UNIVERSITETET
I OSLO

Master's thesis 2023

A molecular and *in planta* investigation of the Q-repeat of the *A. thaliana* transcription factor LRP1

Ellen Margrethe Elnæs Weisteen

Cell biology, Physiology and Neuroscience
60 Credits

Department of Biosciences
Faculty of Mathematics and Natural Sciences

A molecular and *in planta* investigation of the Q-repeat of the *A. thaliana* transcription factor LRP1

Ellen Margrethe Elnæs Weisteen

http://www.duo.uio.no/

Press: Reprosentralen, University of Oslo

Acknowledgements

The work presented in this thesis was carried out at the Department of Bioscience, Faculty of Mathematics and Natural Science, University of Oslo between September 2022 to November 2023.

I would first and foremost like to thank my main supervisor Vilde O. Lalun for always having time for me, for all the invaluable feedback on my thesis, help with experiments, and for always believing in me.

I would also like to thank my co-supervisors Professor Melinka A. Butenko and Professor Kjetill S. Jakobsen for taking the time to read and comment on my thesis.

Thank you to William B. Reinar for the figures you made for my thesis.

Lastly, I want to thank my parents for all the support you have given me throughout all these years.

Hønefoss, December 2023

Ellen M. E. Weisteen

Abstract

Due to their sessility, the ability for plants to adapt to the environment is of great importance. Elucidating the role of genetic variation that underlie phenotypic variation is thus essential for our understanding of adaptation. Over a thousand naturally occurring ecotypes (accessions) have been whole genome sequenced, providing data about genomic structural variations such as short tandem repeats (STRs). STRs have been shown to have a higher occurrence near and within coding regions in many *Arabidopsis thaliana (A. thaliana)* genes, and many STRs had variable length between natural accessions (Reinar et al., 2021). The occurrence of STRs have been shown to be associated with environmental factors and are therefore thought to be involved in adaptation (Reinar et al., 2023). One of the genes found to contain a variable STR between natural accessions of *A. thaliana* was *LATERAL ROOT PRIMORDIUM 1 (LRP1)*. The STR in *LRP1* encodes a Glutamine (Q) repeat ranging from 4 to 12 between populations. LRP1 is a transcription factor (TF) that has been shown to be involved in root elongation and is expressed in various stages of lateral root formation (Singh et al., 2020). Roots are essential for nutrient and water absorption, and they have high levels of plasticity to respond to variations in the rhizosphere. In this study we aimed to elucidate the molecular function of the tri-nucleotide STR encoding a Q-repeat found in the *LRP1* gene.

We investigated this by comparing the most abundant version of LRP1 containing 7 Q-repeats with a version of the gene where the Q-repeat has been removed. We have shown that they both have nuclear localization, and that they form aggregates when transiently expressed in *Nicotiana benthamiana*. Through Fluorescence recovery after photobleaching (FRAP) we have seen indications of mobility differences between the protein variants. We have also seen indications that the repeat affects stability and functionality of the protein. *In planta* experiments have been performed to investigate the phenotypic effects of overexpressing the two LRP1 variants. Lastly, we have furthered our understanding of LRP1 by identifying the spatiotemporal *pLRP1* activity in root development, and through the phenotypic effect of CRISPR mediated *lrp1* knock-out.

Table of Contents

1. Introduction

1.1. Arabidopsis *thaliana* as a model system for population studies

Arabidopsis thaliana (*A. thaliana*) is a commonly used model organism. It has a small genome (135 Mb) relative to most other plants with a well annotated genome. Ecotypes (accessions) used in the lab are typically inbred with high levels of homozygosity compared to naturally occurring accessions, and there are many available tools for forward and reverse genetics, enabling the study of genes and their effect on the organism (Reviewed in Bolle et al., 2011). Highly relevant for my project is that over a thousand natural accessions, sampled from Eurasia, North Africa, and North America have been whole genome sequenced - providing researchers with data about genome wide polymorphisms such as single nucleotide polymorphisms (SNPs), insertions, and deletions (1001 Genomes Consortium., 2016). These data have been used to analyze the evolutionary history, divergence between populations, and population structure of *A. thaliana* (Cao et al., 2011; 1001 Genomes Consortium., 2016; Long et al., 2013; Brennan et al., 2014). Additionally, the importance of polymorphisms for physiological responses, protein function, and phenotype can be studied in a laboratory setting under various growth conditions providing an indication of how genetic variability affects adaptation. While the effects of SNPs on adaptation have been extensively studied, less data is available on the effects of structural variations, such as short tandem repeat (STR), in the genome across populations (Long et al., 2013; Göktay et al., 2021).

1.2. Short Tandem Repeats

STRs, also known as microsatellites, refer to DNA motifs consisting of 1-6 basepairs (though the definition of STR length varies) (Reviewed in Verbiest et al., 2023) that are tandemly repeated in the genome (Fig. 1.1). They are highly mutable due to replication slippage and can in that way increase or decrease in length from one generation to the next (Levinson and Gutman, 1987; Weber and Wong, 1993).

Mononucleotide repeat:	(C)n
Dinucleotide repeat:	(CA)n
Trinucleotide repeat:	(CAA)n
Tetranucleotide repeat:	(CAAT)n
Pentanucleotide repeat:	(CAATC)n
Hexanucleotide repeat:	(CAATCG)n

Figure 1.1 Example of short tandem repeats (STR) unit sizes. The figure shows examples of STRs with different repeat unit size. STRs can consist of 1-6 bases tandemly repeated. n is the number of repeat units

With high mutation rates of 10^{-3} to 10^{-7} per cell division (Reviewed in Gemayel et al., 2010) compared to approximately 10^{-8} to 10^{-10} for SNPs (Reviewed in Baer et al., 2007), STRs may be an important driver for diversification and adaptation, although this is not yet established as an evolutionary mechanism. The effect of STRs on morphological divergence through breeding was seen in dogs where glutamine (Q) and alanine (A) homopolymer repeats in the transcription factor (TF) encoded by the *Runt-related transcription factor 2* gene correlated with midface length and dorsoventral nose bend within and between breeds depending on the Q to A ratio composition in the protein sequence. The mechanism was suggested to be due to the opposing effects of Q-repeats and A-repeats (Fondon and Garner, 2004) since Q-repeats in TFs have been associated with transcriptional activity (Gerber et al., 1994), while A-repeats with transcriptional repression (Janody et al., 2001). The phenotypic variation in form of rapid morphological facial changes were attributed to length variation in the tri-nucleotide repeats encoding the Q and A tracts given the low rate of point mutations and the small genetic diversity within breeds (Fondon and Garner, 2004).

A. thaliana can be found across different environmental clines (1001 Genomes Consortium, 2016). This is reflected by genetic polymorphism, such as STR length variation, between populations which is likely to be important for adaptation (1001 Genomes Consortium., 2016). STR length variation in regions between genes, and within and surrounding coding regions was uncovered through an analysis of the genomes of natural *A. thaliana* accessions. The distribution of STRs were shown to be higher near transcription start sites (TSS) or within genes (Fig. 1.2) involved in developmental processes, hormone pathways, and response to stimuli raising the question of their importance in adaptation (Reinar et al., 2021).

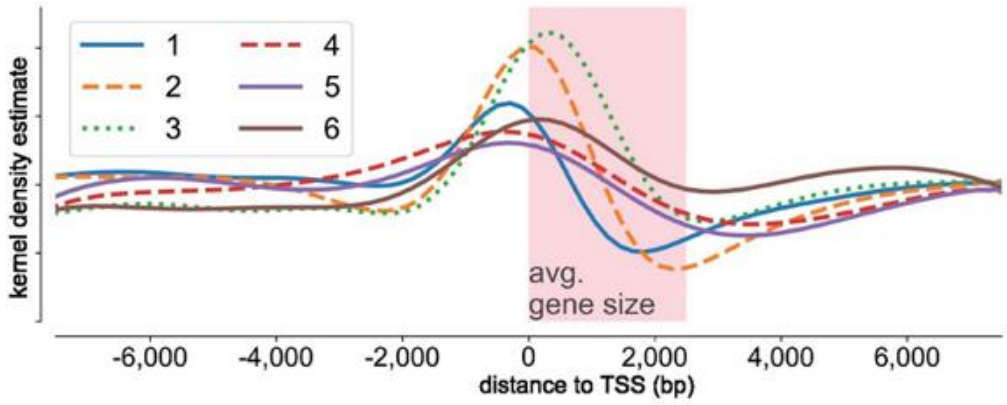

Figure 1.2 Occurrence of various Short Tandem Repeat (STR) unit sizes near Transcription Start Site (TSS). Shows an increase in the occurrence of di- and trinucleotide repeats near and within genes. Figure from Reinar et al., 2021.

Recently, correlations between STR length variations in protein coding regions and environmental conditions in the location the accessions with the STRs were sampled from have been found through a global analysis of *A. thaliana* genes. It was also found that STRs encoding Q and Asparagine (N) homopolymer tracts had the strongest associations with environmental factors, and it is therefore suggested that the amino acids Q and N in particular play an adaptive role (Reinar et al., 2023). Previous studies investigating the Q encoding trinucleotide repeat in the *A. thaliana* gene *EARLY FLOWERING 3* (*ELF3*), encoding a scaffolding protein involved in thermosensing showed that the Q-repeat affected ELF3 protein aggregate formation in the nucleus in response to elevated temperatures (Jung et al., 2020). This mechanism allows for transcriptional activation of thermal responsive genes by sequestering ELF3. The binding partner ELF4 was shown to stabilize the function of ELF3, (Jung et al., 2020) and the interaction between ELF3 and ELF4 was also shown to be affected by the length of the repeat (Press and Queitsch, 2017).

The importance of STRs in protein coding regions, and the effect of Q-repeats on protein function and the association with environmental conditions became the basis for choosing a protein of interest for this thesis. One gene found to have a variable CAA tri-nucleotide STR encoding a Q-repeat was *LATERAL ROOT PRIMORDIUM 1 (LRP1)* (Reinar et al., 2021).

1.3. The LATERAL ROOT PRIMORDIUM 1 transcription factor modulates root development in *A. thaliana*

LRP1 encodes a TF, and has been shown to be expressed in the A. thaliana root (Singh et al., 2020; Smith and Fedoroff, 1995). Many TFs are important for modulating gene expression in response to environmental factors and internal cues by repressing or activating transcription (Reviewed in Hrmova and Hussain, 2021). They typically act by binding to regulatory DNA elements either at promoters or enhancers through a DNA binding domain (DBD), and often in conjunction with other TFs through a dimerization domain (Reviewed in Hrmova and Hussain, 2021). *LRP1* is a member of the *SHORT INTERNODES/STYLISH (SHI/STY)* gene family consisting of 9 active members in *A. thaliana*, with numerous homologues in other plant species (Zhao et al., 2020; Eklund et al., 2010b). TFs in the *SHI/STY* family have a conserved RING finger-like zinc finger motif as the DNA binding domain, as well as an IGGH domain unique to this family (Fridborg et al., 2001), enabling homo- and/or heterodimerization between the different TFs of the SHI/STY family (Eklund et al., 2020a). LRP1 has been shown to interact with the SHI/STY members SHI, STY1, SRS3, SRS6, SHI-RELATED SEQUENCE7 (SRS7), and itself in a yeast two hybrid assay, suggesting that they function as a complex (Kuusk et al., 2006; Singh et al., 2020). All the members except one are confirmed to be expressed in roots, with *SRS5*, *SRS7*, and *LRP1* having the highest expression (Mergner et al., 2020; Liu et al., 2012).

β-glucuronidase (GUS) promoter reporter lines (*pLRP1:GUS*) show activity of the *LRP1 promoter* in young leaves, gynoecium, shoot apical regions, root meristem, and in early lateral root primordia (LRP), as well as at the base of emerging lateral roots (LRs) (Singh et al., 2020; Smith and Fedoroff, 1995). However, a hybridized RNA probe showed *LRP1* expression only in early LRs and adventitious root primordia formation (Smith and Fedoroff, 1995). An increased root length was seen when the *LRP1* repressor LYSINE-SPECIFIC HISTONE DEMETHYLASE 1 (LDL1, also known as SWP1) was knocked out (KO) (Krichevsky et al., 2009) as well as in transgenic *A. thaliana* lines overexpressing (OE) *LRP1* (Singh et al., 2020). The altered phenotype was suggested to be caused by altered auxin homeostasis through increased auxin accumulation in the root tip (Singh et al., 2020). The members STY1 and LRP1

are confirmed to be involved in auxin homeostasis by increasing the levels of the flavin monooxygenases YUCCA (YUC) (Singh et al., 2020; Sohlberg et al., 2006), which are involved in auxin biosynthesis (Zhao et al., 2001). Transgenic *A. thaliana* lines expressing both the *YUC4 promoter* fused to a GUS reporter (*pYUC4:GUS*), and *LRP1* under the constitutively expressed 35S promoter (LRP1 OE) showed increased *YUC4* expression in root meristem and leaves compared to a transgenic line with only *pYUC4:GUS*. Auxin levels in *LRP1* OE lines were shown to be increased, and expression of *LRP1* was also increased in response to auxin treatment (Singh et al., 2020).

Using genomic data from the 1001 genomes project (1001 Genomes Consortium, 2016) it was possible to identify the variability of the STR repeat corresponding to the Q-repeat in LRP1 across the *A. thaliana* accessions. The Q-repeat ranged from 4 to 12 Qs with 7 Qs being the most common (Fig. 1.3 A) (Reinar et al., 2021). The distribution of the repeats across accessions in Eurasia, showing a slight increase in distribution of longer repeats in parts of southern Europe, and a higher occurrence of shorter repeats in south-western Europe (Fig. 1.3 B) could indicate a that there are different environmental clines where accessions with a given repeat in LRP1 have an adaptive advantage.

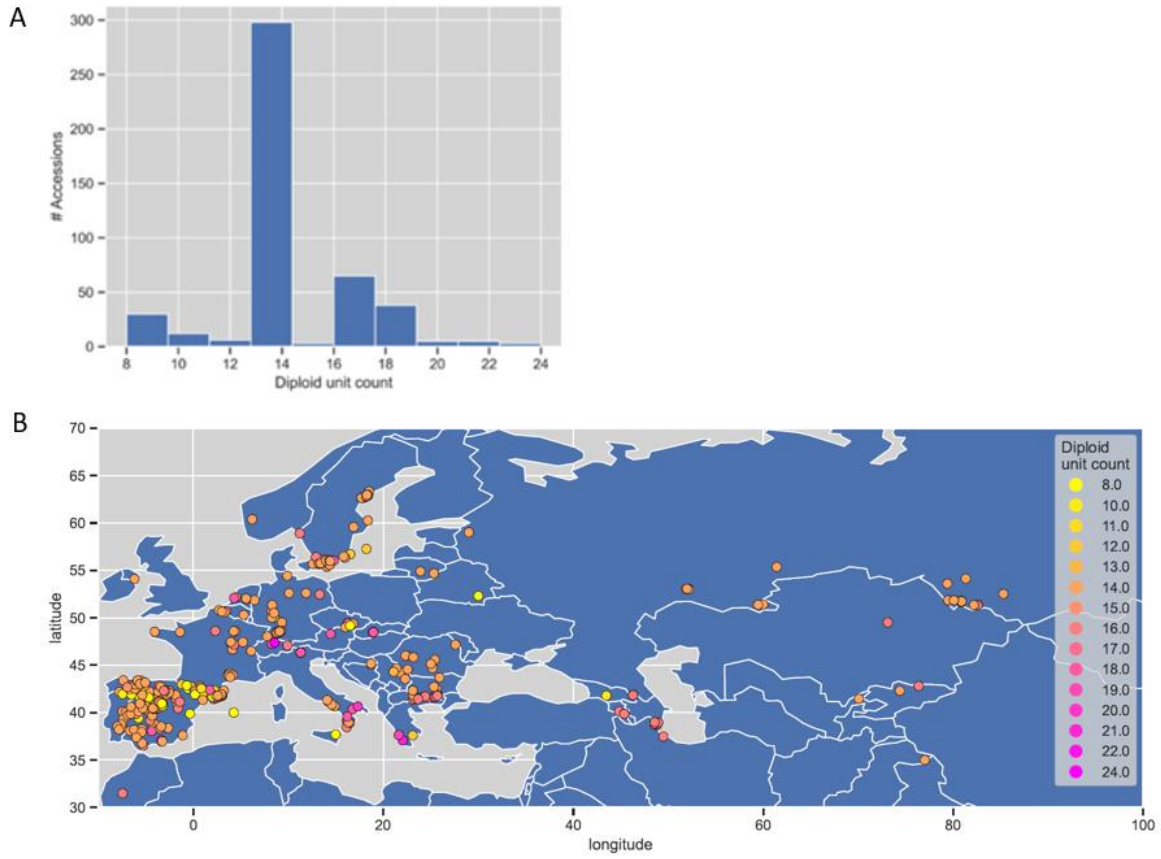

Figure 1.3 Occurrence and distribution of *LATERAL ROOT PRIMORDIUM 1* (*LRP1*) with various short tandem repeat (STR) unit lengths in natural *Arabidopsis thaliana (A.thaliana)* accession A) Bar graph showing the occurrence of various repeats in diploid unit count B) Distribution of various short tandem repeat lengths in *LRP1* in natural *A. thaliana* accessions across Eurasia. Repeat length is shown in diploid unit count. Diploid unit count means that the repeat has been counted for both *LRP1* gene copies since *A. thaliana* contains two chromosome copies, the unit count is therefore double that of the repeat present in the *LRP1* gene. Data used to create figure is from Reinar et al., 2021, and the figure is made by William B. Reinar.

The LRP1 Q-repeat is localized between the DBD and IGGH domain (Fig. 1.4). The spacing and amino acid composition between the domains can affect protein conformation and thus binding and dimerization abilities (Reviewed in Reddy Chichili et al., 2012). The effect of repeats on dimerization abilities was demonstrated in a study on cold tolerance in rice. COLD11 was identified as a protein involved in double stranded break repair, and was found to have an A-repeat that varied between rice cultivars where cultivars with a longer A-repeat in the COLD11 protein had a higher chilling tolerance, likely due to the protein's reduced dimer formation when containing a longer A-repeat (Li et al., 2023). The differences in the Q-repeats

observed in LRP1 between accessions might therefore affect root and shoot formation and adaptation by affecting LRP1's ability to modulate *YUC4* transcription which subsequently affects auxin biosynthesis.

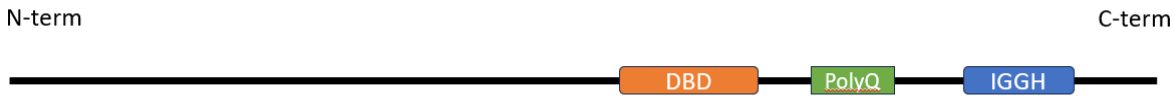

Figure 1.4 Illustration of LATERAL ROOT PRIMORDIUM 1. The black line represents the full-length protein showing the approximate location of the DNA binding domain, the glutamine (Q) -repeat, and the IGGH domain close to the C-terminal.

1.3.1. A. thaliana root system architecture is affected by genetic variation and environmental factors

Roots are essential for plant growth and survival and are thus an important adaptational trait. They enable absorption of water and nutrients from soil, attachment and mechanical support. Due to the sessile nature of plants, it is important that they can modify the root system architecture in response to environmental factors and heterogeneity in the rhizosphere (Reviewed in Smith and De Smet, 2012). *A. thaliana* has a taproot system meaning it consists of one primary root (PR) with emerging LRs (Fig. 1.5). The general appearance of the taproot has been shown to vary between ecotypes, and the phenotypes were associated with environmental conditions. Higher temperatures seemed to negatively influence various root traits such as PR length and LR density, and low levels of precipitation favored length distribution (Deja-Muylle et al., 2022). In addition, the phenotype between ecotypes also varied when grown under the same conditions indicating that genetic variations affect root phenotype (Deja-Muylle et al., 2022). STR length variation in coding regions of genes involved in root development might therefore be involved in local adaptation, and repeat length could influence responsiveness to environmental factors as has been indicated by the repeat length in ELF3 (Jung et al., 2020).

Figure 1.5: Taproot of *A. thaliana*. Blue arrow pointing to primary root, orange arrow pointing to lateral root on the Col-0 ecotype. Modified from Deja-Myulle et al., 2022.

1.3.2. Organization and development of the A. thaliana root

To better follow the development of the root system architecture of *A. thaliana* it is useful to have an overview of the cell types and developmental zones of the root.

A. thaliana roots are organized along a radial axis, and an apical-basal axis. The radial organization consists of the stele at the center, which is divided into the phloem, procambium, metaxylem, and protoxylem. Surrounding the stele is the pericycle, where pericycle cells at the phloem pole are referred to as phloem pole pericycle cells, and pericycle cells at the xylem pole are xylem pole pericycle (XPP) cells. Then there is the endodermis, followed by the cortex, and the epidermis as the outermost layer (Fig 1.6) (Reviewed in De Smet et al., 2015).

The apical-basal organization is divided into the meristematic zone (MZ), elongation zone (EZ), and the differentiation zone (DZ) (Dolan et al., 1993). The MZ can be divided into the apical meristem with higher levels of cell divisions, and the basal meristem with lower levels of cell division. The area between the basal meristem where cell division stops prior to elongation can be referred to as the transition zone (TZ) (Fig. 1.6) (Reviewed in De Smet et al., 2015).

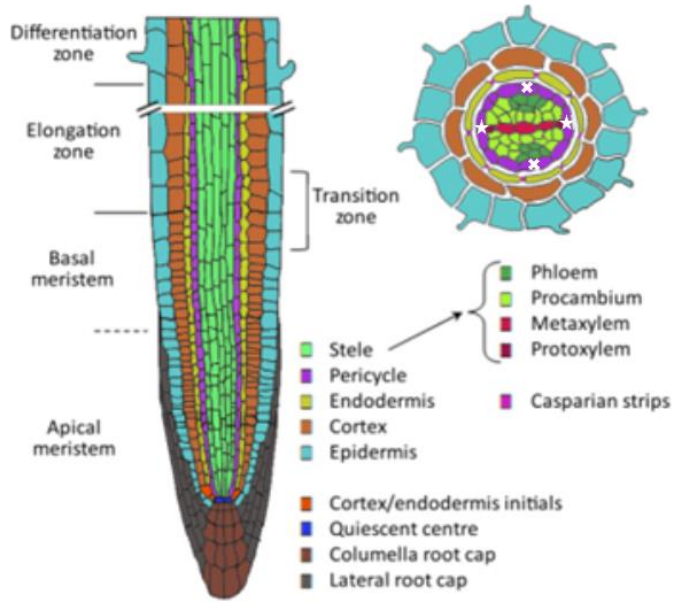

Figure 1.6: *A.thaliana* root structure. Left, longitudinal organization. Right, Radial organization. White stars indicate the location of the xylem pole pericycle cells, white crosses indicate location of phloem pole pericycle cells. Modified from De Smet et al., 2015

1.3.3. Primary root formation and elongation

LRP1 was shown to be expressed in the root meristem, and *LRP1* OE lines showed an increase in root length indicating a role of LRP1 in root elongation in *A. thaliana*. The root apical meristem (RAM) (Fig. 1.6), which is responsible for primary root growth throughout the life span of the plant (Reviewed in Perilli et al., 2012), is established during embryogenesis by an auxin-cytokinin gradient (Reviewed in Su et al., 2015). It consists of the stem cell niche (SCN) and part of the MZ. Local production of auxin in the quiescent center in the SCN has been shown to be essential for its maintenance, and without it the SCN degenerates (Brumos et al., 2018). Low levels of auxin at the SCN have been found to be important for primary root elongation, conversely excessive amounts have been shown to reduce growth (Hu et al., 2021). Auxin produced in the SCN is important for the establishment of the auxin gradient in the root meristem (Fig. 1.7). In the meristem auxin promotes cell division and when the cells reach the TZ an auxin minima allows for cell cycle arrest followed by cell elongation, while a cytokinin maxima at this site promotes differentiation (reviewed in Perrot-Rechenmann, 2010).

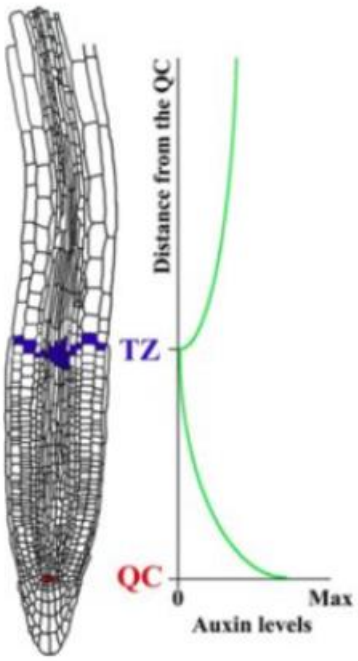

Figure 1.7 Auxin gradient in root. Auxin has a maximum at the quiescent center and a minimum at the transition zone (TZ), and the auxin levels increase again past the TZ. Figure modified from Di Mambro et al., 2017.

1.3.4. Lateral root formation

LRs provide the root system with high levels of plasticity where various nutrient and environmental conditions can affect LR initiation, density, and growth (Gruber et al., 2013; Deja-Muylle et al., 2022). Genetic variation has been shown to affect the root architecture, and this was associated with the environmental cline (Deja.Myulle et al., 2022). Many proteins and hormones are involved in the modulation of LR development, among them is LRP1. LRP1 has as mentioned been shown to be expressed in various stages of LRP formation (Singh et al, 2020). The variable STR in *LRP1* might therefore be important for optimal modulation of LR development for the environmental cline the various *LRP1* STRs are found.

In *A. thaliana* LRs form at regular intervals alternating between the left and right side on the primary root (De Smet et al., 2007). The interval of LR formation is likely dependent on an oscillatory auxin maxima in the primary root, as well as fluctuating expression of various genes, which primes XPP cells at the basal meristem to become LRs (Moreno-Risueno et al., 2010). The expression pattern in the primed XPP cells change as they move from the MZ to the EZ

and to the start of the DZ at a site called the pre-branch site (Taiz et al., 2023). Following this, local production of auxin in primed XPP cells establishes the lateral root founder cells (Fig. 1.8 A) (Dubrovsky et al., 2008). These will further develop into a LRP. LRP development is divided into stages (I-VIII) that correlate with the number of cell layers. Stage I starts with an anticlinal asymmetric division, and the following stages are formed by several periclinal divisions (Fig. 1.8 B). In order for LRPs to emerge through the overlying cells, their properties are affected through regulation of gene expression by an auxin maxima produced at the tip of the LRP. Eventually the LRP will emerge as an LR through the epidermis and continue to grow (Reviewed in Banda et al., 2019).

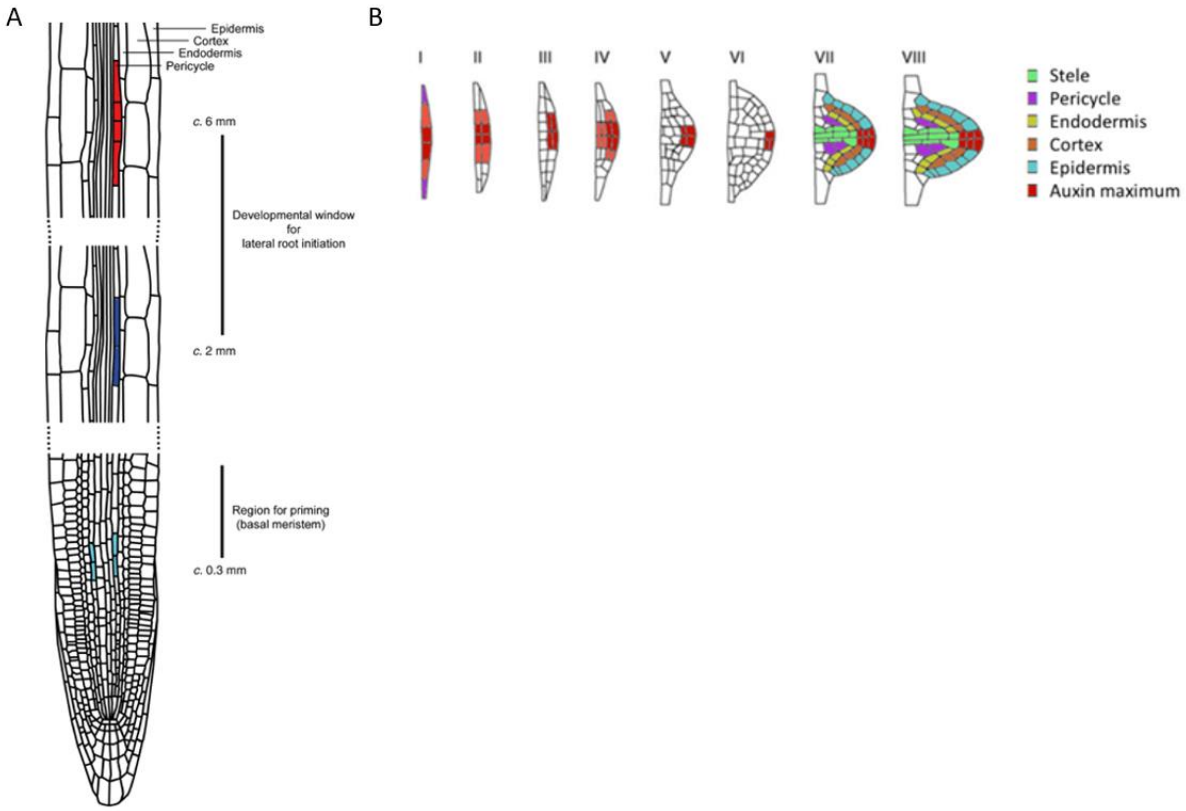

Figure 1.8: Lateral root primordium (LRP) formation. A) Figure showing approximate location of priming of xylem pole pericycle (XPP) cell (light blue), establishment of lateral root founder cells (LRFC) (dark blue), and the asymmetric division (red) of LRFC that leads to LRP formation. Figure modified from De Smet 2012. B) Figure from De Smet et al., 2015) showing the stages (I-VIII) of LRP development.

1.4. Auxin and LRP1 in leaf development

Leaf development and morphology is affected by auxin levels, this has been demonstrated with elevated auxin levels which led to epinastic (downturned) leaves (King et al., 1995; Qin et al., 2005). Conversely, reduced auxin through downregulation of YUC2 and YUC6 has been shown to cause hyponastic (upturned) leaves (Li et al., 2008). *YUC4* OE has also been shown to affect leaf morphology, with elongated petioles and downward curled leaves (Munguía-Rodríguez et al., 2020), and since *LRP1* has been shown to be expressed in the shoot apical region and young leaves (Singh et al., 2020), LRP1 might be involved in leaf development through its ability to increase YUC4 levels (Singh et al., 2020).

Leaves develop from the shoot apical meristem (SAM), which consists of the central zone important for maintaining the stem cell niche, and the peripheral zone (PZ) where leaves emerge from (Reviewed in Du, F. et al., 2018). Initiation of leaf development is dependent on an auxin maxima at the PZ. This leads to the recruitment of founder cells which become a leaf primordium and form a bud (Reviewed in Nakata and Okada, 2013). The primordium grows distally away from the SAM, establishing the proximal-distal polarity. The proximal side will give rise to the petiole, while the distal side gives rise to the blade that will later become the leaf (Reviewed in Manuela and Xu, 2020). Simultaneously, an asymmetry of the adaxial-abaxial and medio-lateral is formed. A polar distribution of auxin of the abaxial-adaxial axis has been reported with high levels of auxin at the abaxial side and low levels at the adaxial side (Guan et al., 2017). The abaxial-adaxial auxin polarity has been shown to be important for the medio-lateral polarity and subsequent growth and flattening of the blade (Guan et al., 2017). The blade forms from a region between the adaxial and abaxial sides (Reviewed in Du, F. et al., 2018). Cell division and cell differentiation separates the petiole and the blade, and the blade is shaped, followed by a rapid distal and lateral expansion of the blade to form the leaf (Fig. 1.9) (Reviewed in Xiong and Jiao, 2019).

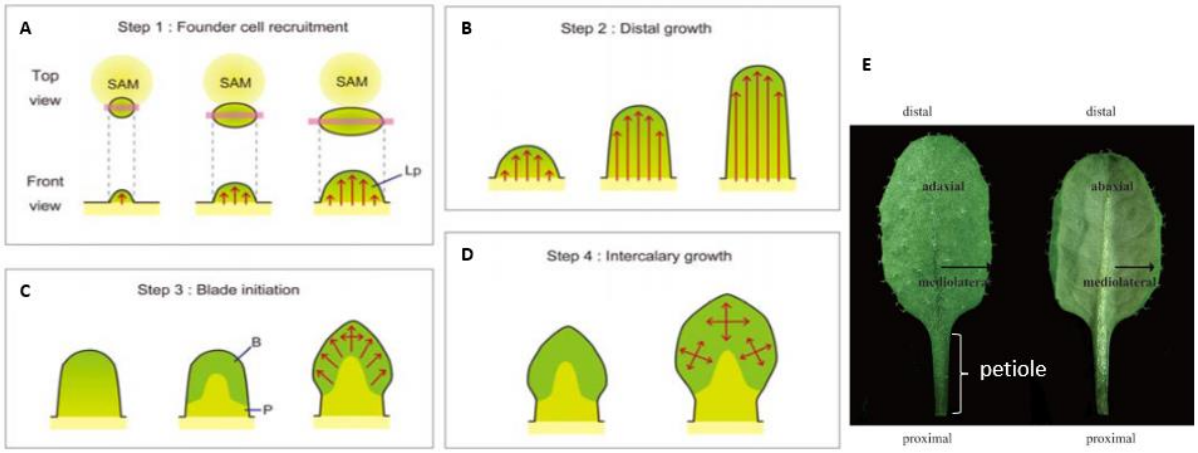

Figure 1.9 Leaf formation and polarity A) Founder cells are recruited in the SAM to form a primordium, B) primordium grows distally, C) initiation of the blade with growth in several directions, separating the petiole from the blade, D) intercalary growth of the blade that gives it the leaf shape A-D) Modified from Nakata and Okada, 2013. E) Picture showing adaxial and abaxial sides, mediolateral axis and proximal-distal axis, from Manuela and Xu, 2020. B = blade, P = petiole, SAM = shoot apical meristem. Red arrows indicate growth direction.

1.5. Aims of study

The main aim of this study is to contribute to the understanding of the functional importance of the tri-nucleotide STR found in the coding region of the *LRP1* gene. We will investigate this by comparing the wild-type version of LRP1 found in Col-0 which is the most abundant version harboring a 7 amino acid Q-repeat to an LRP1 version where the Q-repeat is removed. Although LRP1 without a Q-repeat is not found among the natural *A. thaliana* accessions, studies that look at repeats in plant proteins often create a gene variant without a repeat as this can give a good indication of the potential importance of the repeat (Jung et al., 2020; Li et al, 2023; Press and Queitsch, 2017).

To elucidate the functional differences of LRP1 with a 7 Q tract and without a Q tract, we will first explore the protein variants fused to a fluorescent protein through transient expression in *Nicotiana benthamiana* (*N. benthamiana*) to a) investigate cellular localization and b) determine the mobility of the LRP1 variants by fluorescence recovery after photobleaching (FRAP). Next, given that LRP1 activates *pYUC4*, we want to investigate if the two variants of LRP1 differ in a luciferase assay set up to measure *pYUC4* activity.

Further, we want to address the function of the native *LRP1* gene, as well as the potential functional differences of the two LRP1 variants *in planta*. To do this, two *pLRP1* reporter lines will be used to identify spatiotemporal expression of LRP1. Transgenic *A.thaliana* lines overexpressing the *LRP1* versions with and without a Q tract will be created to compare phenotypes. Lastly, CRISPR-Cas9 will be used to create a KO mutant *lrp1* line to investigate potential root phenotype aberrations in plants lacking a functional LRP1 protein.

2. Materials and Methods

2.1. DNA techniques

2.1.1. Isolation of genomic DNA

DNA isolation was performed on Columbia-0 (Col-0) ecotype of *A. thaliana* leaves to obtain genomic DNA for use in amplifying specific sequences with PCR (Section 2.1.3).

A small piece (approximately 0.5 cm x 0.5 cm) of a leaf was placed in an Eppendorf tube with 150 µl extraction buffer (200 mM Tris-Cl pH 7.5, 250 mM NaCl, 25 mM EDTA, 0.5 % SDS) and ground with a small pestle until there was no visible tissue. Another 300 µl extraction buffer was added before centrifuging for 5 minutes (min) at full speed. 350 µl supernatant was transferred to a new tube and 350 µl isopropanol was added. The solution was left for 5 min at room temperature (RT) before centrifuging for 5 min, max speed. Supernatant was removed and pellet was left to dry in 37 °C incubator before being resuspended in 50-100 µl double distilled H2O (ddH_2O).

2.1.2. Primers

Primers were designed manually using the available gene sequences from “ensemble plants”, with the exception of primers used in genotyping of Salk T-DNA transgenic plants (Section 2.1.4).

Table 2.1: Primers used for amplification of specific DNA sequences. Primers are written in the 5’->3’ direction. Sequences are found on the reverse strand. Fw = forward, Rv = reverse

Primer name	Sequence	Ensemble ID/location
promRLP1_2000 Fw	5’CGAGTTTTAATGTTACCACCC ‘3	Chromosome 5: 3,989,833-3,991,833
promRLP1_Rv	5’AACCCATAAATCTACACAAATCTG ‘3	
promRLP1_2000 attb1	5’GGGGACAAGTTTGTACAAAAAAGCAGGCTTG CGAGTTTTAATGTTACCACCC ‘3	

promRLP1_ attb2	5’GGGGGACCACTTTGTACAAGAAAGCTGGGTC AACCCATAAATCTACACAAATCTG ‘3	
LRP1 Attb1	5’GGGGACAAGTTTGTACAAAAAAGCAGGCTTG ATGTACATTGGAGCTTTGTG’3	AT5G12330.4
LRP1 Attb2 NS	5’GGGGGACCACTTTGTACAAGAAAGCTGGGTC ACTGTAAAACCCACCGC’3	
LRP1 CDS fw	5’ATGTACATTGGAGCTTTGTGC’3	
LRP1 CDS NS Rv	5’ACTGTAAAACCCACCGC’3	
LRP1_0 rep Fw	5’GCCACTTCTCATACTTCAACTTCT’3	
LRP1_0 rep Rv	5’AGACCCTACGATCCTCG’3	
pYUCCA4 Fw	5’TCTCAGATGTCCAACATG’3	Chromosome 5: 3,613,640-3,616562
pYUCCA4 Rv	5’GTCGACTAATAAAAGCGAAAG’3	

2.1.3. Polymerase chain reaction

DNA sequences of interest were amplified using PCR, and the templates used are shown in table 2.3. These were used in subsequent cloning steps and were therefore amplified using the proofreading polymerase Q5® High-Fidelity DNA (New England BioLabs) An exception was *pYUC4* where Taq DNA polymerase (New England BioLabs) was used. Taq was also used for confirmation of the presence of specific DNA sequences in transformed bacterial colonies (Section 2.2.1), and in Salk genotyping (section 2.1.4)

Protocols from New England Biolabs were used for the respective polymerases.

2.1.4. Genotyping of Salk T-DNA lines

One T-DNA line (Table 2.2) that should have *lrp1* KO was ordered from The Nottingham Arabidopsis Stock Centre (NASC). The line has a T-DNA insert in exon 3 of *LRP1* (Fig. 2.1). Genotyping of the T-DNA line was performed using PCR to ensure that it contains the T-DNA insert (S. Fig. 1). DNA was isolated using the method described in section 2.1.1. The primers used are shown in table 2.2 and were designed using the Salk Institute Genomic Analysis Laboratory (SIGnAL) T-DNA primer design. The genotyping protocol from SIGnAL was followed.

The lines used and the corresponding left border (LB) and right border (RB) primers used for wild-type detection are shown in table 2.2 For T-DNA confirmation LBb1.3 for SALK_201247 with the corresponding RB primer.

Table 2.2: Primers used for SALK genotyping, listed in 5'->3' direction. N/A = not applicable. LB = left border, RB = right border.

SALK line	Name	Sequence
SALK_201247	SALK_201247 LB	5'TGATAAGTGCATGAGAAAATGG'3
	SALK_201247 RB	5'ACACACCACCTCAAAGTTTCG'3
N/A	LBb1.3	5'ATTTTGCCGATTTCGGAAC'3

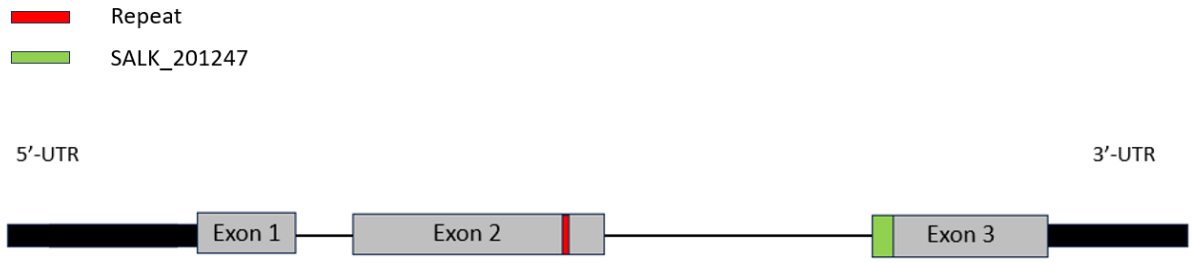

Figure 2.1 Illustration of LATERAL ROOT PRIMORDIUM 1 (AT5G12330.4) in the 5'->3' direction showing the approximate position of T-DNA insertion of SAIL_70_H09 and SALK_201247.

2.1.5. TOPO TA cloning

TOPO TA cloning utilizes the enzyme DNA topoisomerase I that function as a restriction enzyme and a ligase, making this a one-step cloning method (Shuman, 1994). The enzyme is bound to phosphate on the 3' thymidine overhang of a linearized TOPO vector (Fig. 2.2). A PCR product with complementary A'overhangs is required for insertion and it can be inserted

either in the forward or reverse direction. It is therefore necessary to screen for vectors with the PCR product in the correct direction by using restriction enzymes.

TOPO TA cloning was used to create entry clones with AttL4-and AttR1-sites compatible with the Gateway system, shown in table 2.4, to later be used to create expression vectors in an LR reaction (section 2.1.6). The vector used for TOPO cloning was pENTR'5. The protocol from ThermoFisher was followed.

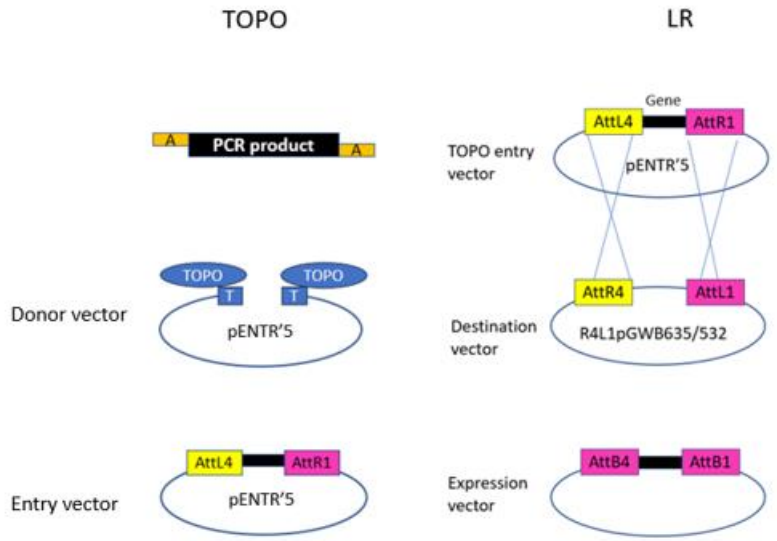

Figure 2.2 Illustration of TOPO and LR gateway cloning. A PCR product with adenine (A) overhangs is used together with a TOPO vector which has thymidine overhangs. Topoisomerase attached to thymidine catalyzes ligation of the PCR product with the vector. The product is a TOPO entry vector. This vector can be used in LR cloning to create an expression vector. Figure inspired by ThermoFisher Multisite Gateway Manual.

2.1.6. Gateway® cloning

Gateway® cloning is based on the ability of the bacteriophage λ to recombine sequences between plasmids (Landy, 1989). There are two main steps to this method; The first step is to create an entry clone through a BP reaction where a PCR product flanked by att-sites are recombined by BP clonase into a donor vector containing complementary att-sites, creating an entry clone. The second step is an LR reaction where the entry clone from BP cloning (or TOPO

cloning) is used in an LR reaction where recombination of att-sites of a destination vector by LR clonase creates an expression vector.

The vectors contain an antibiotic resistant gene allowing for selection of bacterial colonies containing the vector. Additionally, the donor vectors contain a *ccdB* gene that acts as selection against bacteria that might have been transformed with a vector that has not been recombined as this gene prevents growth of the bacteria.

Gateway® cloning was used to create some of the constructs listed in table 2.3 and in table 2.4, and the protocol from ThermoFisher was followed.

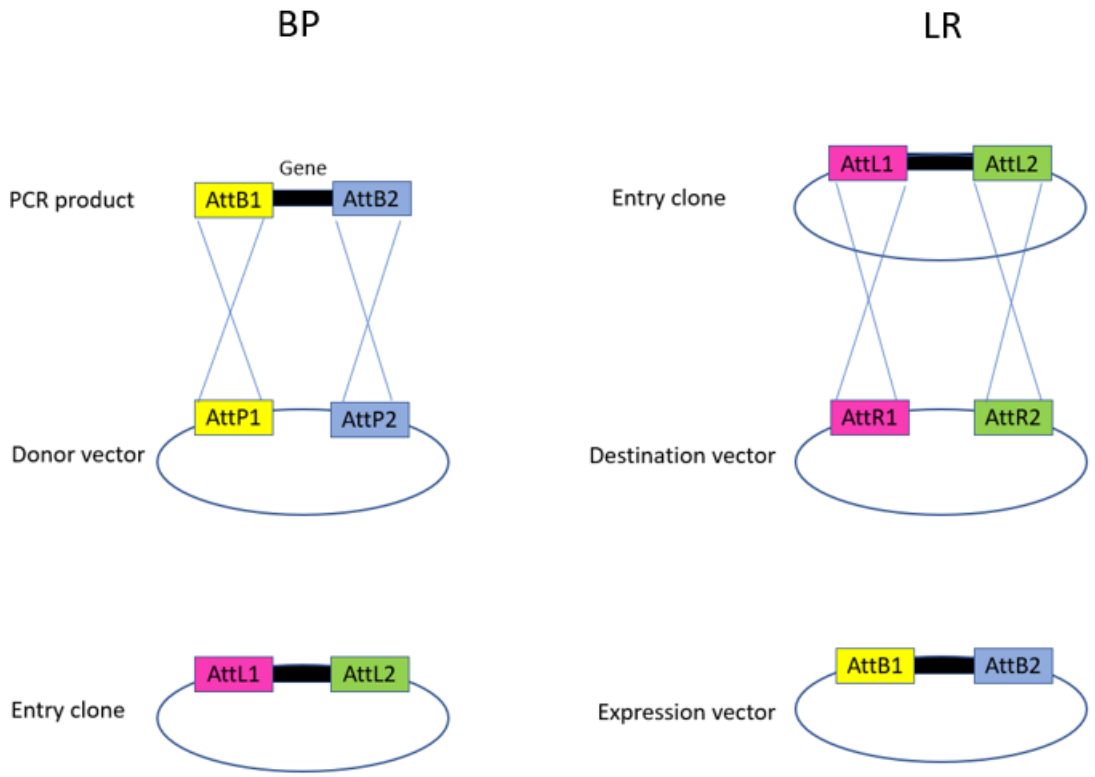

Figure 2.3 Illustration of BP and LR cloning. BP cloning is performed with a PCR product with flanking att-sites. BP clonase will catalyze recombination of att-sites between the PCR product and donor vector creating an entry clone. This entry clone can be used in LR cloning to create an expression vector. Figure inspired by ThermoFisher Multisite Gateway Manual.

2.1.7. Site-directed mutagenesis

Site-directed mutagenesis was used to generate *0QLRP1*, a version of *7QLRP1* with no CAA-repeat. The primers LRP1_0 rep Fw and LRP1_0 rep Rv (Table 2.1) were designed to bind on each side of the Q-tract, orienting away from it (Fig. 2.4). PCR was performed with *7QLRP1-pDONR/Zeo* as template. This leads to a PCR product without the repeat. The PCR product was run on gel (Section 2.1.13), the correct band of approximately 3300 basepairs was cut out of the gel and purified (Section 2.1.10), then ligated with T4 ligase (New England Biolabs) following the provider's manual. The ligated vector was then used in transformation (Section 2.2.1), and gateway cloning (Section 2.1.6).

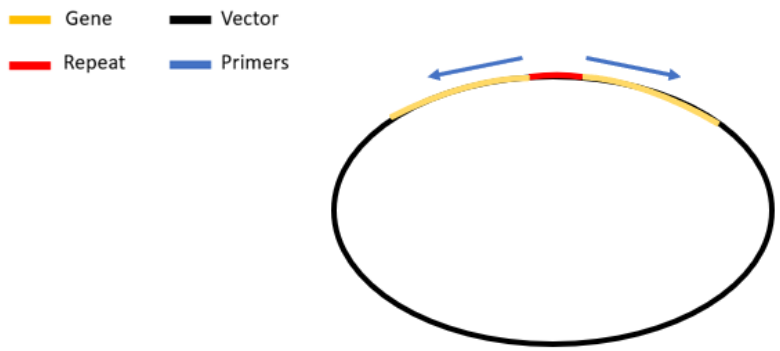

Figure 2.4 Illustration of vector containing a gene (yellow) with a repeat (red) and binding sites for primers (blue) going in opposite directions away from the repeat.

Table 2.3 Overview of entry clones created using BP cloning, TOPO cloning, or site directed mutagenesis (SDM). Zeo = Zeocin, Km = Kanamycin. Constructs were confirmed with Sanger sequencing.

Gene/promoter	Template	Vector	Method	Resistance	Reference
7QLRP1	PCR with att-sites on Col-0 cDNA	pDONR^{TM}/Zeo(Invitrogen)	BP	Zeo	This study
0QLRP1	7QLRP1-pDONR^{TM}/Zeo	pDONR^{TM}/Zeo(Invitrogen)	SDM	Zeo	This study
pLRP1	PCR on Col-0 gDNA PCR with att-sites on Col-0 gDNA	pENTR'5 (Invitrogen) pDONR^{TM}/Zeo (Invitrogen)	TOPO BP	Km Zeo	This study This study
pYUC4	PCR on Col-0 gDNA	pENTR'5 (Invitrogen)	TOPO	Km	This study

Table 2.4 Overview of expression clones made using LR cloning. Sp = Spectinomycin, Km = Kanamycin, Hyg = Hygromycin. KO = knockout. Est.ind = estradiol inducible. GFP = green fluorescent protein, YFP = yellow fluorescent protin, LUC = luciferase, Tomat is a red fluorescent protein. N/A = not applicable. Constructs were confirmed with Sanger sequencing.

Construct	Vector	Promoter	Resistance	Resistance in plants	C-term tag	Purpose	Reference
est.ind35S:7QLRP1-GFP ***35S:7QLRP1-YFP***	pAB117 (Bleckmann et al., 2010) pEG101 (Earley et al., 2006)	LexA-46 35S CaMV 35S	Sp Km	N/A BASTA	GFP YFP	Infiltration Floral dip	This study
est.ind35S:0QLRP1-GFP	pAB117 (Bleckmann et al., 2010)	LexA-46 35S	Sp	N/A	GFP	Infiltration	This study

35S:0QLRP1-YFP	pEG101 (Earley et al., 2006)	CaMV 35S	Km	BASTA	YFP	Floral dip	
est.ind35S:7QgLRP1-GFP	pAB117 (Bleckmann et al., 2010)	LexA-46 35S	Sp	N/A	GFP	-	This study
pLRP1:GUS	R4L1pGWB532 (Nakamura et al., 2009)	-	Sp	Hyg	GFP-GUS	Floral dip	This study
pLRP1:H2B-Venus	pAB146 (Somssich et al., 2016)	-	Km	N/A	H2B-YFP	Floral dip	This study
pYUC4:luc	R4L1pGWB635 (Tanaka et al., 2013)	-	Sp	N/A	LUC	Luciferase assay	This study
CRISPR Guide11	pKI1.1R (Tsutsui and Higashiyama, 2017)		Sp	Hyg	-	KO	This study
CRISPR Guide19	pKI1.1R (Tsutsui and Higashiyama 2017)		Sp	Hyg	-	KO	This study
dsTomat-H2B			Sp	N/A		Infiltration	Sergio G. Trigo

2.1.8. CRISPR Knock-Out of LRP1

CRISPR/Cas9 is based on a bacterial antiviral system and can be used to KO the function of genes or introduce desired mutations. A Cas protein containing two domains (HNH and RuvC) with nuclease activity introduce a double stranded break (DSB) in the DNA. Cas recognizes the cleavage site through the association with a single guide RNA (sgRNA) that can be designed to recognize a specific gene sequence. The sequence must also have an adjacent PAM site for the nuclease to cut the target sequence. When a DSB has been introduced, the cell will try to repair it, this often leads to the addition or removal of bases which can lead to a frame-shift mutation, causing an earlier stop codon, and the gene will code for a truncated protein which ideally will be non-functional (Jinek et al., 2012).

CRISPR/Cas9 was used to create a *lrp1* KO in Col-0 plants. Two different sgRNAs were chosen from the CRISPR-P 2.0 design tool; sgRNA11 and sgRNA19. The primers used are shown in Table 2.5 and were designed by my supervisor Vilde O. Lalun. The sgRNAs were cloned into the vector pKIR1.1 (Table 2.4), which was used to transform Col-0 through floral dip (Section 2.3.2). Mutants were selected by plating seeds on Murashige Skoog (MS-2) plates with appropriate selection (Table 2.8). DNA was isolated (Section 2.1.1) from seedlings that survived, and PCR was performed using primers shown in table 2.6. PCR product was genotyped using Sanger sequencing (Section 2.1.12) to confirm mutation, and to check if it is homo- or heterozygous for the mutation.

Table 2.5 Primers used to create CRISPR vector with Guide 11 or Guide 19. Primers designed by Vilde O. Lalun. Primers written in the 5'->3' direction. Fw = forward, Rv = reverse

Name	Sequence
LRP1_CR_Guide11 Fw	5'ATTGGCTTATCACCACCAGAACGC'3
LRP1_CR_Guide11 Rv	5'AAACGCGTTCTGGTGGTGATAAGC'3
LRP1_CR_Guide19 Fw	5'ATTGGTTCAAGTGTGTTAGAGTAA'3
LRP1_CR_Guide19 Rv	5'AAACTTACTCTAACACACTTGAAC'3

Table 2.6 Primers used for sequencing CRISPR mutants. Primers are written in the 5'->3 direction. g11 represents single guide RNA11, g19 represents single guide RNA19. Fw = forward, Rv = reverse

Name	Sequence
g11 Fw	5'CTACCGACGTCGGATTCCGGT'3
g11 Rv	5'GCCACGGCTCTTGCAGCA'3
g19 Fw	5'CCAGCTCCAGCCGACAAGG'3
g19 Rv	5'CCACCGCCTGAACCTCCACC'3

Binding sites for the sgRNAs are shown in figure 2.5. The protocol from Tsutsui and Higashiyama (2017) was followed.

Figure 2.5 Illustration of binding sites for CRISPR guide 11 (blue) and guide 19 (yellow). Location of the *LRP1* STR (repeat) is shown in red. *LRP1 = LATERAL ROOT PRIMORDIUM 1*, STR = short tandem repeat

2.1.9. Plasmid isolation

Isolation of plasmid DNA from bacterial cultures was performed using the Wizard® Plus Miniprep DNA Purification System kit (Promega), following the protocol from the supplier.

A "home-made" plasmid isolation method was also used. 1.8 mL overnight culture in Eppendorf tubes was centrifuged at top speed for 1 min. Supernatant was discarded, and 1 µL RNAse A and 100 µL ice-cold sterilized Solution 1 (50 mM Glucose, 25 mM Tris-Cl (pH 8.0), 10 mM EDTA (pH 8.0)) was carefully mixed with pellet followed by adding 200 µl Solution

2 (0.2 N NaOH, 1 % (w/v) SDS) freshly made. The tubes were inverted 5-10 times and incubated at RT for up to 3 min until the solution has become clear. Then 150 µL Solution 3 (5 M Potassium Acetate, 11.5 % glacial acetic acid, H_2O) was added, and tubes were inverted vigorously 5-10 times and placed on ice for 5 min before centrifuging for 5 min max speed. Supernatant was added to a new Eppendorf tube. 900 µL 100 % ethanol (EtOH) was added and was mixed by inverting tubes 5-10 times, then centrifuged for 5 min max speed. Supernatant removed without disrupting pellet. Add 750 µL 75 % EtOH and vortexed for 10 seconds (s). Was then spun down for 30 s max speed. Pipette out supernatant and allow pellet to dry before resuspending in 100 µL dH_2O.

2.1.10. PCR and gel clean up

PCR and gel clean-up (Promega) was used to isolate DNA from gel in site directed mutagenesis (Section 2.1.7). Protocol from supplier was followed.

2.1.11. General cleanup from enzymatic reactions

Cleanup from enzymatic reactions from geneJET (ThermoFisher) was used to isolate digested vector for CRISPR (Section 2.1.8). Protocol from the supplier was followed.

2.1.12. Sequencing

All constructs were prepared for Sanger sequencing following the protocol from supplier and sequenced by Eurofins Genomics.

2.1.13. Gel electrophoresis

Gel electrophoresis was used to visualize the presence of an amplified band from PCR, and to separate different sized fragments after digestion reactions. The DNA samples were mixed with

6 X Orange Loading Buffer and was added to 1% agarose gel made with 1x TEA and 10,000 X GelRed® (Biotium, 41003-1, VWR). To determine DNA fragment sizes a 1 kb GeneRuler with known fragment sizes was used. The gel was run at 90-110 V for 20-30 min.

2.2. Methods in Bacteria

2.2.1. Transformation of *Escherichia coli*

Chemically competent *Escherichia coli* (*E.coli*) strain Dh5α (Thermo Scientific, EC0112) was used for all constructs except for the CRISPR constructs where TOP10 (Invitrogen) was used. Protocols from the suppliers were followed.

All transformants were plated on LB-medium (LB-medium with 15 g/l Bacto Agar) agar plates containing the appropriate selection (Table 2.4) and concentrations (Table 2.7) and incubated at 37°C overnight.

2.2.2. Transformation of *Agrobacterium tumefaciens*

Electrocompetent *Agrobacterium tumefaciens (A. tumefaciens)* (C58 GV3101) were transformed by electroporation. This is done by adding 50 µL *A. tumefaciens* mixed with approximately 100 µg isolated construct placing in a chilled electroporation cuvette. This was pulsed at 2.5 kV, and 250 µL S.O.C medium was added to the cuvette and mixed before being plated. All transformants were plated on YEB (YEB medium, 15 g/l bacto agar) plates containing the appropriate selection (Table 2.4) and concentrations (Table 2.7) and incubated at 28 °C for 2-3 days.

2.2.3. Overnight culture

Bacteria were grown in overnight cultures in approximately 5 mL LB or 3 mL YEB medium with appropriate selection (Table 2.4) and concentrations (Table 2.7) at 37 °C (*E. coli*) or 28 °C (*A. tumefaciens*) with 220 rotations per minute (rpm) for 1-2 days.

Table 2.7 Antibiotics and concentrations used for selection of bacterial growth. Carb = Carbencillin, Km = Kanamycin, Rif = Rifampicin, Sp = Spectinomycin, Zeo = Zeocin

Name	**Abbreviation**	**Stock concentration**	**User concentration**
Carbencillin	Carb	100 mg/mL	100 µg/mL
Kanamycin	Km	100 mg/mL	100 µg/mL
Rifampicin	Rif	50 mg/mL	50 µg/mL
Spectinomycin	Sp	100 mg/mL	10 µg/mL
Zeocin	Zeo	100 mg/mL	25 g/mL

2.3. Methods for *A. thaliana* transformation

2.3.1. Seed sterilization and plant growth

Seeds were surface sterilized to prevent contamination by submerging them in 70% EtOH for 5 min, followed by a bleach solution (20 % Klorix, 0.1 % Tween20, ddH_2O) for 5 min, and washing them with a wash solution (0.001 % Tween20, ddH_2O) before submerging them in agar solution. They were then plated on Murashige and Skoog-2 agar plates (MS-2 plates) containing the appropriate selection if needed (Table 2.4). Antibiotic concenctrations are shown in Table 2.8.

Seeds were then vernalized for approximately 1-3 days at 4 °C, then transferred to long day (16 hours (h) light, 8 h dark) conditions at 22 °C.

If seedlings were to be used to produce seeds, they were placed in soil to grow at 22 °C (16 h light, 8 h dark). When stems started to appear, they were cut at the base to induce the production of more stems which increased seed yield.

2.3.2. *A. thaliana* transformation by Floral dipping

A.tumefaciens have an innate ability to transform plants due to the presence of a Ti-plasmid containing a T-DNA sequence that can be inserted randomly into the plant genome (Alonso et al., 2003). Floral dipping is a method that utilizes this to create transformed seeds (Clough and Bent, 1998).

To perform the floral dip, the constructs (Table 2.4) were grown over night in baffled Erlenmeyer flasks to increase agitation with approximately 100 mL liquid YEB medium with appropriate selection (Table 2.4) and concentration (Table 2.7). at 28 °C, 220 rpm. Optical density (OD) was checked the next day, if over 0.8 they were diluted to approximately OD 0.4 and incubated until the OD had increased to approximately 0.8, this is done to ensure the bacteria are in a growth phase. They were then centrifuged at 5000 rpm for 10 min at 4 °C. Supernatant was poured off, and the pellet was resuspended in a resuspension solution (ddH_2O, 5% sucrose, and 0.02% Silwett) to an OD of 0.8. If flowers had started to appear, they were cut to reduce the number of Col-0 seeds produced. The plants were then dipped in the solution, covered with aluminum foil and placed in a dark place for ~24 h before being transferred to growth room (18 or 22 °C, 16 h light, 8 h dark)

Seeds were harvested when the plants and siliques were dry.

2.3.3. Selection of transformants and identifying one copy lines

Seeds harvested from the floral dipped plants (T_0) were plated on MS2 plates with selection (table 2.4) to select for transformed seeds (T_1). Antibiotic concentrations used for selection are found in table 2.8.

Seedlings that survived were transferred to soil and are the primary transformants (T_1). Seeds from T_1 (T_2 seeds) were harvested separately as each individual T_1 plant will have the T-DNA inserted in different places and have different copy numbers of the insert (Alonso et al., 2003). To find one copy lines, T_2 seeds were plated on MS2 plates containing appropriate selection. The inheritance of T-DNA inserts follows mendelian inheritance. T1 seeds containing one insert will in the following generation give rise to seeds where 25 % will have no T-DNA insert,

and 75 % will have one insert and be either homo- or heterozygous meaning that one copy lines will have approximately 75 % survival on agar plates with selection.

Table 2.8 Antibiotics and concentrations used for selection of *A. thaliana* transformants. Hyg = Hygromycin, BASTA = Glufosinate Ammonium

Name	**Abbreviation**	**Stock concentration**	**User concentration**
Hygromycin	Hyg	25mg/ml	25mg/l
Glufosinate Ammonium	BASTA	1 M	100

2.4. Phenotyping of transgenic lines

2.4.1. Root phenotyping of *LRP1* OE and *lrp1* lines

Seedlings of one copy lines of *35S:7QLRP1-YFP* and *35S:0QLRP1-YFP* containing a YELLOW FLUORESCENT PROTEIN (YFP) were grown vertically on ½ MS2 plates for 7 days. The plates were scanned using an Epson scanner, ImageJ was used to measure the root length starting from the base of the hypocotyl.

2.4.2. Leaf phenotyping of *LRP1* OE lines

Seedlings of one copy lines of *35S:7QLRP1-YFP* and *35S:0QLRP1-YFP* were grown vertically on MS2 plates until they contained the two first true leaves. The plates were scanned using an Epson scanner. ImageJ was used to measure length and diameter of leaves starting from the beginning of the petiole.

2.5. Methods in *Nicotiana benthamiana*

2.5.1. Agrobacterium infiltration

To infiltrate *N. benthamiana* with the constructs (Table 2.4), overnight cultures of transformed *A. tumefaciens* (Section 2.2.2), in addition to the helper plasmid p19 which inhibits post-transcriptional gene silencing (Lakatos et al., 2004), were set up with appropriate antibiotic concentrations (Table 2.7) of Carbamycin, Rifampicin and the appropriate selection listed in Table 2.4 in 3mL of liquid YEB medium.

The next day, they were centrifuged (2700rpm, 4 °C, 8 min), followed by removing supernatant, and resuspending pellet with 1mL resuspension solution (ddH_2O, 10 mM MgCl and 150 µM acetosyringone). They were then chilled on ice for 1-4 h, and more resuspension solution was added to bring the solutions to approximately 0.8 OD before infiltration.

Equal amounts of p19, construct, and resuspension solution were mixed before injecting it with a syringe into *N. benthamiana* leaves.

2.5.2. Estradiol induction

Transient expression of *est.ind35S:7QLRP1-GFP* and *est.ind35S:0QLRP1-GFP* containing a GREEN FLUORESCENT PROTEIN (GFP) was induced by spraying *N. benthamiana* leaves with estradiol approximately 2 days after infiltration (Section 2.5.1). To determine the ideal time for imaging following induction, expression was checked using a fluorescence microscope 2, 4, 6, and 16 h after induction. (S. Fig. 2)

16 h was chosen as the ideal time for practical reasons. Due to being highly overexpressed at this time, optimization with different estradiol concentrations (20 mM, 15 mM, 10 mM, and 5 mM) was done to see if this would affect the amount of expressed protein. (S. Fig. 3)

It was decided that all measurements would be done after 16 h with 5 mM estradiol for induction.

2.6. Microscopy

2.6.1. Light microscopy

Zeiss Axioplan was used to take pictures of GUS-stained seedlings (Section 2.7.1) and for estradiol optimization (Section 2.5.1).

2.6.2. Confocal microscopy

Zeiss LSM 880 confocal microscope was used for FRAP experiments (Section 2.6.3), and for nuclei and aggregate quantification (Section 2.6.4).

Olympus FV1000 was used for one replica of aggregate quantification and for imaging of transgenic *A. thaliana* lines.

2.6.3. Fluorescence recovery after photobleaching

FRAP is a method in microscopy used to study the dynamics of proteins tagged with fluorescence in living cells. To perform a FRAP experiment, an area with the fluorescent signal is bleached using a high intensity laser (Fig 2.6 A). This bleaching is permanent – meaning the proteins that have been bleached will not recover their fluorescence. The recovery of fluorescence in the bleached area will therefore depend on the movement of the other tagged proteins (Axelrod et al., 1976).

The fluorescence intensity is measured before, during, and after the bleaching to provide the data necessary to calculate the mobile fraction (Mf) and immobile fraction. Whether the proteins are bound to a binding partner or not will influence the speed of the diffusion – a bound protein will typically move less than one that is free. The movement is also affected by the proteins properties such as charge, where a positively charged protein moves faster than a negatively charged protein (Xu et al., 2013). To get a standardized result, it is important to bleach an area of the same size each time in the different structures. Additionally, measurements of background signal is important to account for natural fluctuations in background signal. From these data, a fluorescence recovery curve can be made (Fig 2.6 B)

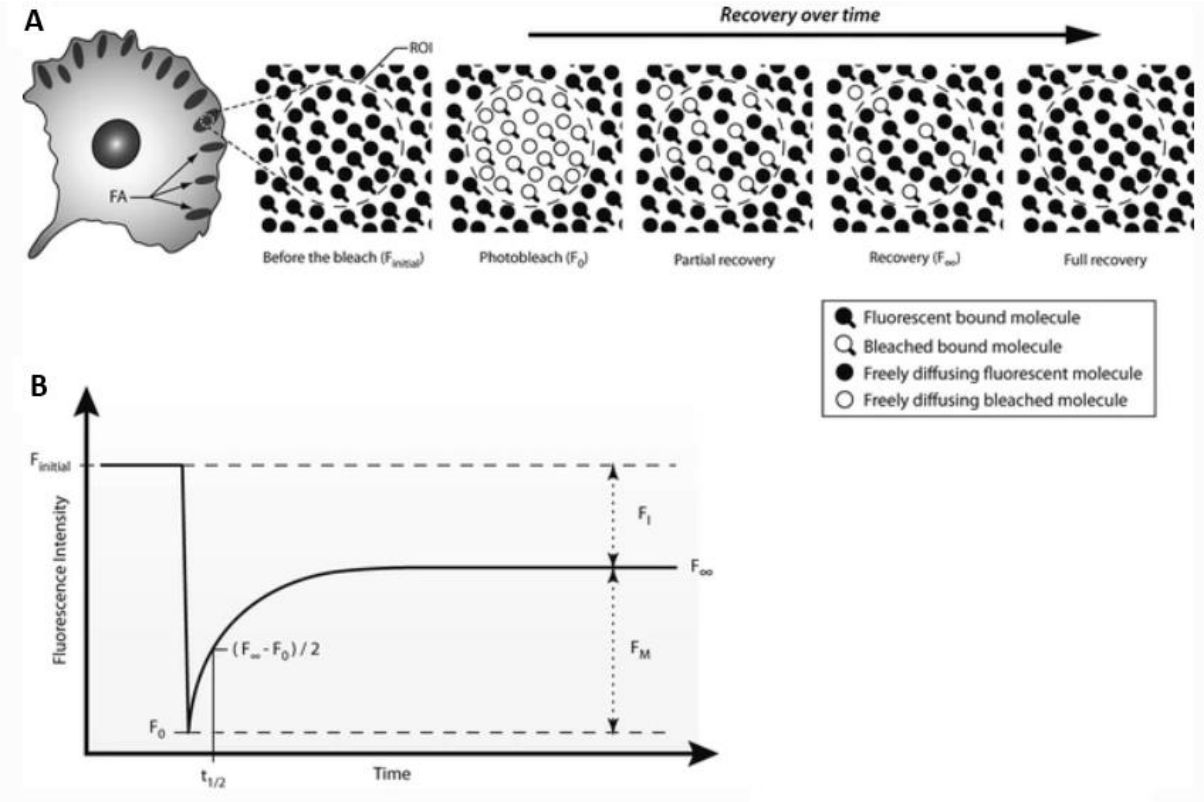

Figure 2.6 Fluorescence recovery after photobleaching (FRAP). A) Illustration of how FRAP is performed. An area with fluorescently tagged proteins is bleached, and the recovery of fluorescence is measured B) Fluorescence recovery curve showing $F_{initial}$ as the highest fluorescence before bleach F_0 as the lowest fluorescence intensity after bleach, F_∞ is the highest recovery, F_I is immobile fraction, F_M is mobile fraction. FRAP = fluorescence recovery after photobleaching. Figure from Carisey et al., 2011

2.6.3.1. Experimental setup for FRAP

Three regions of interest (ROI) were measured; ROI 1 measures the bleached area inside the nucleus, ROI2 measures the whole nucleus, and ROI3 measures a dark area outside of the nucleus. The sizes of the areas were 20 µm x 20 µm and this was used for all the experiments.

The following FRAP settings were used on Zeiss LSM880; bleaching after 10 scans, repeat bleach after 1 scan, 5 iterations, stop when intensity drops to 30 %, use 405 nm laser at 100 % for bleach. 300 scans were taken with an interval of 100 ms.

2.6.3.2. Analysis of FRAP data

FRAP data was first corrected by subtracting the background intensity (ROI2) from bleached area (ROI1) and reference area (ROI3).

The corrected bleach (I_{bleach}) was normalized to corrected reference (I_{ref}) with the equation from Pelkmans et al., 2001, where $I_{bleach(0)}$ is the average intensity of the bleach area pre-bleach, $I_{ref(0)}$ is the average intensity of the reference area pre-bleach, $I_{bleach(t)}$ is the intensity of the bleach area at time t, and $I_{ref(t)}$ is the intensity of the bleach area at time t:

$$Ft = \frac{I_{ref(0)}}{I_{bleach(0)}} \times \frac{I_{bleach(t)}}{I_{ref(t)}}$$

The average of the normalized data was fitted in ImageJ using the exponential recovery curve fitter (Webster and Wachsmuth, 2014). F_0 and F_∞,were determined from the fitted curve. F_0 is the fluorescence intensity post-bleach, F_∞ is the highest recovery post-bleach. From this curve the Mf was calculated using the following equation from Lippincott-Schwartz et al., 2001;

$$Mobile\ fraction\ (Mf) = 1 - \frac{1 - F_\infty}{1 - F_0}$$

2.6.4. Nuclei aggregate quantification

N. benthamiana leaves on separate plants were infiltrated (Section 2.5.1) with *est.ind35S:7QLRP1-GFP* and *est.ind35S:0QLRP1-GFP* along with *dsTomat-H2B* to visualize the nucleus. dsTomat-H2B encodes a RED FLUORESCENT PROTEIN (RFP) and H2B is a core histone protein. In the nuclei where dsTomat-H2B is produced, H2B will be incorporated into histones, and the nucleus will be visualized with red fluorescence. Stack images were taken of random nuclei to quantify the number of nuclei with aggregates. Pictures were taken with 60 x oil or glycerin objective, 2 x zoom, and a picture was taken at intervals of 0.5 µm.

ImageJ was used to create a 3D image from the stack images to determine if the aggregates (if any) are inside or outside of the nucleus (as a Z-stack image cannot accurately determine this). The quantification of aggregates was decided to be “aggregates or no aggregates”.

2.7. Assays

2.7.1. β-glucuronidase assay

GUS assay was performed on *pLRP1:GUS* transformed *A. thaliana* plants to visualize where in the root *pLRP1* is expressed. This is possible because GUS hydrolyses 5-bromo-4-chloro-3-indolyl ß-d-glucuronide (x-Gluc) creating the blue pigment 5,5′-dibromo-4,4′-dichloro-indigo where the promoter is active (Jefferson et al, 1987).

T2 *pLRP1:GUS* seeds were plated on five square ½MS plates that were vernalized. Seedlings were prefixed with ice cold 90% acetone for 10 min, then de-stained with GUS solution (50 nM NaPO4, 2 mM K4FE(CN)6, 2 mM K3FE(CN)6, 0,1 % Triton X-100, pH = 7.2) without x-Gluc for 10 min. Seedlings were then covered with foil and incubated at 37 °C with GUS solution for approximately 24-48 h.

Optimalization of GUS-staining was done to see when we had the best staining, from these results we concluded that 7 day old seedlings had the optimal staining. Because of this, the age of the seedlings would be 7 days in subsequent experiments.

2.7.2. β-glucuronidase fluorometric assay

GUS fluorometric assay was used to quantify promoter activity of *pLRP1* exposed to various stress conditions. If the activity of a promoter is increased in response to a specific stress condition, more GUS will be produced allowing for quantification of promoter activity. The measurement is based on GUS cleavage of 4-Methylumbelliferyl beta-D-glucuronide (4-MUG) to create 4-MU which can be detected with a fluorimeter (Fior et al., 2009).

T2 *pLRP1:GUS* seedlings were grown vertically on ½ MS2 plates for 6 days. 5-6 seedlings were transferred to different wells in a 12-well plate with 1 mL MS2 liquid medium with 60 µM Mannitol, 50 mM NaCl, 20 µg/mL Chitin, 1 µM Flagellin, as well as an untreated control

in separate wells.Additionally, seedlings that had grown horizontally with roots growing into the agar plate were incubated with only MS2 liquid medium. The seedlings were then incubated in growth chamber (22 °C, 16 h light, 8 h dark) for 24 h, then treated with a reaction mix (1 mM 4-MUG, 0.1% Triton X-100, 50 mM NaPO4 (pH 7.0), 0.1 % SDS, 10 mM EDTA (pH 8.0), dH_2O) for approximately 24 h before transferring 100 µl of the solution to 5-6 different wells in a 96-plate well with 50 µl STOP reagent (1 M Na2CO3, dH_2O) to stop reaction. Total fluorescence was measured with Wallac 1420 VICTOR2 microplate luminometer (PerkinElmer).

Data was normalized to the mean of the untreated control.

2.7.3. Luciferase reporter assay

Luciferase reporter assay can be used to measure the activity of a promoter either by activation by a specific transcription factor or by environmental factors. It is based on the ability of the luciferase enzyme to oxidize luciferin which leads to the emission of light (Reviewed in Navizet et al., 2011).

This method was used to measure the activation of *pYUC4* by 7QLRP1 and 0QLRP1 in *N. benthamiana* leaves. *pYUC4* was cloned into a vector containing the luciferase gene (Section 2.1.5). The method of infiltration is explained in Section 2.5.1.

On the same plant, one leaf was infiltrated with *est.ind35S:7QLRP1-GFP* and *pYUC4:luc* and another leaf was infiltrated with *est.ind35S:0QLRP1-GFP* and *pYUC4:luc* (Fig. 2.7). Another plant was infiltrated with *est.ind35S:7QLRP1-GFP*, *est.ind35S:0QLRP1-GFP*, and *pYUC4:luc* with an unrelated promoter, on separate leaves as controls. Initially, *pYUC4:Luc* without a promoter was used as a control, however the luminescence was much higher than it should have been, so we had to have a control using an unrelated gene together with the promoter and therefore have no control for replica 1

The leaves were sprayed with estradiol approximately 16 h prior to the experiment to induce expression of the *est.ind35S:LRP1-GFP* constructs.. Pieces of equal size were cut and floated in water for 2 h, then transferred to a 96-well plate with 200 µl luciferin solution (H_2O, 35.67 µM luciferin) for approximately 10 min before measuring the bioluminescence with Wallac 1420 VICTOR2 microplate luminometer (PerkinElmer).

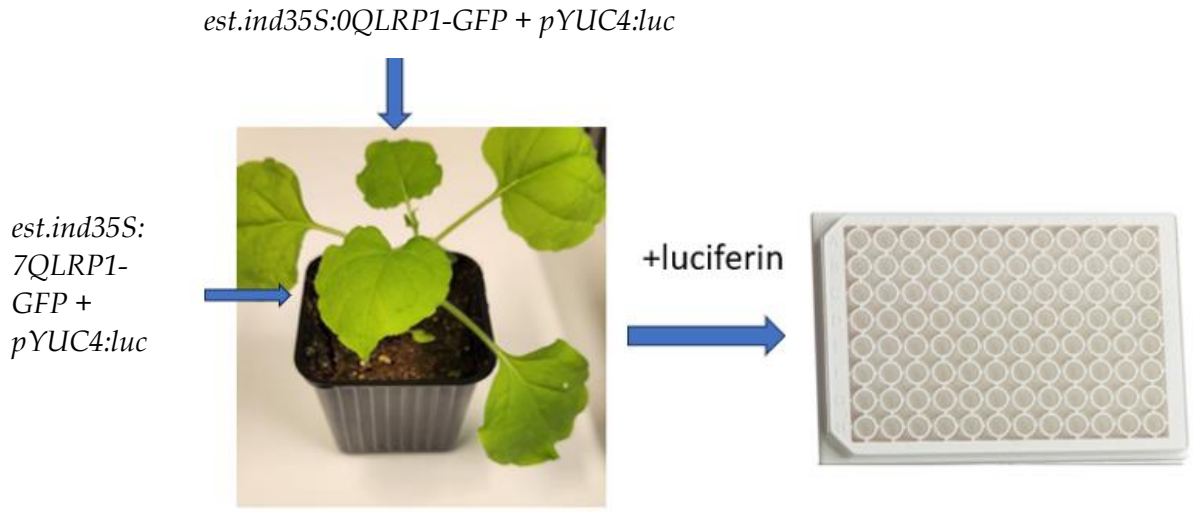

Figure 2.7: Experimental setup for Luciferase assay. *est.ind35S:7QLRP1-GFP + pYUC4:luc* were infiltrated with a syringe into one leaf of a plant, and *est.ind35S:0QLRP1-GFP + pYUC:luc* was infiltrated on another leaf on the same plant. The leaves were treated with estradiol approximately 16 hours prior to the experiment. 6 equally sized pieces were added to separate wells in a 96-well plate together with luciferin solution. The same setup was used for controls.

2.8. Statistical analyses

To determine statistical significance between two mean values, One-Way ANOVA was used. The analysis was performed using OriginLabs. Significance level was set to $P \leq 0.05$.

3. Results

3.1. Investigating the role of the LRP1 polyQ tract

3.1.1. Subcellular localization of LRP1 with different Glutamine homopolymer repeats

3.1.1.1. The presence of introns in LRP1 does not affect subcellular localization of the LRP1 protein

The presence of introns has been shown to affect protein localization. This has been shown with the human Estrogen-related receptor beta gene where alternative splicing could produce three different mRNAs where two of them had nuclear localization, and the third mostly had expression in the cytoplasm (Zhou et al., 2006). Therefore, before investigating the potential importance of the Q repeat for subcellular localization of LRP1, we wanted to explore if the intron in *LRP1* affected protein localization of LRP1 since there are four reported splice variants of *LRP1* (Yates et al., 2022).

We created expression clones by cloning the genomic region of *LRP1* and the cDNA of *LRP1* from Col-0 that contains an STR encoding a homopolymer of 7 Q into an estradiol inducible vector with a 35S promoter and a C-terminal GFP tag (est.ind*35S:7QgLRP1-GFP* and *est.ind35S:7QLRP1-GFP*, respectively) (section 2.1.6, Table 2.4). The proteins encoded by the vectors were transiently expressed in *N. benthamiana* leaves (Section 2.5.2).

All leaf tissue showed GFP localizing to the nucleus independent of the vector expressed (Fig. 3.1 A, B), indicating that the introns in *est.ind35S:7QgLRP1-GFP* did not affect the localization of LRP1 in the cell. We therefore continued our experiments with the *est.ind35S:7QLRP1-GFP*. To investigate the effect of the Q-repeat on protein localization, we made an additional construct where the Q-repeat was removed (*est.ind35S:0QLRP1-GFP*) and used this construct to compare subcellular localization to *est.ind35S:7QLRP1-GFP*.

3.1.1.2. 7QLRP1 and 0QLRP1 localize primarily in the nucleus

In a study on the *Populus trichocarpa* ANGUSTIFOLIA (PtAN1) protein, it was demonstrated that the length of the Q-repeat affected subcellular localization, with PtAN1 containing 11Q primarily present in the nucleus, 13Q in both nucleus and cytosol, and 15Q solely in cytosol (Bryan et al., 2018). We therefore wanted to investigate if the Q-repeat in LRP1 was important for its subcellular localization by transiently expressing *est.ind35S:7QLRP1-GFP* and *est.ind35S:0QLRP1-GFP* in *N. benthamiana* to compare the cellular localization of the proteins.

We saw that both proteins primarily localized to the nucleus irrespective of the length of the Q-repeat (Fig. 3.1 A), as well as what appeared to be protein aggregates in the cytosol (Fig. 3.1 B). We also observed nuclear aggregate formation and sought to explore if there was a correlation between the Q-repeat in the LRP1 protein and the formation of nuclear aggregates. To investigate this we quantified the level of aggregate formation.

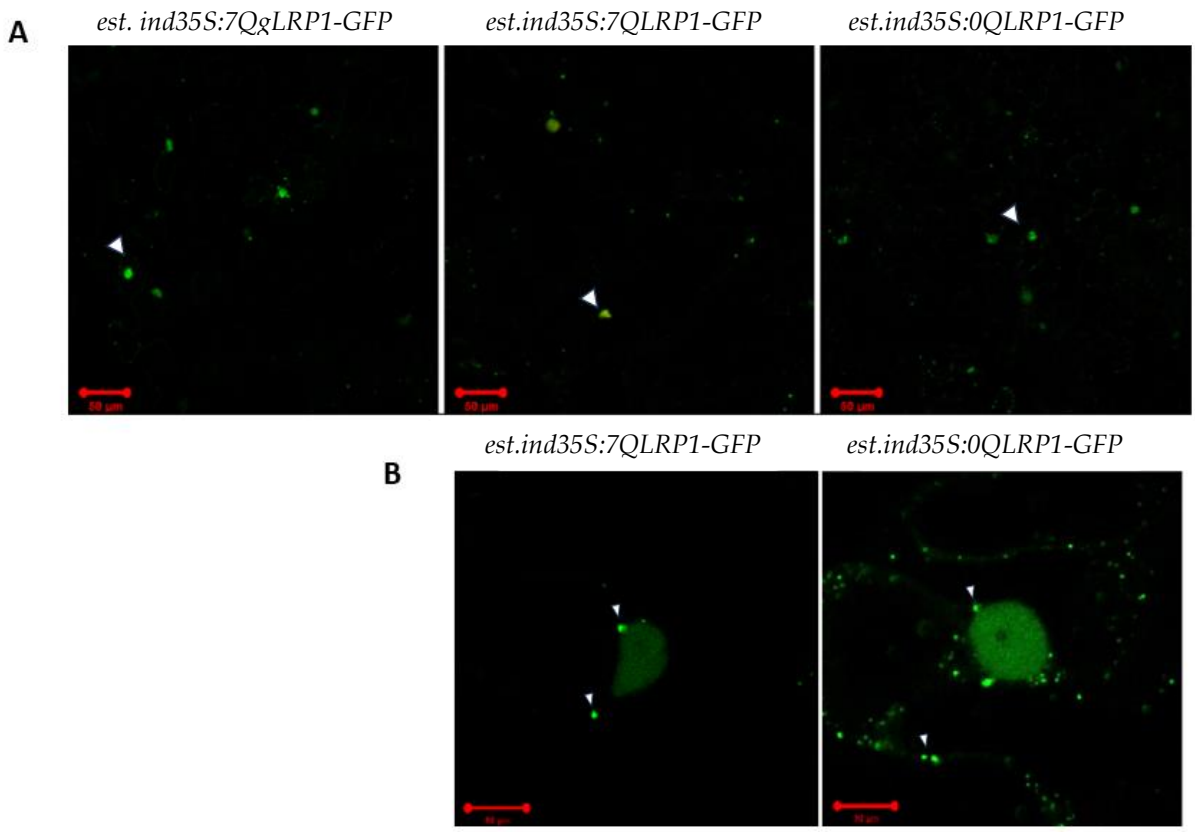

Figure 3.1 Localization of 7QgLRP1-GFP, 7QLRP1-GFP and 0QLRP-GFP1 transiently expressed in *N. benthamiana* leaves. A) 7QgLRP1-GFP, 7QLRP1-GFP, and 0QLRP1-GFP have nuclear localization. Arrowheads point to a nucleus. Expression was induced with 5µM estradiol 16h prior to imaging. Scale bar = 50µm B) Aggregates of both 7QLRP1-GFP and 0QLRP1-GFP were seen in the cytosol, arrowheads point to aggregates. Scale bar = 10µm. A-B) Pictures taken with Zeiss LSM880 AiryScan confocal microscope. A) Pictures taken with 20x objective B) Pictures taken with 60 x Oil objective.

3.2. 7QLRP1 and 0QLRP1 have a propensity to form nuclear aggregates when overexpressed

Q-repeats have been linked to the formation of protein aggregates (Satyal et al., 2000; reviewed in Todd and Lim 2013). This has been demonstrated in ELF3 where the formation of aggregates (speckles) were correlated with repeat length where a longer Q-repeat showed a slight increase in aggregate formation, and 0Q ELF3 had much lower formation. (Jung et al., 2020). Formation

of aggregates can also occur when proteins are targeted for degradation due to over- or mis-expression or when misfolded (Fu et al., 2021).

We therefore wanted to investigate if there was a difference in the occurrence of aggregate formation in 7QLRP1-GFP compared to 0QLRP1-GFP by quantifying the number of nuclei where aggregates were formed on the inside, not counting the nuclei with aggregates appearing on the outside. To do this, *est.ind35S:7QLRP1-GFP* and *est.ind35S:0QLRP1-GFP* were transiently expressed in *N. benthamiana* leaves. These were co-expressed with *35S:H2B-Tomat*, a construct encoding the histone protein H2B coupled with Tomato, a RFP, enabling visualization of the nuclei. Stack images were taken of the nuclei with a 0.5 µm interval and z-stack images with maximum projection were created using ImageJ. Due to difficulties in determining the presence of nuclear aggregates solely from stack images due to the presence of aggregates outside of the nucleus (Fig 3.2) we created 3D projections from the stack images to be better able to quantify the nuclei (movie 1, movie 2, movie 3).

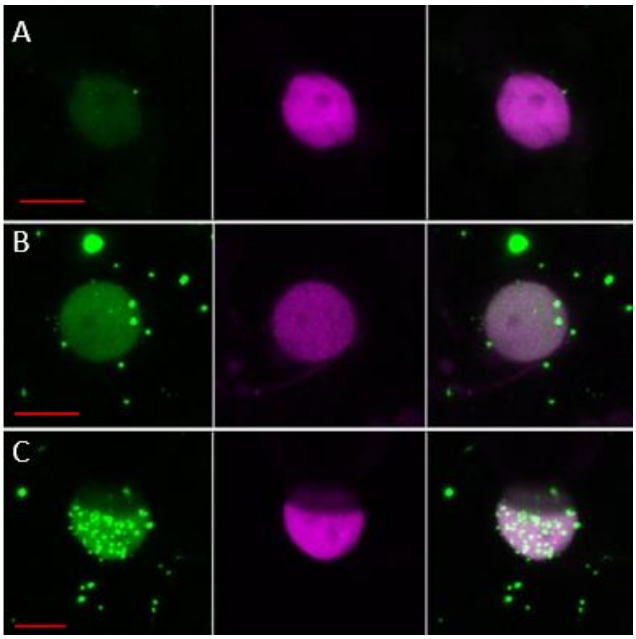

Figure 3.2 Example of nuclei co-expressed with est.*ind35S:7QLRP1-GFP* and *35S:H2B-Tomat* showing A) no aggregates, B) nucleus where aggregates appear to be in the nucleus but are actually located on the outside of the nucleus, and C) nucleus with aggregates on the inside. Left to right: GFP channel, RFP channel, merged. Scale bar = 10µm. Pictures taken with Zeiss LSM880 AiryScan Confocal Microscope, 60 x Oil objective.

When comparing the proteins, both had some nuclei with and some without aggregate formation (Fig. 3.3 A), however we observed an overall trend of protein aggregates forming in the nuclei for both 7QLRP1-GFP and 0QLRP1-GFP. Interestingly in one of the replicas there was almost no protein aggregate formation in the nuclei for 0QLRP1-GFP (Fig. 3.3 B) indicating that the Q-repeat could influence aggregate formation and thus affect the

functionality of the LRP1 protein, such as its ability to move within the nucleus and be accessible to binding partners and DNA binding.

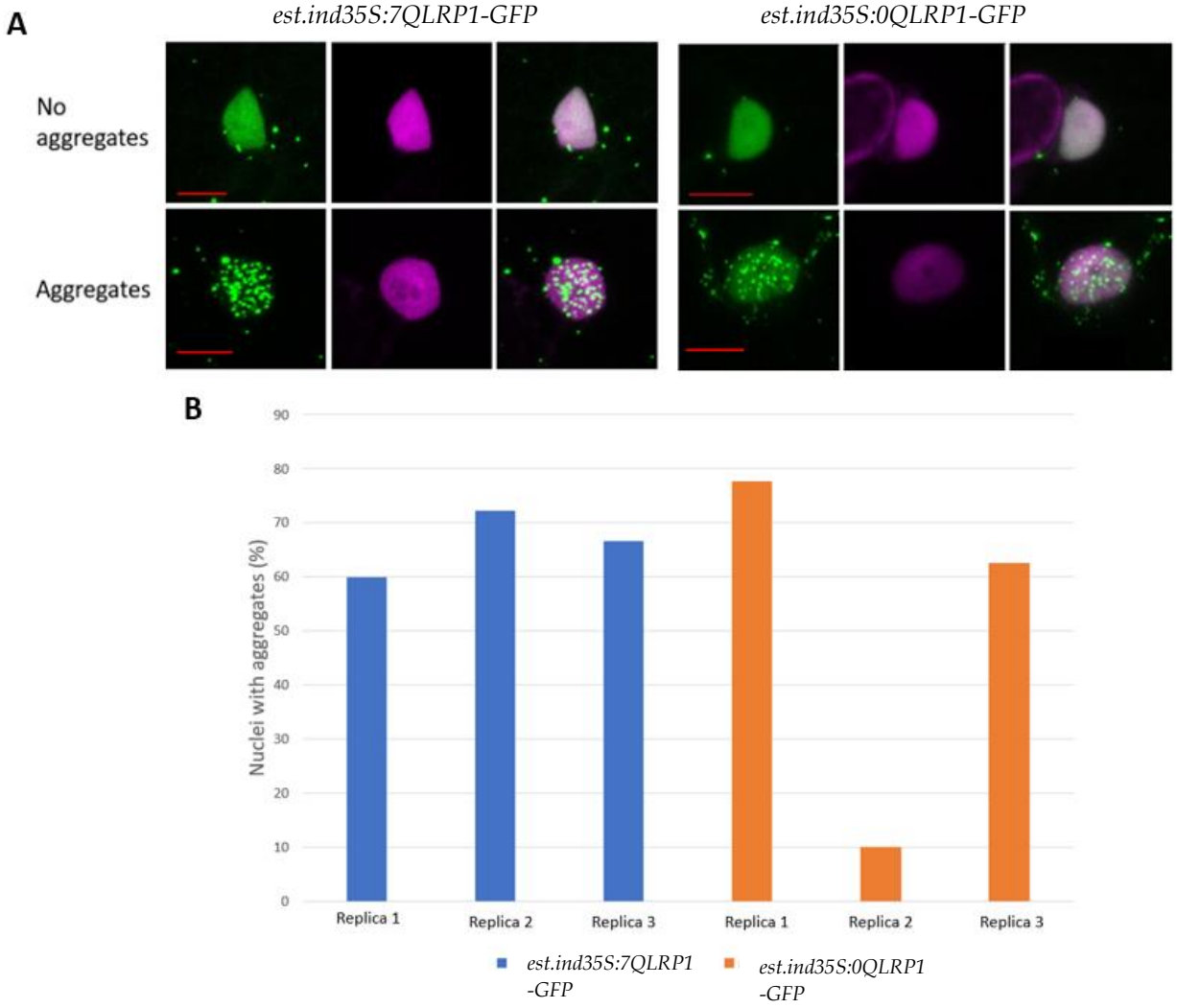

Figure 3.3 Aggregate formation in *N. benthamiana* leaves expressing 7QLRP1-GFP and 0QLRP1-GFP. A) Representative pictures of nuclei without and with aggregates for 7QLRP1-GFP and 0QLRP1-GFP. Pictures taken with the Zeiss LSM880 AiryScan Confocal Microscope, 60 x Oil objective. Scalebar = 10 µm. B) Quantification of aggregate formation in leaves expressing 7QLRP1-GFP and 0QLRP1-GFP. The graph shows three biological replicas for each of the constructs indicated. Data is presented in percentage of nuclei with aggregates. n = 10, 11, 6, 9, 10, 8 from left to right.

3.3. FRAP indicates a slight difference in fluorescence recovery and recovery speed between 7QLRP1 and 0QLRP1

The mobility of proteins in the nucleus is thought to be dependent on free diffusion, and the level of mobility can be affected by interactions with other proteins, chromatin or DNA (Phair and Misteli, 2000). These interactions however are usually transient, and for a TF it is important for interactions to DNA to be short lasting to allow for rapid changes in transcriptional activity (Phair et al., 2004; Reviewed in Swift and Coruzzi, 2017). Protein diffusion rates are also dependent on protein charge. Positively charged proteins typically move faster than negatively charged proteins, this factor is also dependent on size as positively charged proteins typically are smaller (Xu et al., 2013). The diffusion speed, size, and folding of a protein affects interactions with interaction partners, and changes in amino acid sequences can influence protein folding (Reviewed in Valastyan and Lindquist, 2014). It is therefore possible that the difference in Q repeat length in LRP1 affects its mobility and we thus investigated if 7QLRP1 and 0QLRP1 would show differences in mobility in the cell. Again, we transiently expressed *est.ind35S:7QLRP1-GFP* and *est.ind35S:0QLRP1-GFP* in *N. benhamiana* leaves and performed FRAP. Three ROIs were chosen, the first ROI is the bleach area, the second measures the background signal, while the third ROI measured the entire nucleus. The fluorescence intensity was measured in all ROIs before, during, and after bleach (Section 2.6.3). From these data we calculated Mf which is the amount of mobile protein (section 2.6.3.2)

Since LRP1 is a TF we only performed FRAP in the nucleus. We first tried to perform FRAP measurements on nuclei with uniform distribution of the TF (S. Fig 4), However, it proved challenging due to the rapid diffusion of unbleached LRP1-GFP into the bleaching area before we could reach the desired bleaching intensity. This experiment led to bleaching of the whole nucleus without the possibility to measure the recovery fluorescence (S. Fig. 4).

Due to most of the nuclei forming aggregates (Fig. 3.3), and the challenge with FRAP on nuclei without aggregates, we decided to attempt FRAP on nuclei with aggregates as the proteins in

the aggregates could have different mobilities (Fig. 3.4 A). Difference in mobility in protein aggregates with different Q-repeat lengths was shown in a study on Atrophin-1 (ATN1), a human protein involved in dentatorubropallidoluysian atrophy where the aggregates of the 19Q ATN1 had faster recovery than 71Q ATN1 which formed aggregates with variable mobility, ranging from low mobility to higher mobility (Hinz et al., 2012).

When comparing the FRAP measurements in the nuclear aggregates of 7QLRP1-GFP and 0QLRP1-GFP, we saw that there was overall very little recovery of fluorescence for both constructs. In the first replica there was a very similar recovery for both proteins and the Mf was very similar (S. Fig. 5). In the second replica however, there seemed to be a slight difference in Mf for 7QLRP1-GFP and 0QLRP1-GFP with 7QLRP1-GFP having a much higher Mf than 0QLRP1-GFP (Fig. 3.4 B, C), the results therefore show that there is more mobile protein in 7QLRP1-GFP compared to 0QLRP1-GFP in replica 2.

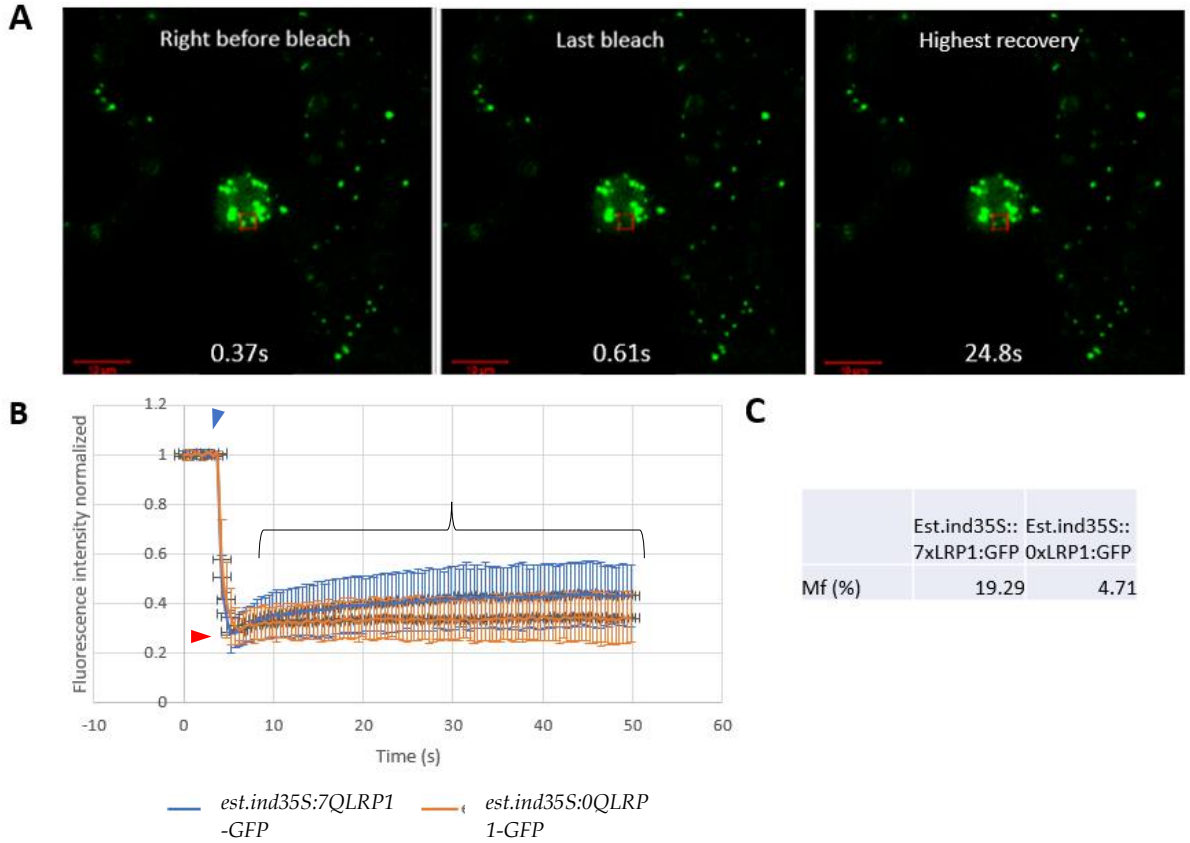

Figure 3.4 Fluorescence recovery after photobleaching (FRAP) replica 2. A) Representative image of a FRAP experiment performed on a nucleus with aggregates from *est.ind35S:0QLRP1-GFP*. Red square represents the region of interest (ROI) that was bleached, containing two aggregates. ROI

measuring background and entire nucleus is not shown. Right before bleach is when the fluorescence intensity is highest, last bleach has the lowest fluorescence intensity, highest recovery is where the fluorescence intensity was no longer increasing post bleach and we see a slight increase in fluorescence compared to the fluorescence at the last bleach Pictures taken with the Zeiss LSM880 AiryScan Confocal Microscope, 60 x glycerol objective. Scale bar = 50µm B) Graph showing the average of replica 2 of FRAP experiment on *est.ind35S:7QLRP1-GFP* (blue) and *est.ind35S:0QLRP1-GFP* (orange). Highest point is pre-bleach (blue arrowhead), lowest point is after bleach (red arrowhead), the recovery of fluorescence (black brace) occurs following the lowest point. The graph shows higher fluorescence recovery for 7QLRP1-GFP than for 0QLRP1-GFP indicating a higher Mobile fraction (Mf) for 7QLRP1-GFP. n = 5, error bars = ±SD. C) Mf of 7QLRP1-GFP and 0QLRP1-GFP in replica 2, Mf is a measurement of the amount of protein that is mobile in the nucleus.

3.4. 7QLRP1 and 0QLRP1 have similar activation of *pYUC4*

Both protein mobility and localization may influence the function of a TF. Since LRP1 has been shown to increase levels of YUC4 (Singh et al., 2020), and we noticed indications of differences between 7QLRP1-GFP and 0QLRP1-GFP in terms of protein mobility and nuclear aggregate formation, we wanted to test if the two LRP1 repeat variants differed in activation of *pYUC4* by performing luciferase assays in *N. benthamiana* leaves transiently expressing *est.ind35S:7QLRP1-GFP* or *est.ind35S:0QLRP1-GFP* and *pYUC:Luc* (Section 2.7.3).

The results show that both 7QLRP1-GFP and 0QLRP1-GFP activate *pYUC4* at similar levels, and the activation indicated by luciferase activity is similar between replicas for replica 2 and 3 (Fig. 3.5). However, in one of the replicas we saw lower activation of *pYUC4* in 0QLRP1-GFP than in 7QLRP1-GFP infiltrated leaves (Fig. 3.5) that was statistically significant (P = 0.03701), indicating that the Q-repeat may influence the ability of LRP1 to activate *pYUC4*.

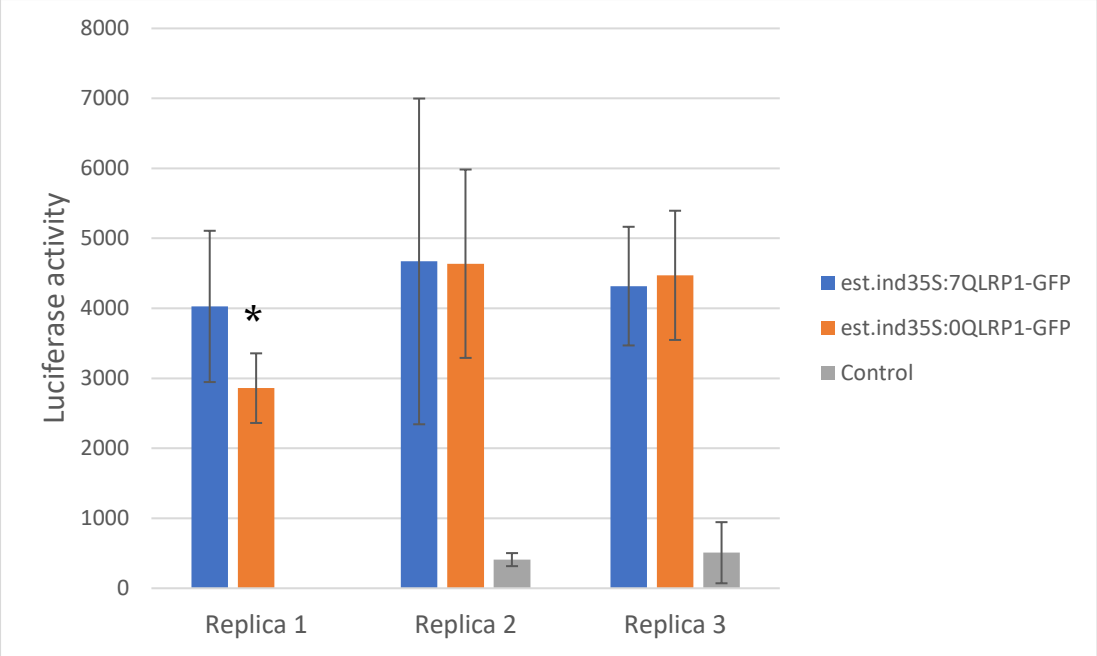

Figure 3.5 *pYUCCA4* (*pYUC4*) activation by 7QLRP1-GFP and 0QLRP1-GFP. Replica 1 showns lower luciferase activity of 0QLRP1-GFP compared to 7QLRP1-GFP. Asterix (*) indicates statistical significance ($P \leq 0.05$). Replica 2 and 3 show that 7QLRP1-GFP and 0QLRP1-GFP have similar activation of *pYUC4* as seen by the luciferase activity. n=6 for all replicas. Error bars = ±SD. No control was included for replica 1 as explained in Section 2.7.3

3.5. Investigating LRP1 using transgenic *A. thaliana* lines

From the experiments in *N. benthamiana,* no significant differences between the two LRP1 variants was observed when considering all experimental replicas. However, the results indicate that 0QLRP1 has a lower tendency to form protein aggregates, shows a lower Mf, and induces a lower transcriptional regulation of *pYUC4* compared to 7QLRP1. We therefore wanted to explore if the LRP1 protein variants would affect the phenotype of *A. thaliana* transgenic lines stably expressing 7QLRP1 and 0QLRP1. Additionally, we were interested in elucidating the spatiotemporal expression of *LRP1* in *A. thaliana* as well as identifying potential mutant phenotypes in *lrp1* KO to gain further insight into LRP1's involvement in root development.

3.5.1. Localization of *LRP1* expression

3.5.1.1. GUS histochemical assay indicates *LRP1* expression at the base of emerged LRs and in developed LRs

Previous work indicated strong *LRP1* expression in all stages of LRPs, and in the root meristem (Singh et al., 2020), however another study showed weak staining in the early stages of LRPs and strong staining in emerged LRs (Smith and Fedoroff, 1995). Due to these minor discrepancies, we aimed to provide additional information about the spatiotemporal expression of *LRP1* in *A. thaliana* by creating *pLRP1:GUS* transgenic lines expressing GUS under the control of *pLRP1*.

pLRP1:GUS seedlings treated with x-Gluc (Section 2.7.1) showed that expression was absent from most of the stages of LRP formation, although there was indication of staining in the vasculature at stages III, IV, and V (Fig. 3.6 A-F). There was clear staining at the base of the emerged LR (Fig 3.6 G), and from the base of the more developed LR to the middle of the LR in the vascular tissue (Fig 3.6 H). This indicates that LRP1 could be involved in the emergence and elongation of LRs.

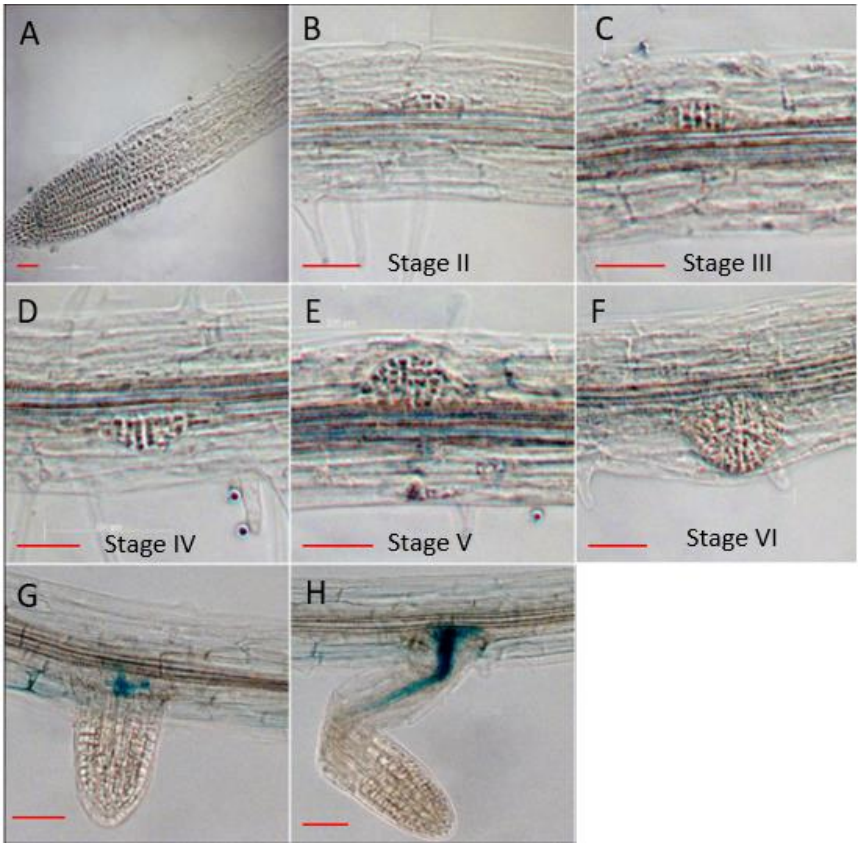

Figure 3.6 GUS staining of 7 day old *pLRP1:GUS* seedlings. A) Root tip, B) C) D) E) F) showing the approximate stage of lateral root primordia (LRP) as indicated in the picture with low GUS activity as indicated by the blue color. The LRP stages represent the number of cell layers with Stage II, III, IV, V and VI having two, three, four, five, and six cell layers respectively. G) Emerged LR with GUS activity at the base, H) More developed LR with GUS activity from the base to approximately the middle of the LR. Pictures taken with Zeiss Axioplan, A) 10x objective, B-H) 20x objective. Representative images of n = 3. Scale bar = ~50µm

3.5.1.2. *LRP1* expression is upregulated in response to stress

While performing GUS histochemical assays we observed a difference in staining of *pLRP1:GUS* roots that had grown into an agar plate compared to roots that had grown vertically on a plate (S. Fig. 6) Roots are constantly exposed to abiotic and biotic stresses such as drought, soil salinity, bacteria, fungi, and the mechanical damage from growing in soil (Reviewed in Potocka and Szymanowska-Pułka, 2018; Reviewed in Iqbal et al, 2021). The ability of the root system to adapt in response to these factors is important for growth in favorable conditions, i.e root growth away from high salinity (Galvan-Ampudia et al., 2013). Roots growing through

dialysis membrane covered agar plates, which was supposed to mimic mechanical stress, had shorter roots than vertically grown roots, and GUS staining showed a slight increase and altered expression of auxin (Okamoto et al., 2008).

We therefore wanted to test if the promoter of *LRP1* is activated by stress by exposing the root to different stress conditions and performing a GUS fluorometric assay. Seedlings were grown vertically for 6 days before exposed for 24 h to either mannitol, NaCl, chitin, or flagellin, Mannitol induces osmotic stress which simulates drought, NaCl induces osmotic stress and ionic stress (Reviewed in Versules et al., 2006). Chitin which is the major component of the fungal cell wall and flagellin which is a component of bacterial flagella triggers an immune response (Gust et al., 2007). In addition, we included seedlings that had grown horizontally into the agar plate simulating mechanical stress, as well as an untreated control. We performed a quantitative fluorometric GUS assay to analyze *pLRP1* expression in the stress treated plants (Section 2.7.2).

We performed two replicas, in the first replica we saw that there overall seems to be a higher activity of *pLRP1* in the stress treated seedlings (S. Fig. 7), however it was not found to be statistically significant with ANOVA. In replica 2 (Fig. 3.7), we saw a very significant upregulation of *pLRP1* activity in the seedlings that had grown downward into agar plates, $P=5.02212x10^{-8}$ compared to the control. The other stress treated seedlings were not statistically different compared to the control using ANOVA, however we do see indications of upregulation of *pLRP1:GUS* in response to Mannitol, Chitin, and Flagellin. Thus our results indicate that *LRP1* is transcriptionally upregulated in response to various stresses, particularly mechanical stress, indicating a possible role of LRP1 in stress responses *in planta*.

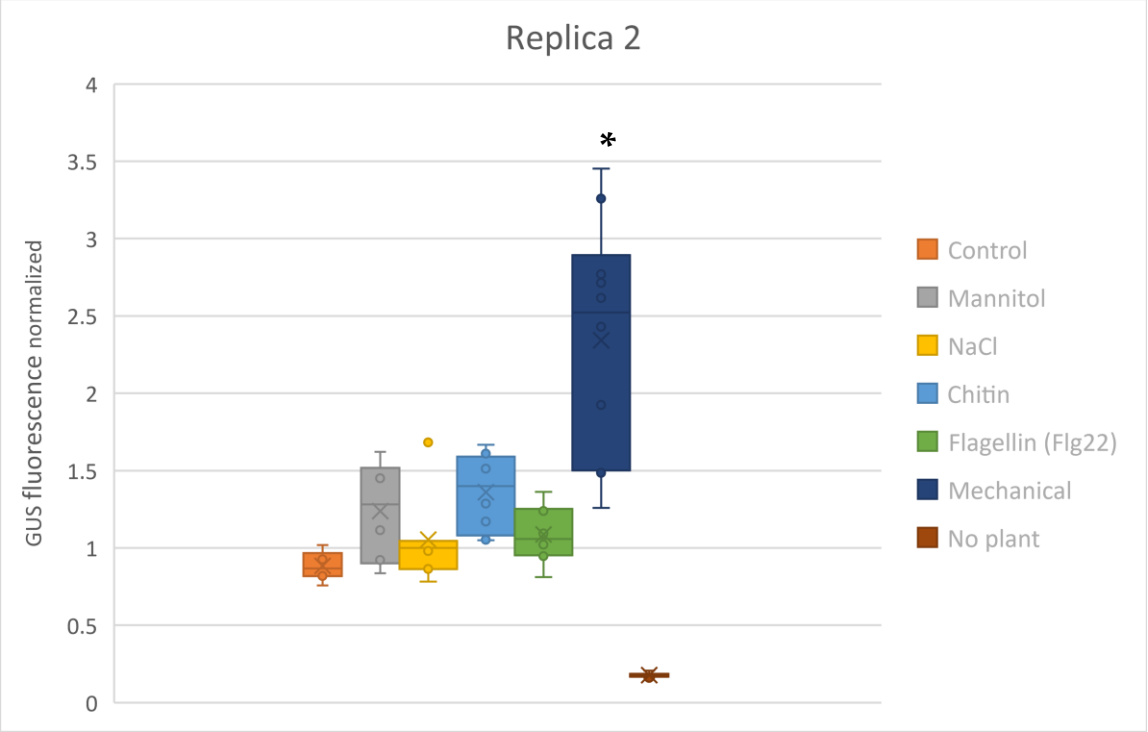

Figure 3.7 Stress test of *pLRP1:GUS* seedlings with Fluorometric GUS Assay. Mechanical stress show a significant upregulation of *pLRP1* activity, while mannitol, Chitin and Flagellin has indications of some upregulation of *pLRP1:GUS*. Asterix (*) indicates statistically significant difference. One-way ANOVA was used for statistics shown in figure, with a significance level of $P \leq 0.05$. n = 7, 6, 7, 8, 10, 10, 10. Mechanical represents seedlings that have grown down into agar plate.

3.5.1.3. *pLRP1:H2B-Venus* shows cell-specific *pLRP1* activity

pLRP1:GUS transgenic *A. thaliana* lines showed GUS activity primarily at the base of emerged LRs, and very little staining at the various stages of LRPs. This was different from what has been previously reported by Singh et al. where they observed staining at all stages of LRP development, however it was concurrent with the findings by Smith and Fedoroff. Additionally, a hybridized RNA probe indicating *LRP1* expression only showed expression in early stages of LRPs (Smith and Fedoroff, 1995). To gain a more detailed view of the spatial-temporal expression of *LRP1*, we created a transgenic *A. thaliana* line (Section 2.3.2) expressing the transcriptional reporter *pLRP1:H2B-Venus* which contains the yellow fluorescent protein (YFP) Venus, coupled to a H2B protein driven by *pLRP1*. H2B is one of the four core histone proteins that together with DNA make up the nucleosomes. When fused to a fluorescent protein, such

as Venus, it allows for visualization of their localization which should be in the nuclei (Howe et al., 2012). When put under the control of a specific promoter, the H2B fusion protein will only be produced in the cells where the promoter is active (Maruyama et al., 2001), and due to the stability of H2B it allows for detection of the reporter even in cells where the promoter is weakly expressed.

Since the GUS reporter line indicated that seedlings grown for 7 days had the highest expression of *LRP1*, this was the age of the seedlings we decided to look at the *pLRP1:H2B-Venus* line. We saw localization of H2B-Venus along most of the root length with higher expression at what appears to be the pericycle and some expression in the endodermis and cortex of the basal meristem and what appears to be the EZ (Fig. 3.8 A). There is also expression in nuclei in most of the cells of the emerged LR with the higher expression at the beginning of the LR. In addition, expression in nuclei was observed in most of the primary root, which cell layers the expression is in is not clear (Fig 3.8 B). There appears to be one nucleus with clear expression at a stage V LRP, but whether this is in the LRP or in the overlying tissue is not clear (Fig 3.8 C).

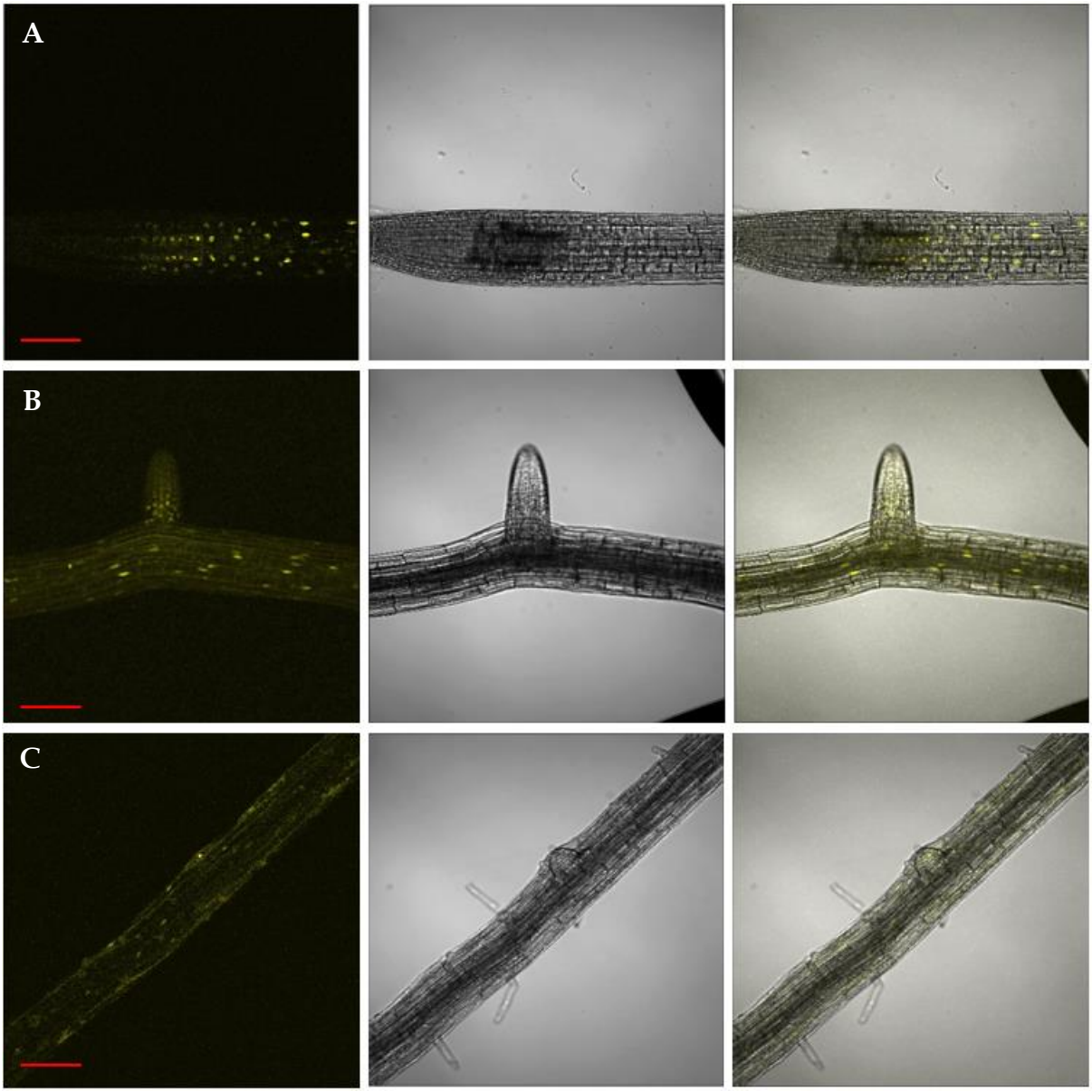

Figure 3.8 Expression of pLRP1 in roots of 7 day old seedlings. A) *pLRP1:H2B-Venus* expression in nuclei of root meristem in and elongation zone B) expression in nuclei of emerged LR, and in tissue of the PR, C) expression in nucleus either in a cell of the LR or in the overlying epidermis, as well as expression in some nuclei of the epidermis of PR. Pictures taken with Olympus FV1000, 20 x objective. Scale bar = 100 µm. Left to right: YFP channel, bright field, merge.

3.5.2. 7QLRP1-YFP and 0QLRP1-YFP in *A. thaliana*

While studying protein behavior and function in *N. benthamiana* can provide useful information, studying the phenotypic effects of differing protein functions in planta can provide insight into the importance of the protein behaviors. We therefore wanted to compare the OE phenotype of *A. thaliana* expressing the two LRP1 variants, as we had some indications that the function of 7QLRP1 and 0QLRP1 could be different.

To study the proteins in *A. thaliana* we created the stable OE lines *35S:7QLRP1-YFP* and *35S:0QLRP1-YFP* which contain YFP (Section 2.1.6).

3.5.2.1. The transgenic overexpression lines differ in leaf phenotype

While selecting for one copy lines for *35S:7QLRP1-YFP* and *35S:0QLRP1-YFP*, we noticed that two of the three 35S:*0QLRP1-YFP* one copy lines (#1 and #2) had a different leaf phenotype than the *35S:7QLRP1-YFP* one copy lines. While this could be caused by the insertion site of the genes, it is generally much less likely if it is seen for more than one line since T-DNA insertion is random (Alonso et al., 2003). *LRP1* has been shown to be expressed in *A. thaliana* leaves (Singh et al., 2020), and since the repeat could potentially affect protein function and stability and we noticed a phenotypic difference, we wanted to measure the length and diameter of the seedling leaves to compare them.

Seedlings from *35S:7QLRP1-YFP#6*, *35S:0QLRP1-YFP#1*, *35S:0QLRP1-YFP#2*, and *35S:0QLRP1-YFP#3* (hereafter *7QLRP1#6*, *0QLRP1#1*, *0QLRP1#2*, *0QLRP1#3*) were grown on selection with the appropriate antibiotic (Table 2.4), while seedlings from *Col-0* were grown without selection. When the seedlings had grown to the two-leaf stage they were scanned. We saw that Col-0, *7QLRP1#6*, and *0QLRP1#3* had similar phenotypes with rounded leaves and a visible petiole, while *0QLRP1#1* and *0QLRP1#2* had no visible petiole and the leaves were oblong (Fig. 3.9 A-E). We measured leaf length and diameter using ImageJ (Section 2.4.2), and the result showed that there was a small but significant difference in leaf length between *7QLRP1#6* and *0QLRP1#3*, ($P = 0.02183$), however they were not statistically different to the other lines (Fig. 3.9 F). The leaf diameter of both *0QLRP1#1* and *0QLRP1#2* was significantly smaller compared to the other lines ($P \leq 0.05$) (Fig. 3.9 G). It also appears that the petiole for

the *0QLRP1#1* and *0QLRP1#2* lines either is non-existent or is developing as a leaf which has not been reported in other OE lines that affect auxin levels. The leaves also appeared to be more downturned which has been reported with mutant *A. thaliana* lines where auxin levels are increased (King et al., 1995; Li et al., 2008). We therefore decided to use two different *0QLRP1* lines moving forward, *0QLRP1#1* and *0QLRP1#3* since this would help determine whether the observed phenotype could be attributed to the repeat length variation or to potential differences in expression levels *in planta*.

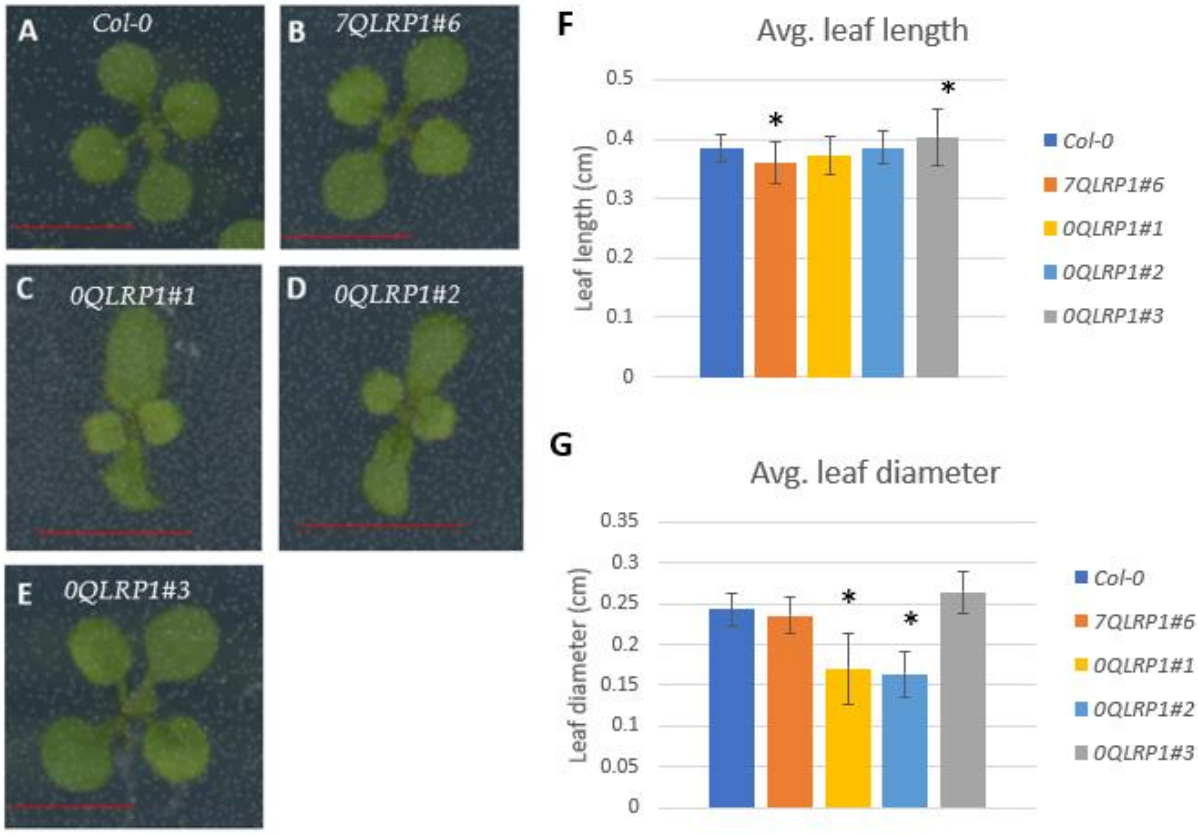

Figure 3.9 Leaf phenotype comparison. A) *Col-0*, B) *7QLRP1#6*, C) *0QLRP1#1* D) *0QLRP1#2* E) *0QLRP1#3*, A-E) Pictures were taken with Epson scanner. Scale bar = ~50 mm, F) Average leaf length, n= 12, 13, 7, 10, 13. In this instance, asterix (*) indicates that the lines are different from each other but not different to the other lines G) Average leaf diameter, n = 10, 9, 8, 6, 8. Asterix (*) indicates statistical difference. Error bars = ±SD. One-way ANOVA was used for statistics with significance level $P \leq 0.05$.

3.5.2.2. *0QLRP1#0* has shorter PR than *7QLRP1#6* and *0QLRP1#3*

Next, we aimed to investigate if *7QLRP1* OE and *0QLRP1* OE would have different effects on the root phenotype previously described in *LRP1* OE lines. A previous study showed longer PR with *LRP1* OE compared to wild-type Col-0 (Singh et al., 2020). Another study looked at the increased LRP1 levels through the null-mutation of the *LRP1* repressor SWP1 which led to increased root length (Krichevsky et al., 2009).

Since we had seen a difference in leaf phenotype for some of the *0QLRP1* lines, we decided to do the phenotyping using one with an abnormal leaf phenotype (*0QLRP1#1*) and one with a leaf phenotype similar to *Col-0* (*0QLRP1#3*). Since the seeds were of T2 generation and thus segregating, the seeds were grown on plates with selection to select against seeds that do not have resistance gene and therefore lack the transgenes. Normally we would compare the length with Col-0 roots. However, considering our primary interest is in comparing 7QLRP1 and 0QLRP1 and the potential growth impact of being grown on selection, we decided against comparing it with Col-0 roots in this experiment. Additionally, longer PR in LRP1 OE lines compared to Col-0 has already been reported (Singh et al., 2020).

The phenotyping (Section 2.4.1) was repeated 4 times. In replica 1 (Fig. 3.10 A) and 2 (Fig. 3.10 B), there was a significant difference in PR length for *0QLRP1#1* compared to *7QLRP1#6* and *0QLRP1#3*. In replica 3 (Fig. 3.10 C) there was a significant difference in PR length between *0QLRP1#1* and *7QLRP1#6* and between *0QLRP1#3* and *0QLRP1#6*. In a fourth replica where the seedlings grew for 8 days instead of 7, there was a statistically significant difference in mean PR length between all lines (S. Fig 8). This indicates that *LRP1* OE can affect PR length.

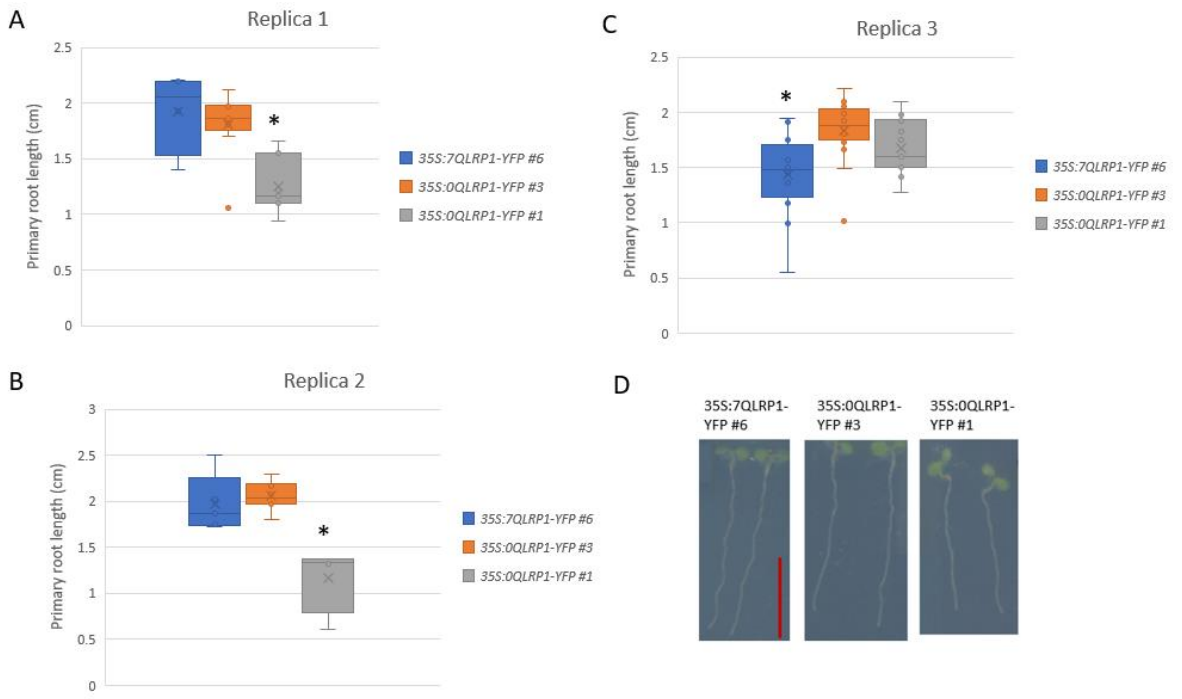

Figure 3.10 Primary root (PR) length quantification of *7QLRP1#6*, *0QLRP1#3*, and *0QLRP1#1*. A) B) We see a statistical difference in the PR length of *0QLRP1#1* compared to the other two lines for both replica 1 and 2. *7QLRP1#6* and *0QLRP1#3* have similar mean PR length for both replicas C) In replica 3, *7QLRP1#6* has a statistically significant shorter mean PR length compared to the other lines, *0QLRP1#1* has a slightly shorter mean PR length however it is not statistically significant in this replica. Asterix (*) indicates statistical significance. One-way ANOVA was used for statistics with significance level $P \leq 0.05$. B) Representative pictures of seedlings. Pictures taken with Epson scanner. Scale bar = ~1 cm. A) n = 10, 9, 7, B) n = 10, 8, 4 C) n = 24, 16, 13

3.5.2.3. *LRP1* OE phenotypes might be attributed to expression levels

Previous studies have shown that expression levels of *LRP1* affect PR length (Section 1.3). Additionally auxin levels are known to affect both PR length and leaf phenotypes. In theory, gene expressed under the control of a *35S* promoter should have the same expression levels, however the expression will also be dependent on the TDNA insertion site (Reviewed in Meyer, 2000). The *LRP1* OE lines might therefore have different expression levels of *LRP1*. We were therefore interested in looking at the apparent protein expression levels in *7QLRP1-YFP#6,*

0QLRP1-YFP#1 and *0QLRP1:YFP#3* to attempt to identify whether the differing phenotypes could be attributed to expression levels or repeat length.

The *0QLRP1-YFP#1 line* shows LRP1-YFP in nuclei near the root cap (Fig. 3.11 A), in the epidermal cells (Fig. 3.11 A, B), and expression in the cotyledon (Fig. 3.11 C). The low apparent expression in root meristem, along the root, and in cotyledons of *0QLRP1-YFP#3* (Fig 3.12) and *7QLRP1-YFP#6* (Fig 3.13) appears to solely be autofluorescence as they look similar to 8 day old Col-0 seedling (S. Fig. 9).

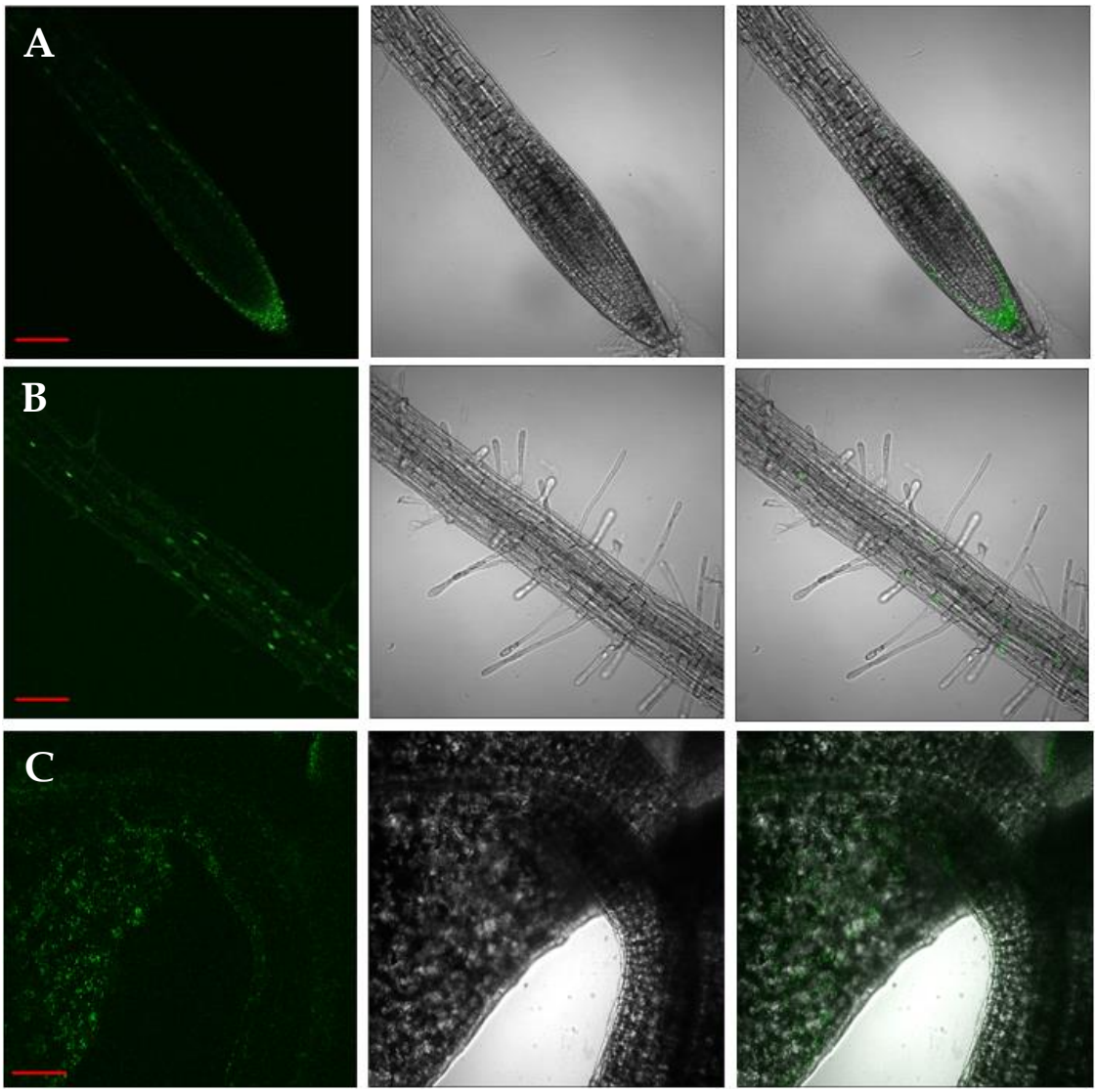

Figure 3.11 Expression of *0QLRP1-YFP#1* in 7 day old seedlings. (A) Expression is seen in nuclei at the root tip and along the epidermis, (B) in parts of the epidermis and possibly vascular tissue along the root, (C) and in leaf. Some of the expression seen in the leaf are likely the stomata. Pictures taken with Olympus FV1000, 20x objective. Scale bar = 100µm. Saturation of overlay images

adjusted. Brightness of GFP images adjusted. Left to right: GFP, brightfield, merge. Representative image of n = 3

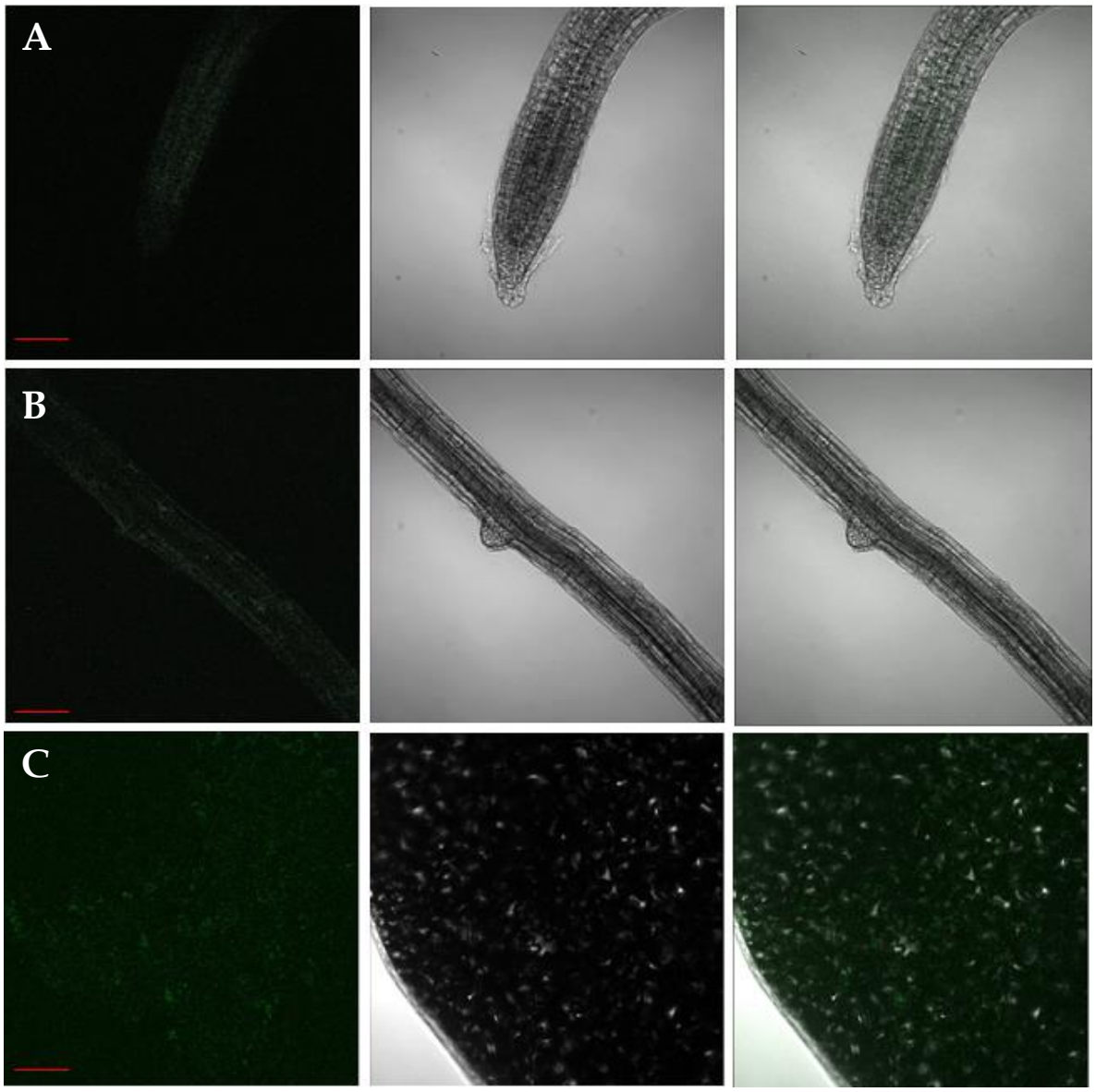

Figure 3.12 Expression of *0QLRP1-YFP#3* in 7 day old seedlings. A) Very low expression in root tip might be autofluorescence, B) at the root length it appears to be some expression in some nuclei, however expression is very low and could be autofluorescence C) GFP signal in leaf is likely the stomata. Pictures taken with Olympus FV1000, 20x objective. Scale bar = 100µm. Brightness of GFP images adjusted. Left to right: GFP, brightfield, merge. Representative image of n = 3

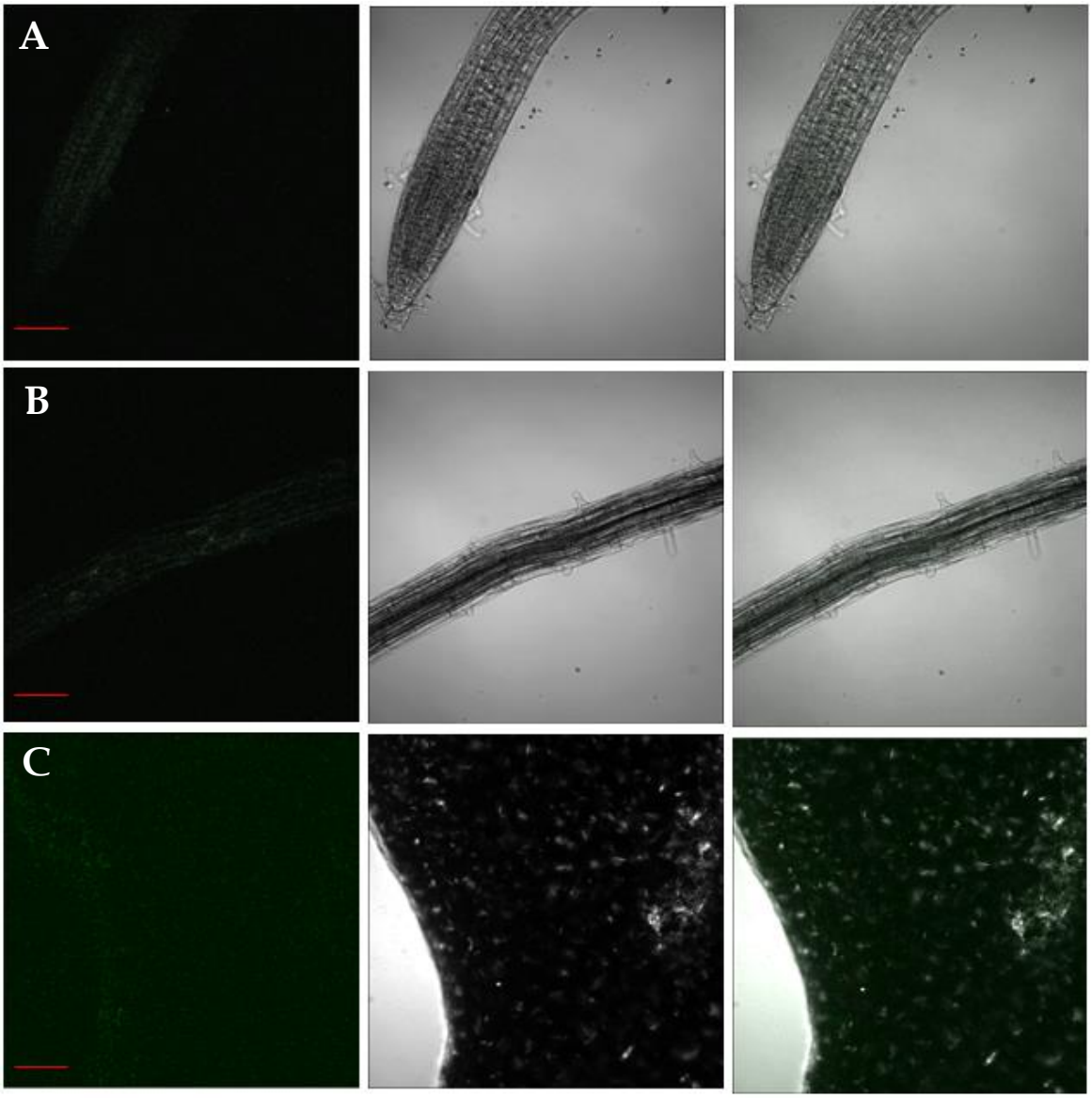

Figure 3.13 Expression of *7QLRP1-YFP* in 7 day old seedlings. A) Very low expression in root tip might be autofluorescence, B) at the root length it appears to be some expression in some nuclei, however expression is very low and could be autofluorescence C) GFP signal in leaf is likely the stomata. Pictures taken with Olympus FV1000, 20x objective. Scale bar = 100µm. Brightness of GFP images adjusted. Left to right: GFP, brightfield, merge. Representative image of n = 3

3.5.3. CRISPR/Cas9 introduced a homozygous mutation

To gain a better understanding of gene functions, the reverse genetics method gene KO can be used. KO using T-DNA is frequently used in plant biology. However, after the advent of CRISPR/Cas9, this is becoming increasingly used due to its relative simplicity and specificity (Reviewed in Zhang et al., 2020). For KO, it is important that the reading frame of the gene is disturbed which can introduce a STOP-codon resulting in a truncated protein. Since *A. thaliana* is diploid, meaning it carries two copies of its chromosomes, it is necessary to have a homozygous mutation.

A CRISPR/Cas9 vector containing either guide 11 or guide 19 directing the Cas9 to the *LRP1* gene was introduced in Col-0 plants by floral dipping (Section 2.3.2) to create a *lrp1* KO line (Section 2.1.8). For CRISPR guide 11 (CRISPR_g11) seedlings, we recovered 8 T1 transformants, and 2 T1 transformants of CRISPR guide 19 (CRISPR_g19) were recovered. They were transferred to soil, and their DNA was isolated (Section 2.1.1) and sequenced (Section 2.1.12). Sequencing results showed that one CRISPR_g19 plant had an extra thymidine in exon 3 of *LRP1*, leading to a STOP codon at amino acid 332 (Fig. 3.14 A) and chromatography results showed that the plant was homozygous for this mutation (Fig. 3.14 B). This is a frameshift mutation that will lead to a truncated protein where the dimerization domain is missing which should affect the functionality of the protein.

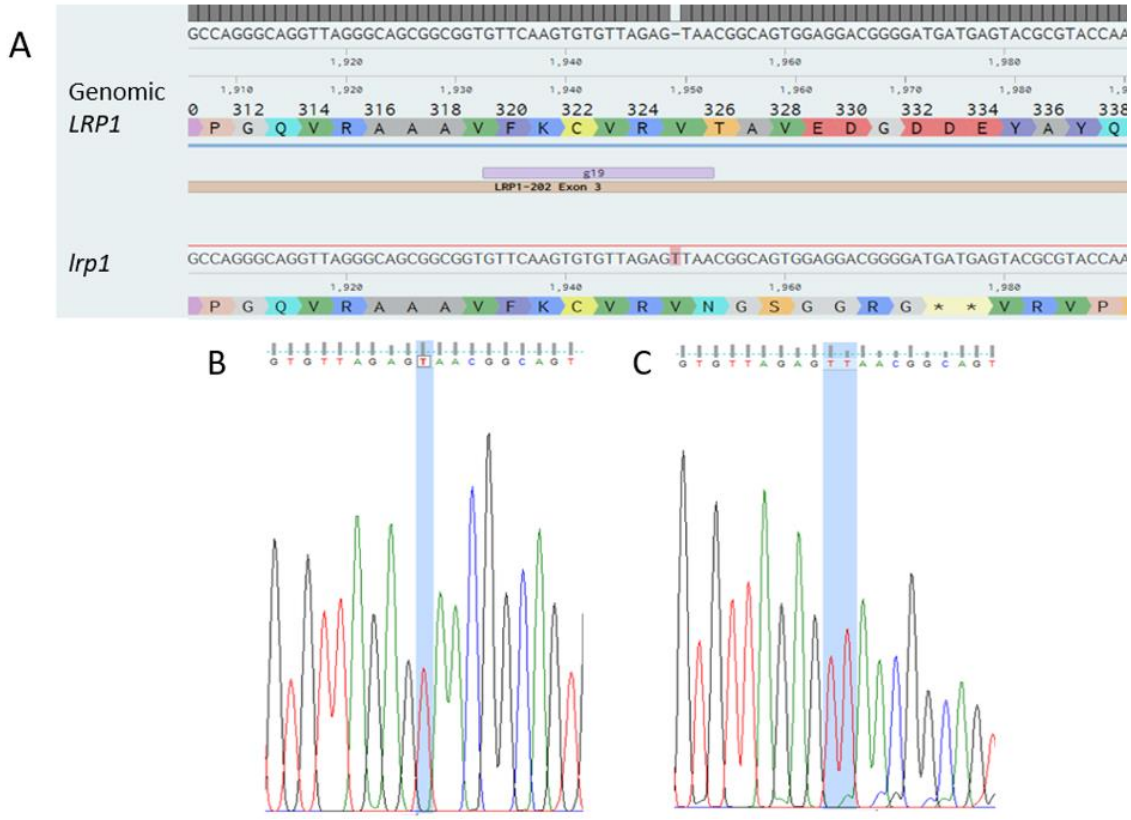

Figure 3.14 A) Shows alignment of Genomic *LRP1* and *lrp1* sequenced from CRISPR guide 19 mutant *A. thaliana* showing an extra thymidine at position 1950 (depicted in red) in the gene. The binding site on exon 3 for guide 19 (g19) is also shown B) Capillary electrophoresis diagrams from Sanger sequencing of genomic *LRP1* and C) *lrp1* showing that the extra thymidine is likely homozygous indicated by the peaks of only one color.

3.5.4. *lrp1* KO has shorter PR than Col-0

No phenotype of *lrp1* has been noted in any *lrp1* T-DNA lines: A study that looked at the effect of a transposon insertion line in *LRP1* noted no difference in phenotype of LR formation (Smith and Fedoroff, 1995), and a paper that looked at gynoecia phenotype in loss-of-function mutants of the *SHI/STY* gene family only noted a mild morphological defect in gynoecia of *sty1-1* mutant plants, and this phenotype was enhanced in multi-mutant plants where several genes in the *SHI/STY* family were mutated (Kuusk et al., 2006). However, they did not look at PR length of *lrp1*, and since *LRP1* is highly expressed in roots and *LRP1* OE was shown to increase PR length, we were interested in investigating the PR length of *lrp1* compared to Col-0.

The T-DNA line *SALK_201247* was chosen to be compared to Col-0 along with the CRISPR KO line *CRISPR_g19*. The T-DNA line was ordered NASC and verified as homozygote *lrp1* mutants by PCR (S. Fig 1). The root phenotyping (Section 2.4.1) was performed three times. In replica 1 (Fig. 3.15 A) we saw a statistically significant difference in PR length between *Col-0* and *CRISPR_g19* (P = 0.00755), and between *CRISPR_g19* and *SALK_201247* (P = 0.00408) where both KO lines were shorter. For the other two replicas there was no significant difference, however the average PR for the KO lines were shorter than the average *Col-0* PR in all replicas (Fig. 3.15). Shorter PR of *lrp1* lines were expected as *LRP1* OE lines have been shown to increase root length (Singh et al., 2020)

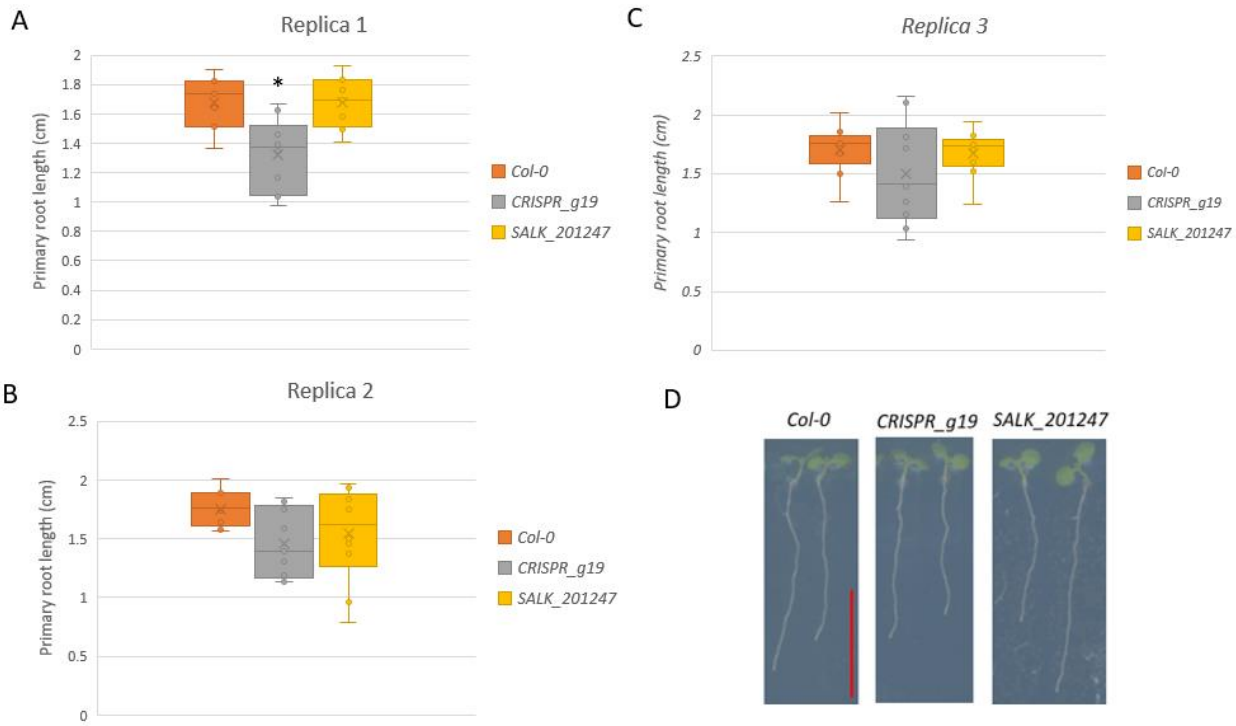

Figure 3.15 Primary root (PR) length phenotyping of *Columbia-0 (Col-0)* and *LATERAL ROOT PRIMORDIUM 1 (LRP1) KO* lines. A) Data of replica 1 shows CRISPR_g19 with a statistically significant shorter PR compared to the other two lines B)C) Data of replica 2 shows no statistically significant difference in PR length between the lines, however CRISPR_g19 and SALK_201247 have a slightly shorter average PR length. Mean values are indicated by x. Asterix (*) indicates significant difference. The mean value is represented by the x D) Representative images of PR of the different lines. Pictures taken with Epson scanner. Scale bar = 1 cm. One-way ANOVA was used for statistics with a significance level of $P \leq 0.05$. A) n = 7, 10, 9 B) n=10, 9, 10. C) n = 9, 10, 9.

4. Discussion

In this section, we will discuss our main findings, encompassing the impact of Q-repeat length on the function, stability, and aggregate formation of LRP1. The effect of abiotic stress factors on *LRP1* expression will be explored, as well as the phenotypic effect of the OE *LRP1* variants and *lrp1* KO *in planta*. Lastly, we will discuss the spatiotemporal expression pattern of *LRP1*.

4.1. Overexpressed LRP1 can form stable aggregates in *N. benthamiana*

We have shown that 7QLRP1 and 0QLRP1 both have a propensity to form nuclear aggregates when overexpressed in *N. benthamiana.* Our results also show that 7QLRP1 has a higher tendency for protein aggregate formation since it formed aggregates in ≥ 60 % of the nuclei in all replicas, while 0QLRP1 in one replica only formed aggregates in 10 % of the nuclei investigated (Fig. 3.3), indicating that there could be a Q-repeat dependent difference in their propensities to form aggregates. Protein aggregates are accumulations of proteins with varying degrees of stability (Reviewed in Fassler et al., 2021). Formation of aggregates have been linked to Q-repeats, and it has been shown that proteins with a higher number of Q's form aggregates faster and are more stable (Krobitsch and Lindquist, 2000). Many aggregate-forming proteins have been shown to form β-sheet interactions (*Perutz et al., 1994*), and the predicted structure of LRP1 shows that it contains β-sheets (Fig. 4.1).

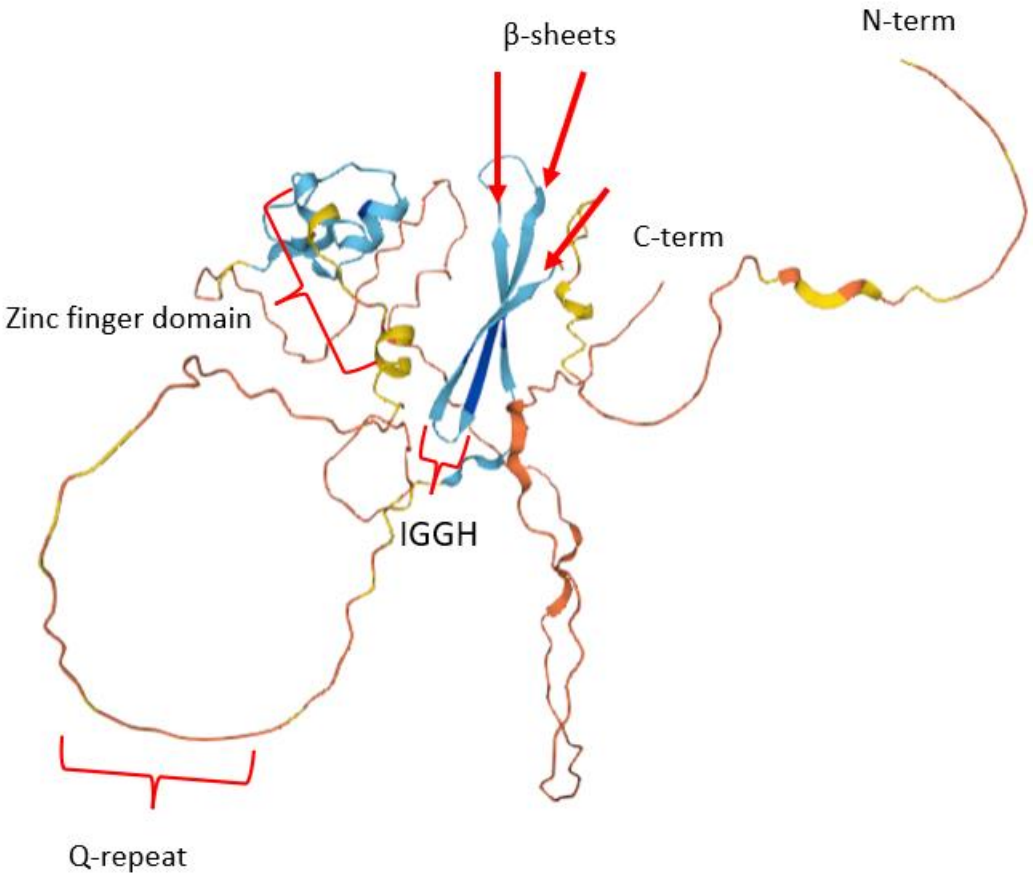

Figure 4.1 AlphaFold-predicted structure of LATERAL ROOT PRIMORDIUM 1. The approximate location of the Zinc-finger domain, IGGH (dimerization) domain, Q-repeat is indicated in the figure. The β-sheets are pointed out with red arrows. Figure from AlphaFold (Varadi et al., 2021; Jumper et al., 2021), code AF-Q94CK9-F1

It has also been reported that Q-repeats can form various structures such as β-sheets (*Perutz et al., 1994),* and affect the propensity of a protein to form β-sheets and α-helices (Davies et al., 2008) which are associated with aggregate formation through the formation of coiled coils (*Kunjithapatham et al., 2005*). Additionally, the Q-repeat in LRP1 is predicted to be located in a disordered region (Fig. 4.1). These regions can adopt an ordered conformation under various circumstances such as protein binding, and have even been shown to be involved in aggregate formation (Reviewed in Tsoi et al., 2023) Aggregate formation is also associated with stress responses which can allow for rapid re-engaging of the processes the proteins are involved in without the need for new synthesis (Saad et al., 2017). If β-sheet interactions are involved in aggregate formation of LRP1, it would be expected to see a higher occurrence of aggregate formation in 7QLRP1 than in 0QLRP1, which our results show for one replica (Fig. 3.3). The

amino acid sequence found in proteins is important for its folding, and it can affect the stability of the protein under various conditions such as temperature and pH (O'Brien et al., 2012). It is therefore possible that the Q-repeat is important for the stability of the protein under various conditions. Since the speed of aggregate formation has been shown to be affected by Q-repeat length, it could be useful to measure this for LRP1 with varying Q-repeat lengths as aggregate formation could have a functional role.

With FRAP experiments, we could investigate the mobility of the two LRP1 variants by measuring the fluorescence recovery after bleaching an area of the nucleus. When looking at our FRAP data, we had one replica with very similar results between 7QLRP1 and 0QLRP1 with similar Mf (S. Fig. 5). For the second replica, 7QLRP1 had a higher Mf than 0QLRP1 (Fig. 3.4) This could indicate that that there is more mobility within the aggregates of 7QLRP1 compared to 0QLRP1 for this replica which could be important for the ability of the proteins to exert their function as TFs.

Performing FRAP experiments where only a part of an aggregate is bleached could allow us to say more about the possible difference in the stability of the proteins in the aggregates. Measuring the speed of the aggregate formation for the different proteins could also give us insight into the importance of the repeat on aggregate formation.

4.2. Both 7QLRP1 and 0QLRP1 activate *pYUC4*

LRP1 had been shown to increase the levels of YUC4 (Singh et al., 2020) we therefore wanted to compare the activation of *pYUC4* by 7QLRP1 and 0QLRP1 since the change in amino acids could affect the conformation of the proteins which in turn could affect the dimerization ability and binding ability to the promoter (Reviewed in Reddy Chichili et al., 2012). For two of the replicas, there was similar activation of *pYUC4* between the proteins (Fig. 3.5). However, in one replica 0QLRP1 had lower activation of *pYUC4:Luc* compared to 7QLRP1 (Fig. 3.5). It is possible that the lower activation of *pYUC4:Luc* by 0QLRP1 is due to the leaf being in worse condition than the leaf expressing 7QLRP1. However, taking into consideration the FRAP results and protein aggregate quantification where 0QLRP1 stood out more for one replica, and since the constructs were infiltrated into leaves of the same *N. benthamiana* plant for the conditions to be as similar as possible, it is tempting to believe that either the external or internal

conditions were less favorable for 0QLRP1 than for 7QLRP1 thus leading to lower activation of *pYUC4* by 0QLRP1 than 7QLRP1. Various factors can stress the plant such as high temperature and ultra violet light (Reviewed in Szymańska et al., 2017). Since 7QLRP1 is the most abundant version of LRP1, it could indicate that this variant can thrive in a variety of conditions. To further examine if 7QLRP1 and 0QLRP1 respond differently to various conditions, luciferase assay experiments could be performed on infiltrated *N. benthamiana* plants exposed to various conditions. Interestingly, we have shown that LRP1 expression is upregulated in response to various stresses (Fig. 3.7; S. Fig. 7).

4.3. *pLRP1* is stress induced

Modulating gene expression in response to stress is an important ability for plants to adapt (Reviewed in Yoon et al., 2020). Several phytohormones are involved in stress responses, including auxin which has been shown to play a role in abiotic stress responses (Reviewed in Jing et al., 2023). Upregulation of auxin in response to salt stress has been shown to increase salt tolerance in *A.thaliana* (Cackett et al., 2022), and upregulation of auxin by YUC6 in potatoes and YUC7 in *A.thaliana* has also been shown to improve drought resistance (Kim et al. 2013, Lee et al., 2012) while a *yuc1yuc2yuc6* triple mutant had decreased resistance to drought (Shi et al., 2014). There are however some indications that the increased drought resistance by YUC6 OE is auxin independent, and rather a result of a decrease in reactive oxygen species which are involved in stress (Cha et al., 2015).

We have shown that *pLRP1* has a slight increase in activation in response to mannitol, chitin, and flagellin, and a large increase in activation in response to mechanical stress (Fig. 3.7; S. Fig. 7). It is then natural to assume that this leads to an increase in YUC4 levels and subsequently increased auxin levels as LRP1 activates *pYUC4* which is involved in auxin biosynthesis. LRP1 might therefore be involved in modulating root length and LR formation in response to stress, as well as increasing stress tolerance. The slight upregulation of *pLRP1* in response to mannitol could indicate that LRP1 is involved in drought resistance, and it could be involved in increasing root length in response to drought. Mechanical stress has been shown to decrease root length, and interestingly *pLRP1* was highly upregulated when exposed to mechanical stress indicating that LRP1 might be involved in reducing root length in a more natural environment.

It is however important to note that some of the GUS solution the seedlings were incubated with evaporated in the first replica, and this evaporation did not seem to be the same for all wells. Consequently, this could have affected the results. Therefore, the experiment should be repeated with one-copy homozygous lines and sealing the wells to prevent evaporation of the GUS solution to get more conclusive results. Stress response to heat is also important and it has been shown to affect auxin levels. It would therefore be interesting to test *pLRP1*'s stress response to heat.

4.4. LRP1 localize to the nucleus in *N. benthamiana* and *A.thaliana*

We have shown that both 7QLRP1 and 0QLRP1 localize to the nucleus in *N. benthamiana*, which was expected for a TF, however there was also localization in what appeared to be aggregates in the cytosol for both protein variants (Fig. 3.1). There might be a difference in the amount of protein present inside and outside of the nucleus for the protein variants that we have not addressed here. This would need measuring and comparing fluorescence intensity between the compartmentalization of proteins.

When looking at LRP1 localization in the *A. thaliana* transgenic *LRP1* OE lines, we also saw in the *0QLRP1#1* line that the protein localized to the nuclei (Fig. 3.11). Unfortunately, we were not able to compare the localization in *A.thaliana* with 7QLRP1 due to low expression of the 7QLRP1 in the analyzed transgenic lines. More lines of 7QLRP1 should be checked for visible expression. We would expect to see localization of 7QLRP1 in nuclei as well, however a comparison of potential expression in cytosol should be done since Q-repeats have the potential to affect localization, which was shown in the *P.trichocarpa* protein PtAN1 (section 3.1.1.2).

4.5. LRP1 affects *A.thaliana* phenotype

4.5.1. *7QLRP1* and *0QLRP1* OE affects PR length

Overexpressed *LRP1* has been shown to increase PR length (Singh et al., 2020), as does the root of *swp1* KO which is a repressor of *LRP1* (Krichevsky et al., 2009). Similarly, *YUC4* OE also leads to a longer root phenotype (Munguía-Rodríguez et al., 2020). Both *LRP1* OE and *YUC4* OE leads to increased auxin levels (Singh et al., 2020; Munguía-Rodríguez et al., 2020), however auxin treated roots has typically been associated with shorter PRs (Hobbie and Estelle, 1994). Auxin production induced in specific cell types in the root negatively affected PR length (Hu et al., 2021) which might indicate that there is a threshold for where auxin increases root length and where it decreases it. When comparing the expression levels of the transgenic *A. thaliana LRP1-YFP* OE lines we observe differences in the YFP expression between independent transformation events (Section 2.3.3).

For the comparison of *7QLRP1#6* and *0QLRP1#3,* if they have comparable expression levels, it could indicate that there is a difference in their *pYUC4* activation and subsequent auxin levels due to the significantly longer root in *0QLRP1#3* than in *7QLRP1#6* after 8 days. Ai et al (2023) looked at increased root length in response to heat and noted that the increased meristem size in response to increased auxin was not the same for all ages of the seedlings, and the PR length of seedlings grown under different temperatures became more different when the seedlings grew older. Due to its higher apparent expression levels *0QLRP1#1* is not comparable to the other two lines (Fig. 3.11; Fig. 3.12; Fig. 3.13), which may suggest that it should have higher auxin levels also corresponding with shorter roots. The mechanism for increased auxin in positive and negative regulation of root length are not entirely known. Singh et al (2020) suggested the increase in root length was caused by increased auxin in the shoot being transported to the root tip. While this may contribute to root elongation, increased production of auxin in the root has been shown to be sufficient for root elongation. A study by Ai et al. (2023) has shown increase in root length in response to higher temperature even when the shoot was removed. Higher temperature in turn increase auxin levels, and blocking transport of auxin from the shoot to the root did not prevent root elongation in response to heat indicating that auxin transport from leaf to root is not necessary for root elongation. Overproduction of auxin in shoots has also been found to be unable to rescue auxin deficiencies (Chen et al., 2014). The lateral root cap (LRC) expresses a cytokinin activated *GH3.17* gene that inactivates auxin in the LRC and is in this way involved in regulating root meristem size, mutants unable to

inactivate auxin had increased meristem size, which should then be related to increased auxin, and an increased meristem size also showed longer root (Di Mambro et al., 2019). We therefore suggest that *LRP1* OE, which previously has been shown to increase GUS staining of *pYUC4* in the root meristem and increased auxin levels (Singh et al, 2020), leads to an increased meristem size possibly due to a shifted auxin gradient. In future experiments it would therefore be interesting to measure and compare the size of the root meristem of *7QLRP1* and *0QLRP1* OE lines with confirmed expression levels.

4.5.2. *lrp1* KO leads to shorter PR

No phenotype of the *lrp1* T-DNA lines have been reported, yet when SWP1, which is a repressor of *LRP1*, was knocked out it showed a longer root indicating that *lrp1* KO should have a shorter root than Col-0 (Krichevsky et al., 2009). Additionally, since *LRP1* OE lines have been shown to have longer roots, it is logical that *lrp1* KO will have shorter roots. We saw that the average root length of all KO lines was shorter than Col-0 for all replicas (Fig. 3.15; S. Fig. 12; S. Fig. 13), although the difference was not statistically significant, it might indicate that LRP1 is important for regulating root growth. If the increased root length seen in the *LRP1* OE lines are caused by an increased meristem size due to increased auxin levels, it is likely that the *lrp1* KO lines would have a reduced meristem size and thus develop a shorter root.

It is possible that our results are not an accurate representation of the effect of *lrp1* CRISPR KO since we have not crossed out the inserted Cas gene. This could lead to introduction of additional mutations which could affect the root phenotype. Another important factor is the function of the truncated gene. We have not confirmed that the gene is KO, and thus it is possible that there is some albeit reduced functionality. A study done on STY1, one of the members of the SHI/STY family LRP1 belongs to, showed that when the dimerization domain was removed it still had activity, albeit reduced compared to the full-length protein (Eklund et al., 2010a). The CRISPR_g19 mutant line has a frame-shift mutation prior to the IGGH dimerization domain, similarly the *SALK_201247* line has a T-DNA insert at the beginning of exon 3 which should disrupt the IGGH domain. Similarly to STY1, the truncated LRP1 in CRISPR_g19 and SALK_201247 could be partially functional. If so, the effects of a fully KO'd *lrp1* would have an even stronger effect on PR length.

4.5.3. *LRP1* OE affects leaf phenotype

We saw that overexpressed *0QLRP1* in two of the lines (#1 and #2) had narrowed leaf phenotype, the leaves were curled downward, and the petiole appeared leaf-like (Fig. 3.9) which has not been previously reported for *LRP1* OE. A downward-curled and narrowed leaf has been reported with increased auxin levels through *YUC4* OE (Munguía-Rodríguez et al., 2020), and *YUC7* activation in *A.thaliana* (Lee et al., 2012). A transgenic Arabidopsis line where the *LRP1 Brassica rapa* (*BrLRP1*) homologue was overexpressed had shorter petiole (Hong et al., 2012) which is similar to the *0QLRP1#1* and *0QLRP1#2* phenotypes. Interestingly, short petioles have not been associated with increased auxin levels, the opposite has been reported where increased auxin levels have led to elongated petioles (Cha et al., 2015). While we only saw an aberrant leaf phenotype in two of the one-copy *0QLRP1* lines, *7QLRP1* lines that were not one-copy lines also showed a similar phenotype (data not shown). Interestingly both *0QLRP1#1* (Fig. 3.11) and *0QLRP1#2* (data not shown) shows high *LRP1* expression when investigating YFP signals in the root tip. This may indicate that the leaf phenotype we see in *0QLRP1#1* and *0QLRP1#2* are OE phenotypes. It is therefore possible that *LRP1* OE leads to increased auxin levels that are localized in a way that differs from other OE lines creating an auxin gradient that affects the boundary between the leaf and the petiole so that the petiole does not develop as it normally would. The downturned leaf phenotype in *0QLRP1#1* and *0QLRP1#2* do correspond with increased auxin level phenotypes previously reported. Interestingly, *BrLRP1* OE was shown to regulate expression of gibberellic acid (GA) and auxin related genes involved in morphogenesis in shoot apical regions (Hong et al., 2012), however with similar YUC expression to Col-0. While AtLRP1 (*A.thaliana* LRP1) has been shown to increase YUC4 levels (Singh et al., 2020), this could indicate that *AtLRP1* is also involved in regulating GA-related genes involved in morphogenesis in shoot apical region leading to an aberrant leaf phenotype. Interestingly, a leafy petiole phenotype was seen in a LEAFY PETIOLE (LEP) activation tagged *A.thaliana* mutant (van der Graaff et al., 2000), and LEP has been shown to be involved in GA response during germination. If AtLRP1 is involved in regulating GA-related genes, there is potential for increased LEP levels which could explain the leafy petiole phenotype we see. Investigating AtLRP1's role in GA related genes could provide insight into this.

4.5.4. *LRP1* is highly expressed in root meristem and emerged LRs

Our GUS-assay results indicate that *pLRP1* is active at the base of emerged LRs, and highly active at the base an along a more developed LR (Fig. 3.6). The potential staining at the other stages is not conclusive. This is different from previously reported results where staining was seen at the root tip and at various stages of LR development (Singh et al., 2020). The growth conditions could have been different; Singh et al. (2020) reports growing the seedlings in 22-24 °C 16 h day 8 h night, while we grew the seedlings at 22 °C 16 h day 8 h night. It is again tempting to speculate that temperature affects our results with LRP1 and therefore might affect *pLRP1* activity. Additionally, the incubation period with GUS solution could have been different. Also the age of our seedlings were different; Singh et al reports using seedlings 5 days after germination, while we used seedlings that had incubated for 7 days. However we did test seedlings of various ages and only saw staining in roots of 7 day old seedlings (data not shown).

The H2B-Venus reporter however shows *pLRP1* activity in many cells along the root, near the root tip and in emerged LRs. This shows that this type of reporter is capable of visualizing low promoter activity, even low activity of *pLRP1* in nuclei will activate transcription of the reporter protein and thus be visible.

One of the pictures of *pLRP1:H2B-Venus* expression at a site where an LR is developing seem to have expression at the tip of the developing LR (Fig. 3.8 C), this might correspond to the area of the LR where an auxin maxima is formed (Fig. 1.8), possibly indicating that LRP1 is involved in creating this auxin maxima and is thus involved in allowing the LR to emerge. The strong signal in the root meristem (Fig. 3.8 A) corresponds with the previously reported *LRP1* expression shown by Singh et al., and it corresponds with the results showing elongated roots, as well as shorter roots in *lrp1* KO lines. The signal in emerged LRs correspond with the signal we see with the GUS assay. Unfortunately, it was challenging to identify the different stages of LRs with the microscope we used for the *pLRP1:H2B-Venus* reporter so we could not determine the expression pattern in nuclei near or in the various stages of LR development.

Ideally identification of cell-specific *LRP1* expression should be repeated with a different microscope where it is possible to identify the LRP stages. Similarly to the GUS fluorometric assay, it would be interesting compare the cell specific activity of *pLRP1:H2B-Venus* when exposed to stress compared to untreated seedlings

4.5.5. Transgenic lines in a natural setting

It is important to take into consideration that the transgenic *A.thaliana* lines are grown and studied in a laboratory setting, and the effect of LRP1 in a natural state could be different as indicated by reduced root length when seedlings grew through a membrane to simulate growth in soil (Okamoto et al., 2008). While *lrp1* KO lines showed reduced root growth, and *LRP1* OE lines displayed increased root growth when grown vertically on agar plates, this could be different if grown under more natural conditions. It would therefore be interesting to compare the OE lines, the KO lines, and WT when grown in a manner that simulates growth in soil. It could also be useful to test the effects of various environmental factors on root growth given that the proteins have different stabilities depending on the environment. Using several transgenic *A.thaliana* lines with additional naturally occurring length variations of the LRP1 Q-repeat, as well as an *lrp1* KO line would be crucial for investigating this issue.

4.5.6. Outstanding issues with the transgenic lines

Due to time constraints, we used segregating lines for all experiments with transgenic lines. This means that approximately 25 % of the seeds will contain no insert, 50 % will be heterozygous for the insert, and 25 % will be homozygous. This can cause issues with the results, particularly for the GUS staining, fluorimetric GUS assay, and the phenotyping.

For the Fluorimetric GUS assay, using segregating lines may skew the results as homozygotes will produce more GUS than the heterozygote seedlings. Similarly for the phenotyping with the *LRP1* OE lines, heterozygotes may express less *LRP1* than homozygotes which can affect the root length and thus skew the results. For the reasons given above, the experiments should therefore be repeated with one-copy homozygous lines to be able to determine differences, and expression levels must be checked to have more comparable lines.

4.6. Summary and future perspectives

We have demonstrated that LRP1 is involved in modulating PR length and leaf phenotype with our OE lines and our KO lines. TFs are important for modulating gene expression in response to various factors, and their functionality can be affected by these factors as has been demonstrated with ELF3 responding to heat-stress, and repeats can affect this response. While the results for the *7QLRP1* and *0QLRP1* OE lines are statistically inconclusive, we have seen indications of a difference in the functionality and mobility of the two LRP1 variants expressed in *N. benthamiana*, This has raised the question of their functionality in response to stress as the experiments do expose the plants to stress by being exposed to bacteria, being exposed to high intensity lasers, and having water pushed into the cells when slides are being prepared.

While we did not look at aggregate formation of LRP1 in *A.thaliana*, this is something we want to do with our transgenic OE lines. Furthermore, while studying aggregate formation in *N. benthamiana* can give insight into the differences in the proteins, the results could be different in *A.thaliana*. It would be interesting to investigate the mechanism and potential importance of the aggregate formation we observe in LRP1. It was recently found that *A.thaliana* produces a chloroplast STROMAL PROCESSING PEPTIDASE which prevents aggregation in cytosol, however heat stress was enough for aggregate formation to occur in (Llamas et al., 2023). Similarly, mitochondrial proteases was shown to prevent aggregate formation of small HEAT-SHOCK PROTEIN in response to heat stress in *A.thaliana* (Maziak et al., 2021). Whether similar processes take place in the nucleus is not known, however it has been shown that ELF3 forms nuclear aggregates in response to higher temperatures in *A.thaliana* (Jung et al., 2020), which could also be the case for LRP1 protein aggregate formation.

To further study the potential effect of the Q-repeat length variation in LRP1, it would be useful to do interaction studies using a yeast two-hybrid method with its known binding partners (Section 1.3) as has been done with ELF3 and COLD11 where repeat length affected interactions (Li et al., 2023; Press and Queitsch, 2017)

Since LRP1 is also reported to be involved in lateral root formation and potentially adventitious root formation (Singh et al., 2020; Smith and Fedoroff, 1995), it would be interesting to look at LRs and the formation of adventitious roots in the KO lines as well as OE lines expressing

LRP1 with various Q-repeat. In this study, we also created mutants using CRISPR guide 11 (Section 2.1.8), which should recognize a site in exon 2 upstream of the zinc finger domain. A STOP codon prior to this domain is expected to have a more deleterious effect on *LRP1*. We were however not able to confirm if any frameshift mutations had been introduced in the CRISPR guide 11 mutants. Further phenotyping of *lrp1* KO mutants should be done with the CRISPR g11 mutants when these are confirmed since it is possible that the KO lines we had did not have *lrp1* fully KO'd.

Lastly, while the comparisons between 7QLRP1 and 0QLRP1 were inconclusive, it is possible that it is possible that there could be a more obvious difference if we were to look at LRP1 versions with more variation in Q-repeat lengths not included in this study.

References

1001 Genomes Consortium. 1,135 genomes reveal the global pattern of polymorphism in *Arabidopsis thaliana*. *Cell* 166, 481–491 (2016).

Ai, H., Bellstaedt, J., Bartusch, K. S., Eschen-Lippold, L., Babben, S., Balcke, G. U., Tissier, A., Hause, B., Andersen, T. G., Delker, C., & Quint, M. (2023). Auxin-dependent regulation of cell division rates governs root thermomorphogenesis. *The EMBO journal*, *42*(11), e111926.

Alexandre Webster (Aravin Lab, Caltech) and Malte Wachsmuth (EMBL)
February 2014. An Easy Protocol for FRAP

Alonso, J. M., Stepanova, A. N., Leisse, T. J., Kim, C. J., Chen, H., Shinn, P., Stevenson, D. K., Zimmerman, J., Barajas, P., Cheuk, R., Gadrinab, C., Heller, C., Jeske, A., Koesema, E., Meyers, C. C., Parker, H., Prednis, L., Ansari, Y., Choy, N., Deen, H., … Ecker, J. R. (2003). Genome-wide insertional mutagenesis of Arabidopsis thaliana. *Science (New York, N.Y.)*, *301*(5633), 653–657.

Andrew D. Yates, James Allen, Ridwan M. Amode, Andrey G. Azov, Matthieu Barba, Andrés Becerra, Jyothish Bhai, Lahcen I. Campbell, Manuel Carbajo Martinez, Marc Chakiachvili, Kapeel Chougule, Mikkel Christensen, Bruno Contreras-Moreira, Alayne Cuzick, Luca Da Rin Fioretto, Paul Davis, Nishadi H. De Silva, Stavros Diamantakis, Sarah Dyer, Justin Elser, Carla V. Filippi, Astrid Gall, Dionysios Grigoriadis, Cristina Guijarro-Clarke, Parul Gupta, Kim E. Hammond-Kosack, Kevin L. Howe, Pankaj Jaiswal, Vinay Kaikala, Vivek Kumar, Sunita Kumari, Nick Langridge, Tuan Le, Manuel Luypaert, Gareth L. Maslen, Thomas Maurel, Benjamin Moore, Matthieu Muffato, Aleena Mushtaq, Guy Naamati, Sushma Naithani, Andrew Olson, Anne Parker, Michael Paulini, Helder Pedro, Emily Perry, Justin Preece, Mark Quinton-Tulloch, Faye Rodgers, Marc Rosello, Magali Ruffier, James Seager, Vasily Sitnik, Michal Szpak, John Tate, Marcela K. Tello-Ruiz, Stephen J. Trevanion, Martin Urban, Doreen Ware, Sharon Wei, Gary Williams, Andrea Winterbottom, Magdalena Zarowiecki, Robert D. Finn and Paul Flicek.
Ensembl Genomes 2022: an expanding genome resource for non-vertebrates.
Nucleic Acids Research 2022

Axelrod, D., Koppel, D. E., Schlessinger, J., Elson, E., & Webb, W. W. (1976). Mobility measurement by analysis of fluorescence photobleaching recovery kinetics. *Biophysical journal*, *16*(9), 1055–1069.

Baer, C., Miyamoto, M. & Denver, D. Mutation rate variation in multicellular eukaryotes: causes and consequences. *Nat Rev Genet* 8, 619–631 (2007).

Banda, J., Bellande, K., von Wangenheim, D., Goh, T., Guyomarc'h, S., Laplaze, L., & Bennett, M. J. (2019). Lateral Root Formation in Arabidopsis: A Well-Ordered LRexit. *Trends in plant science*, *24*(9), 826–839.

Bleckmann, A., Weidtkamp-Peters, S., Seidel, C.A., and Simon, R. (2010). Stem cell signaling in Arabidopsis requires CRN to localize CLV2 to the plasma membrane. Plant Physiol 152:166-176.

Bolle, C., Schneider, A., & Leister, D. (2011). Perspectives on Systematic Analyses of Gene Function in Arabidopsis thaliana: New Tools, Topics and Trends. *Current genomics*, *12*(1), 1–14.

Brennan, A. C., Méndez-Vigo, B., Haddioui, A., Martínez-Zapater, J. M., Picó, F. X., & Alonso-Blanco, C. (2014). The genetic structure of Arabidopsis thaliana in the south-western Mediterranean range reveals a shared history between North Africa and southern Europe. *BMC plant biology*, *14*, 17.

Brumos J., Robles L.M., Yun J., Vu T.C., Jackson S., Alonso J.M., Stepanova A.N. 2018. Local auxin biosynthesis is a key regulator of plant development. *Developmental Cell,* 47, 306–318.e5

Bryan, A. C., Zhang, J., Guo, J., Ranjan, P., Singan, V., Barry, K., Schmutz, J., Weighill, D., Jacobson, D., Jawdy, S., Tuskan, G. A., Chen, J. G., & Muchero, W. (2018). A Variable Polyglutamine Repeat Affects Subcellular Localization and Regulatory Activity of a *Populus* ANGUSTIFOLIA Protein. *G3 (Bethesda, Md.)*, *8*(8), 2631–2641.

Cackett L, Cannistraci CV, Meier S, Ferrandi P, Pěnčík A, Gehring C, Novák O, Ingle RA, Donaldson L. Salt-Specific Gene Expression Reveals Elevated Auxin Levels in *Arabidopsis thaliana* Plants Grown Under Saline Conditions. Front Plant Sci. 2022 Feb 10;13:804716.

Cao, J., Schneeberger, K., Ossowski, S. *et al.* Whole-genome sequencing of multiple *Arabidopsis thaliana* populations. *Nat Genet* 43, 956–963 (2011).

Carisey, A., Stroud, M., Tsang, R., Ballestrem, C. (2011). Fluorescence Recovery After Photobleaching. In: Wells, C., Parsons, M. (eds) Cell Migration. Methods in Molecular Biology, vol 769. Humana Press.

Cha, J. Y., Kim, W. Y., Kang, S. B., Kim, J. I., Baek, D., Jung, I. J., Kim, M. R., Li, N., Kim, H. J., Nakajima, M., Asami, T., Sabir, J. S., Park, H. C., Lee, S. Y., Bohnert, H. J., Bressan, R. A., Pardo, J. M., & Yun, D. J. (2015). A novel thiol-reductase activity of Arabidopsis YUC6 confers drought tolerance independently of auxin biosynthesis. *Nature communications*, *6*, 8041.

Chen, Q., Dai, X., De-Paoli, H., Cheng, Y., Takebayashi, Y., Kasahara, H., Kamiya, Y., & Zhao, Y. (2014). Auxin overproduction in shoots cannot rescue auxin deficiencies in Arabidopsis roots. *Plant & cell physiology*, *55*(6), 1072–1079.

Clough, S. J., & Bent, A. F. (1998). Floral dip: a simplified method for Agrobacterium-mediated transformation of Arabidopsis thaliana. *The Plant journal : for cell and molecular biology*, *16*(6), 735–743.

Davies, P., Watt, K., Kelly, S. M., Clark, C., Price, N. C., & McEwan, I. J. (2008). Consequences of poly-glutamine repeat length for the conformation and folding of the androgen receptor amino-terminal domain. *Journal of molecular endocrinology*, *41*(5), 301–314.

De Smet I. (2012). Lateral root initiation: one step at a time. *The New phytologist*, *193*(4), 867–873.

De Smet S, Cuypers A, Vangronsveld J, Remans T. Gene Networks Involved in Hormonal Control of Root Development in Arabidopsis thaliana: A Framework for Studying Its Disturbance by Metal Stress. Int J Mol Sci. 2015 Aug 14;16(8):19195-224.

De Smet, I., Tetsumura, T., De Rybel, B., Frei dit Frey, N., Laplaze, L., Casimiro, I., Swarup, R., Naudts, M., Vanneste, S., Audenaert, D., Inzé, D., Bennett, M. J., & Beeckman, T. (2007). Auxin-dependent regulation of lateral root positioning in the basal meristem of Arabidopsis. *Development (Cambridge, England)*, *134*(4), 681–690.

Deja-Muylle, A., Opdenacker D., Parizot B., Motte H., Lobet G., Storme V., Clauw P., Njo M., Beeckman T. (2022). Variability of Arabidopsis thaliana Mature Root System Architecture and Genome-Wide Association Study. *Frontiers in Plant Science*.

Di Mambro, R., Svolacchia, N., Dello Ioio, R., Pierdonati, E., Salvi, E., Pedrazzini, E., Vitale, A., Perilli, S., Sozzani, R., Benfey, P. N., Busch, W., Costantino, P., & Sabatini, S. (2019). The Lateral Root Cap Acts as an Auxin Sink that Controls Meristem Size. *Current biology : CB*, *29*(7), 1199–1205.e4.

Dolan L, Janmaat K, Willemsen V, Linstead P, Poethig S, Roberts K, Scheres B. Cellular organisation of the Arabidopsis thaliana root. Development. 1993 Sep;119(1):71-84.

Du, F., Guan, C., & Jiao, Y. (2018). Molecular Mechanisms of Leaf Morphogenesis. *Molecular plant*, *11*(9), 1117–1134.

Dubrovsky, J. G., Sauer, M., Napsucialy-Mendivil, S., Ivanchenko, M. G., Friml, J., Shishkova, S., Celenza, J., & Benková, E. (2008). Auxin acts as a local morphogenetic trigger to specify lateral root founder cells. *Proceedings of the National Academy of Sciences of the United States of America*, *105*(25), 8790–8794.

Earley, K. W., Haag, J. R., Pontes, O., Opper, K., Juehne, T., Song, K., & Pikaard, C. S. (2006). Gateway-compatible vectors for plant functional genomics and proteomics. *The Plant journal : for cell and molecular biology*, *45*(4), 616–629.

Eklund, D. M., Ståldal, V., Valsecchi, I., Cierlik, I., Eriksson, C., Hiratsu, K., Ohme-Takagi, M., Sundström, J. F., Thelander, M., Ezcurra, I., & Sundberg, E. (2010a). The Arabidopsis thaliana STYLISH1 protein acts as a transcriptional activator regulating auxin biosynthesis. *The Plant cell*, *22*(2), 349–363.

Eklund, D. M., Thelander, M., Landberg, K., Ståldal, V., Nilsson, A., Johansson, M., Valsecchi, I., Pederson, E. R., Kowalczyk, M., Ljung, K., Ronne, H., & Sundberg, E. (2010b). Homologues of the Arabidopsis thaliana SHI/STY/LRP1 genes control auxin biosynthesis and affect growth and development in the moss Physcomitrella patens. *Development (Cambridge, England)*, *137*(8), 1275–1284.

Fassler, J. S., Skuodas, S., Weeks, D. L., & Phillips, B. T. (2021). Protein Aggregation and Disaggregation in Cells and Development. *Journal of molecular biology*, *433*(21), 167215.

Fior, S.; Vianelli, A.; Gerola, P.D. A novel method for fluorometric continuous measurement of β-glucuronidase (GUS) activity using 4-methyl-umbelliferyl-β-d-glucuronide (MUG) as substrate. Plant Sci. 2009, 176, 130–135

Fondon, J. W., 3rd, & Garner, H. R. (2004). Molecular origins of rapid and continuous morphological evolution. *Proceedings of the National Academy of Sciences of the United States of America*, *101*(52), 18058–18063.

Fridborg, I., Kuusk, S., Robertson, M., & Sundberg, E. (2001). The Arabidopsis protein SHI represses gibberellin responses in Arabidopsis and barley. *Plant physiology*, *127*(3), 937–948.

Fu, A., Cohen-Kaplan, V., Avni, N., Livneh, I., & Ciechanover, A. (2021). p62-containing, proteolytically active nuclear condensates, increase the efficiency of the ubiquitin-proteasome system. *Proceedings of the National Academy of Sciences of the United States of America*, *118*(33), e2107321118.

Galvan-Ampudia, C. S., Julkowska, M. M., Darwish, E., Gandullo, J., Korver, R. A., Brunoud, G., Haring, M. A., Munnik, T., Vernoux, T., & Testerink, C. (2013). Halotropism is a response of plant roots to avoid a saline environment. *Current biology : CB*, *23*(20), 2044–2050.

Gemayel, R., Vinces, M. D., Legendre, M., & Verstrepen, K. J. (2010). Variable tandem repeats accelerate evolution of coding and regulatory sequences. *Annual review of genetics*, *44*, 445–477.

Gerber, H. P., Seipel, K., Georgiev, O., Höfferer, M., Hug, M., Rusconi, S., & Schaffner, W. (1994). Transcriptional activation modulated by homopolymeric glutamine and proline stretches. *Science (New York, N.Y.)*, *263*(5148), 808–811.

Göktay, M., Fulgione, A., & Hancock, A. M. (2021). A New Catalog of Structural Variants in 1,301 A. thaliana Lines from Africa, Eurasia, and North America Reveals a Signature of Balancing Selection at Defense Response Genes. *Molecular biology and evolution*, *38*(4), 1498–1511.

Gruber, B. D., Giehl, R. F., Friedel, S., & von Wirén, N. (2013). Plasticity of the Arabidopsis root system under nutrient deficiencies. *Plant physiology*, *163*(1), 161–179.

Guan, C., Wu, B., Yu, T., Wang, Q., Krogan, N. T., Liu, X., & Jiao, Y. (2017). Spatial Auxin Signaling Controls Leaf Flattening in Arabidopsis. *Current biology : CB*, *27*(19), 2940–2950.e4.

Gust, A. A., Biswas, R., Lenz, H. D., Rauhut, T., Ranf, S., Kemmerling, B., Götz, F., Glawischnig, E., Lee, J., Felix, G., & Nürnberger, T. (2007). Bacteria-derived peptidoglycans constitute pathogen-associated molecular patterns triggering innate immunity in Arabidopsis. *The Journal of biological chemistry*, *282*(44), 32338–32348.

Hinz, J., Lehnhardt, L., Zakrzewski, S., Zhang, G., & Ignatova, Z. (2012). Polyglutamine expansion alters the dynamics and molecular architecture of aggregates in dentatorubropallidoluysian atrophy. *The Journal of biological chemistry*, *287*(3), 2068–2078.

Hobbie, L., & Estelle, M. (1994). Genetic approaches to auxin action. *Plant, cell & environment*, *17*(6), 525–540.

Hong, J. K., Kim, J. A., Kim, J. S., Lee, S. I., Koo, B. S., & Lee, Y. H. (2012). Overexpression of Brassica rapa SHI-RELATED SEQUENCE genes suppresses growth and development in Arabidopsis thaliana. *Biotechnology letters*, *34*(8), 1561–1569.

Howe, E. S., Clemente, T. E., & Bass, H. W. (2012). Maize histone H2B-mCherry: a new fluorescent chromatin marker for somatic and meiotic chromosome research. *DNA and cell biology*, *31*(6), 925–938.

Hrmova, M., & Hussain, S. S. (2021). Plant Transcription Factors Involved in Drought and Associated Stresses. *International journal of molecular sciences*, *22*(11), 5662.

Hu, Y., Omary, M., Hu, Y. *et al.* Cell kinetics of auxin transport and activity in *Arabidopsis* root growth and skewing. *Nat Commun* 12, 1657 (2021).

Janody, F., Sturny, R., Schaeffer, V., Azou, Y., & Dostatni, N. (2001). Two distinct domains of Bicoid mediate its transcriptional downregulation by the Torso pathway. *Development (Cambridge, England)*, *128*(12), 2281–2290.

Jefferson, R. A., Kavanagh, T. A., & Bevan, M. W. (1987). GUS fusions: beta-glucuronidase as a sensitive and versatile gene fusion marker in higher plants. *The EMBO journal*, *6*(13), 3901–3907.

Jinek, M., Chylinski, K., Fonfara, I., Hauer, M., Doudna, J. A., & Charpentier, E. (2012). A programmable dual-RNA-guided DNA endonuclease in adaptive bacterial immunity. *Science (New York, N.Y.)*, *337*(6096), 816–821.

Jing, H., Wilkinson, E. G., Sageman-Furnas, K., & Strader, L. C. (2023). Auxin and Abiotic Stress Responses. *Journal of experimental botany*, erad325. Advance online publication.

Jumper, J *et al*. Highly accurate protein structure prediction with AlphaFold. *Nature* (2021).

Jung, JH., Barbosa, A.D., Hutin, S. *et al.* A prion-like domain in ELF3 functions as a thermosensor in *Arabidopsis*. *Nature* 585, 256–260 (2020).

Kim, J. I., Baek, D., Park, H. C., Chun, H. J., Oh, D. H., Lee, M. K., Cha, J. Y., Kim, W. Y., Kim, M. C., Chung, W. S., Bohnert, H. J., Lee, S. Y., Bressan, R. A., Lee, S. W., & Yun, D. J. (2013). Overexpression of Arabidopsis YUCCA6 in potato results in high-auxin developmental phenotypes and enhanced resistance to water deficit. *Molecular plant*, *6*(2), 337–349.

King, J. J., Stimart, D. P., Fisher, R. H., & Bleecker, A. B. (1995). A Mutation Altering Auxin Homeostasis and Plant Morphology in Arabidopsis. *The Plant cell*, *7*(12), 2023–2037.

Krichevsky, A., Zaltsman, A., Kozlovsky, S. V., Tian, G. W., & Citovsky, V. (2009). Regulation of root elongation by histone acetylation in Arabidopsis. *Journal of molecular biology*, *385*(1), 45–50.

Krobitsch, S., & Lindquist, S. (2000). Aggregation of huntingtin in yeast varies with the length of the polyglutamine expansion and the expression of chaperone proteins. *Proceedings of the National Academy of Sciences of the United States of America*, *97*(4), 1589–1594.

Kunjithapatham, R., Oliva, F. Y., Doshi, U., Pérez, M., Avila, J., & Muñoz, V. (2005). Role for the alpha-helix in aberrant protein aggregation. *Biochemistry*, *44*(1), 149–156.

Kuusk, S., Sohlberg, J.J., Magnus Eklund, D. and Sundberg, E. (2006), Functionally redundant *SHI* family genes regulate Arabidopsis gynoecium development in a dose-dependent manner. The Plant Journal, 47: 99-111.

Lakatos, L., Szittya, G., Silhavy, D., & Burgyán, J. (2004). Molecular mechanism of RNA silencing suppression mediated by p19 protein of tombusviruses. *The EMBO journal*, *23*(4), 876–884.

LANDY, A. 1989. Dynamic, structural, and regulatory aspects of lambda site-specific recombination. Annual Review of Biochemistry, 58, 913-949.

Lee, M., Jung, J. H., Han, D. Y., Seo, P. J., Park, W. J., & Park, C. M. (2012). Activation of a flavin monooxygenase gene YUCCA7 enhances drought resistance in Arabidopsis. *Planta*, *235*(5), 923–938. https://doi.org/10.1007/s00425-011-1552-3

Li, L. C., Qin, G. J., Tsuge, T., Hou, X. H., Ding, M. Y., Aoyama, T., Oka, A., Chen, Z., Gu, H., Zhao, Y., & Qu, L. J. (2008). SPOROCYTELESS modulates YUCCA expression to regulate the development of lateral organs in Arabidopsis. *The New phytologist*, *179*(3), 751–764.

Li, Z., Wang, B., Luo, W., Xu, Y., Wang, J., Xue, Z., Niu, Y., Cheng, Z., Ge, S., Zhang, W., Zhang, J., Li, Q., & Chong, K. (2023). Natural variation of codon repeats in *COLD11* endows rice with chilling resilience. *Science advances*, *9*(1), eabq5506.

Lippincott-Schwartz, J., Snapp, E., & Kenworthy, A. (2001). Studying protein dynamics in living cells. *Nature reviews. Molecular cell biology*, *2*(6), 444–456.

Liu J, Jung C, Xu J, et al. Genome-wide analysis uncovers regulation of long intergenic noncoding RNAs in Arabidopsis. The Plant Cell. 2012 Nov;24(11):4333-4345. DOI: 10.1105/tpc.112.102855.

Llamas, E., Koyuncu, S., Lee, H.J. *et al.* In planta expression of human polyQ-expanded huntingtin fragment reveals mechanisms to prevent disease-related protein aggregation. *Nat Aging* 3, 1345–1357 (2023).

Long, Q., Rabanal, F. A., Meng, D., Huber, C. D., Farlow, A., Platzer, A., Zhang, Q., Vilhjálmsson, B. J., Korte, A., Nizhynska, V., Voronin, V., Korte, P., Sedman, L., Mandáková, T., Lysak, M. A., Seren, Ü., Hellmann, I., & Nordborg, M. (2013). Massive genomic variation and strong selection in Arabidopsis thaliana lines from Sweden. *Nature genetics*, *45*(8), 884–890.

Manuela, D., & Xu, M. (2020). Patterning a Leaf by Establishing Polarities. *Frontiers in plant science*, *11*, 568730.

Maruyama, J., Nakajima, H., & Kitamoto, K. (2001). Visualization of nuclei in Aspergillus oryzae with EGFP and analysis of the number of nuclei in each conidium by FACS. *Bioscience, biotechnology, and biochemistry*, *65*(7), 1504–1510.

Maximilian Oliver Press, Christine Queitsch, Variability in a Short Tandem Repeat Mediates Complex Epistatic Interactions in *Arabidopsis thaliana*, *Genetics*, Volume 205, Issue 1, 1 January 2017, Pages 455–464,

Maziak, A., Heidorn-Czarna, M., Weremczuk, A., & Janska, H. (2021). FTSH4 and OMA1 mitochondrial proteases reduce moderate heat stress-induced protein aggregation. *Plant physiology*, *187*(2), 769–786.

Mergner, J., Frejno, M., List, M. *et al.* Mass-spectrometry-based draft of the *Arabidopsis* proteome. *Nature* 579, 409–414 (2020).

Meyer P. (2000). Transcriptional transgene silencing and chromatin components. *Plant molecular biology*, *43*(2-3), 221–234.

Moreno-Risueno, M. A., Van Norman, J. M., Moreno, A., Zhang, J., Ahnert, S. E., & Benfey, P. N. (2010). Oscillating gene expression determines competence for periodic Arabidopsis root branching. *Science (New York, N.Y.)*, *329*(5997), 1306–1311.

Munguía-Rodríguez, A. G., López-Bucio, J. S., Ruiz-Herrera, L. F., Ortiz-Castro, R., Guevara-García, Á. A., Marsch-Martínez, N., Carreón-Abud, Y., López-Bucio, J., & Martínez-Trujillo, M. (2020). YUCCA4 overexpression modulates auxin biosynthesis and transport and influences plant growth and development via crosstalk with abscisic acid in Arabidopsis thaliana. *Genetics and molecular biology*, *43*(1), e20190221.

MURASHIGE, T. & SKOOG, F. 1962. A revised medium for rapid growth and bio assays with tobacco tissue cultures. Physiologia Plantarum, 15, 473-497

Nakamura, S., Nakao, A., Kawamukai, M., Kimura, T., Ishiguro, S., & Nakagawa, T. (2009). Development of Gateway binary vectors, R4L1pGWBs, for promoter analysis in higher plants. *Bioscience, biotechnology, and biochemistry*, *73*(11), 2556–2559.

Navizet, I., Liu, Y.-J., Ferré, N., Roca-Sanjuán, D., & Lindh, R. (2011). The Chemistry of Bioluminescence: An Analysis of Chemical Functionalities. *Chemphyschem*, *12*(17), 3064–3076.

O'Brien, E. P., Brooks, B. R., & Thirumalai, D. (2012). Effects of pH on proteins: predictions for ensemble and single-molecule pulling experiments. *Journal of the American Chemical Society*, *134*(2), 979–987.

Okamoto, T., Tsurumi, S., Shibasaki, K., Obana, Y., Takaji, H., Oono, Y., & Rahman, A. (2008). Genetic dissection of hormonal responses in the roots of Arabidopsis grown under continuous mechanical impedance. *Plant physiology*, *146*(4), 1651–1662.

Pelkmans, L., Kartenbeck, J. & Helenius, A. Caveolar endocytosis of simian virus 40 reveals a new two-step vesicular-transport pathway to the ER. *Nat Cell Biol* 3, 473–483 (2001).

Perilli, S., Di Mambro, R., & Sabatini, S. (2012). Growth and development of the root apical meristem. *Current opinion in plant biology*, *15*(1), 17–23.

Perutz, M. F., Johnson, T., Suzuki, M., & Finch, J. T. (1994). Glutamine repeats as polar zippers: their possible role in inherited neurodegenerative diseases. *Proceedings of the National Academy of Sciences of the United States of America*, *91*(12), 5355–5358.

Phair RD, Scaffidi P, Elbi C, et al. Global nature of dynamic prot2ein-chromatin interactions in vivo: three-dimensional genome scanning and dynamic interaction networks of chromatin proteins. Molecular and Cellular Biology. 2004 Jul;24(14):6393-6402.

Phair, R., Misteli, T. High mobility of proteins in the mammalian cell nucleus. *Nature* 404, 604–609 (2000).

Qin, G., Gu, H., Zhao, Y., Ma, Z., Shi, G., Yang, Y., Pichersky, E., Chen, H., Liu, M., Chen, Z., & Qu, L. J. (2005). An indole-3-acetic acid carboxyl methyltransferase regulates Arabidopsis leaf development. *The Plant cell*, *17*(10), 2693–2704.

Reddy Chichili, V. P., Kumar, V., & Sivaraman, J. (2013). Linkers in the structural biology of protein-protein interactions. *Protein science : a publication of the Protein Society*, *22*(2), 153–167.

Reinar, W. B., Greulich, A., Stø, I. M., Knutsen, J. B., Reitan, T., Tørresen, O. K., Jentoft, S., Butenko, M. A., & Jakobsen, K. S. (2023). Adaptive protein evolution through length variation of short tandem repeats in *Arabidopsis*. *Science advances*, *9*(12), eadd6960.

Reinar, W. B., Lalun, V. O., Reitan, T., Jakobsen, K. S., & Butenko, M. A. (2021). Length variation in short tandem repeats affects gene expression in natural populations of Arabidopsis thaliana. *The Plant cell*, *33*(7), 2221–2234.

Saad, S., Cereghetti, G., Feng, Y. *et al.* Reversible protein aggregation is a protective mechanism to ensure cell cycle restart after stress. *Nat Cell Biol* 19, 1202–1213 (2017).

Satyal, S. H., Schmidt, E., Kitagawa, K., Sondheimer, N., Lindquist, S., Kramer, J. M., & Morimoto, R. I. (2000). Polyglutamine aggregates alter protein folding homeostasis in Caenorhabditis elegans. *Proceedings of the National Academy of Sciences of the United States of America*, *97*(11), 5750–5755.

Shi H, Chen L, Ye T, Liu X, Ding K, Chan Z. Modulation of auxin content in Arabidopsis confers improved drought stress resistance. Plant Physiol Biochem. 2014 Sep;82:209-17. doi: 10.1016/j.plaphy.2014.06.008. Epub 2014 Jun 20.

Shuman, S. (1994) Novel approach to molecular cloning and polynucleotide synthesis using vaccinia DNA topoisomerasel. *J. Biol. Chem.* 269, 32,678–32,684

Singh, S., Yadav, S., Singh, A., Mahima, M., Singh, A., Gautam, V. and Sarkar, A.K. (2020), Auxin signaling modulates *LATERAL ROOT PRIMORDIUM1* (*LRP1*) expression during lateral root development in Arabidopsis. Plant J, 101: 87-100.

Smith, S., & De Smet, I. (2012). Root system architecture: insights from Arabidopsis and cereal crops. *Philosophical transactions of the Royal Society of London. Series B, Biological sciences*, *367*(1595), 1441–1452.

Sohlberg, J. J., Myrenås, M., Kuusk, S., Lagercrantz, U., Kowalczyk, M., Sandberg, G., & Sundberg, E. (2006). STY1 regulates auxin homeostasis and affects apical–basal patterning of the Arabidopsis gynoecium. *The Plant Journal*, *47*(1), 112-123.

Somssich, M., Bleckmann, A., and Simon, R. (2016). Shared and distinct functions of the pseudokinase CORYNE (CRN) in shoot and root stem cell maintenance of Arabidopsis. J Exp Bot. 67: 4901-4915

Su, Y. H., Liu, Y. B., Bai, B., & Zhang, X. S. (2015). Establishment of embryonic shoot-root axis is involved in auxin and cytokinin response during Arabidopsis somatic embryogenesis. *Frontiers in plant science*, *5*, 792.

Szymańska, R., Ślesak, I., Orzechowska, A., & Kruk, J. (2017). Physiological and biochemical responses to high light and temperature stress in plants. *Environmental and Experimental Botany*, *139*, 165-177.

Taiz, Møller, Murphy, Zeiger, Plant Physiology and Development, 7e

Tanaka, Y., Shibahara, K., & Nakagawa, T. (2013). Development of gateway binary vectors R4L1pGWB possessing the bialaphos resistance gene (bar) and the tunicamycin resistance gene as markers for promoter analysis in plants. *Bioscience, biotechnology, and biochemistry*, *77*(8), 1795–1797.

The Plant Cell, Vol. 7, 735-745, June 1995 O 1995 American Society of Plant Physiologists LRP1, a Gene Expressed in Lateral and Adventitious Root Primordia of Arabidopsis David L. Smith and Nina V. Fedoroff

Todd, T. W., & Lim, J. (2013). Aggregation formation in the polyglutamine diseases: protection at a cost?. *Molecules and cells*, *36*(3), 185–194.

Tsutsui, H., & Higashiyama, T. (2017). pKAMA-ITACHI Vectors for Highly Efficient CRISPR/Cas9-Mediated Gene Knockout in Arabidopsis thaliana. *Plant & cell physiology*, *58*(1), 46–56.

Tsoi, P. S., Quan, M. D., Ferreon, J. C., & Ferreon, A. C. M. (2023). Aggregation of Disordered Proteins Associated with Neurodegeneration. *International journal of molecular sciences*, *24*(4), 3380.

Valastyan, J. S., & Lindquist, S. (2014). Mechanisms of protein-folding diseases at a glance. *Disease models & mechanisms*, *7*(1), 9–14.

van der Graaff, E., Dulk-Ras, A. D., Hooykaas, P. J., & Keller, B. (2000). Activation tagging of the LEAFY PETIOLE gene affects leaf petiole development in Arabidopsis thaliana. *Development (Cambridge, England)*, *127*(22), 4971–4980.

Varadi, M *et al*. AlphaFold Protein Structure Database: massively expanding the structural coverage of protein-sequence space with high-accuracy models. *Nucleic Acids Research* (2021).

Verbiest, M., Maksimov, M., Jin, Y., Anisimova, M., Gymrek, M., & Bilgin Sonay, T. (2023). Mutation and selection processes regulating short tandem repeats give rise to genetic and phenotypic diversity across species. *Journal of evolutionary biology*, *36*(2), 321–336.

Xiong, Y., & Jiao, Y. (2019). The Diverse Roles of Auxin in Regulating Leaf Development. *Plants (Basel, Switzerland)*, *8*(7), 243.

Xu, Y., Wang, H., Nussinov, R., & Ma, B. (2013). Protein charge and mass contribute to the spatio-temporal dynamics of protein-protein interactions in a minimal proteome. *Proteomics*, *13*(8), 1339–1351.

Yoon Y, Seo DH, Shin H, Kim HJ, Kim CM, Jang G. The Role of Stress-Responsive Transcription Factors in Modulating Abiotic Stress Tolerance in Plants. *Agronomy*. 2020; 10(6):788.

Zhang, D., Zhang, Z., Unver, T., & Zhang, B. (2020). CRISPR/Cas: A powerful tool for gene function study and crop improvement. *Journal of advanced research*, *29*, 207–221.

Zhao, S. P., Song, X. Y., Guo, L. L., Zhang, X. Z., & Zheng, W. J. (2020). Genome-Wide Analysis of the Shi-Related Sequence Family and Functional Identification of *GmSRS18* Involving in Drought and Salt Stresses in Soybean. *International journal of molecular sciences*, *21*(5), 1810.

Zhao, Y., Christensen, S. K., Fankhauser, C., Cashman, J. R., Cohen, J. D., Weigel, D., & Chory, J. (2001). A role for flavin monooxygenase-like enzymes in auxin biosynthesis. *Science (New York, N.Y.)*, *291*(5502), 306–309.

Zhou, W., Liu, Z., Wu, J., Liu, J. H., Hyder, S. M., Antoniou, E., & Lubahn, D. B. (2006). Identification and characterization of two novel splicing isoforms of human estrogen-related receptor beta. *The Journal of clinical endocrinology and metabolism*, *91*(2), 569–579.

Appendix 1 Supplementary figures

S. Fig 1

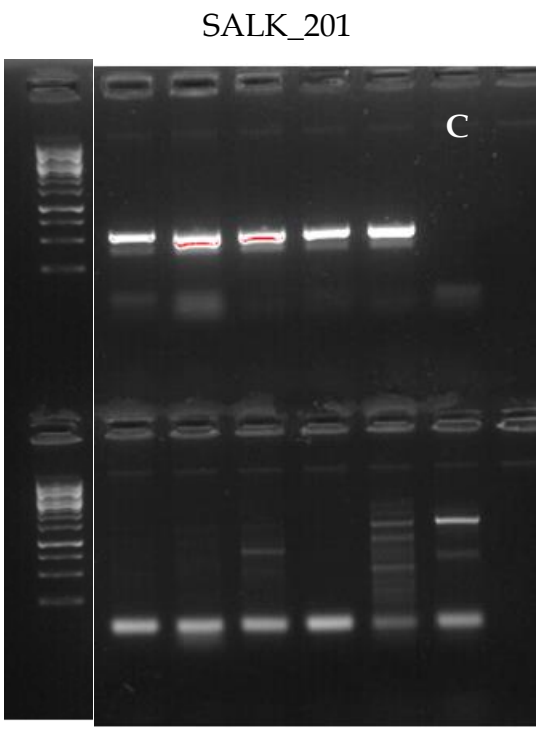

Supplementary figure 1 TDNA genotyping of SALK_201247. Upper wells are to check for TDNA insert, Lower wells are to check for WT gene. C = control with Col-0 DNA. Well number 1, 2, and 4 looks to be homozygous for T-DNA insert.

S. Fig. 2

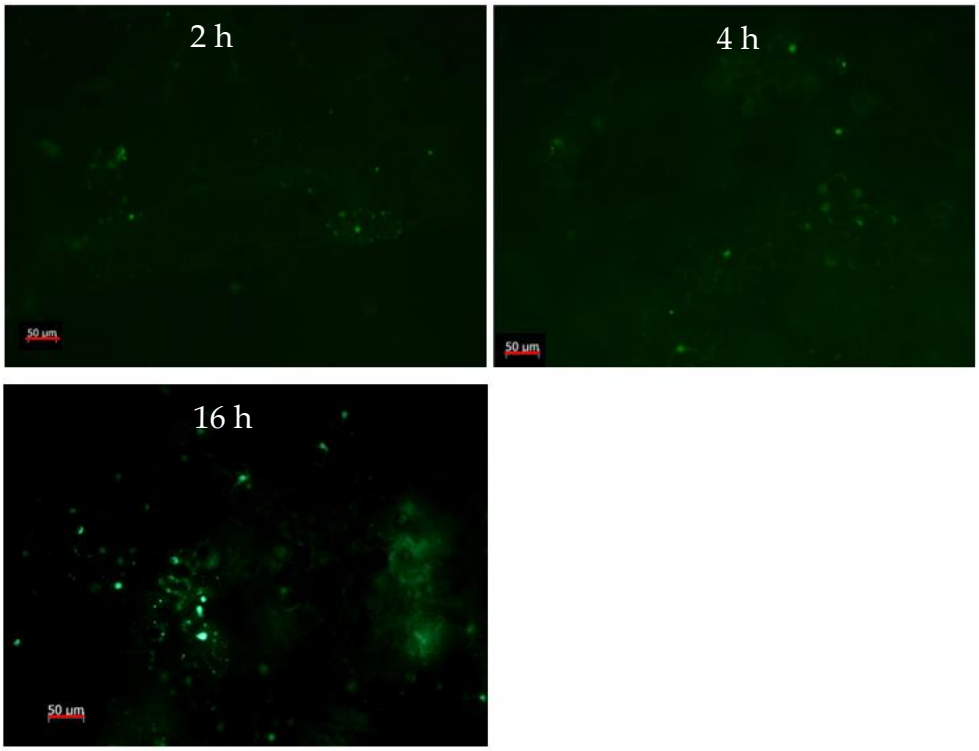

Supplementary figure 2 Time optimization of *est.ind35S:7QLRP1-GFP*. scalebar = 50 µm

S. Fig. 3

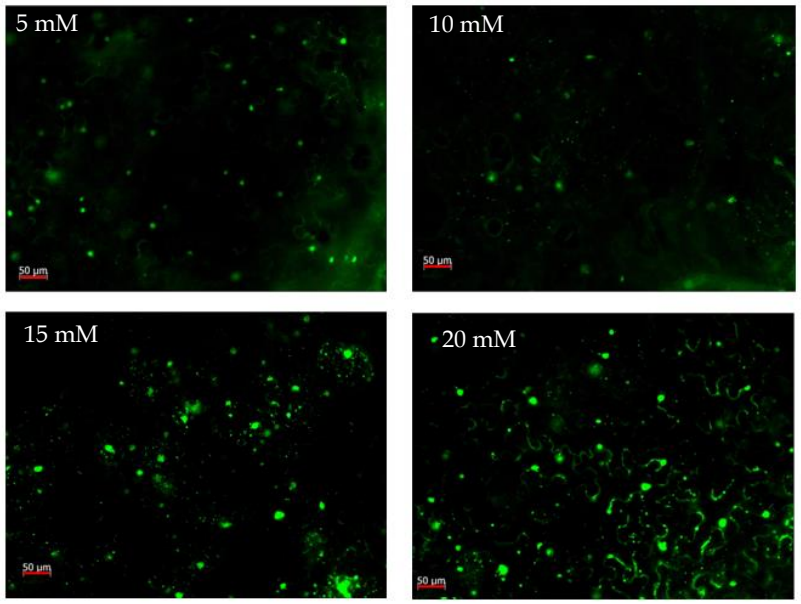

Supplementary figure 3 Estradiol optimization of *est.ind35S:7QLRP1-GFP*. Scalebar = 50 µm

S. Fig. 4

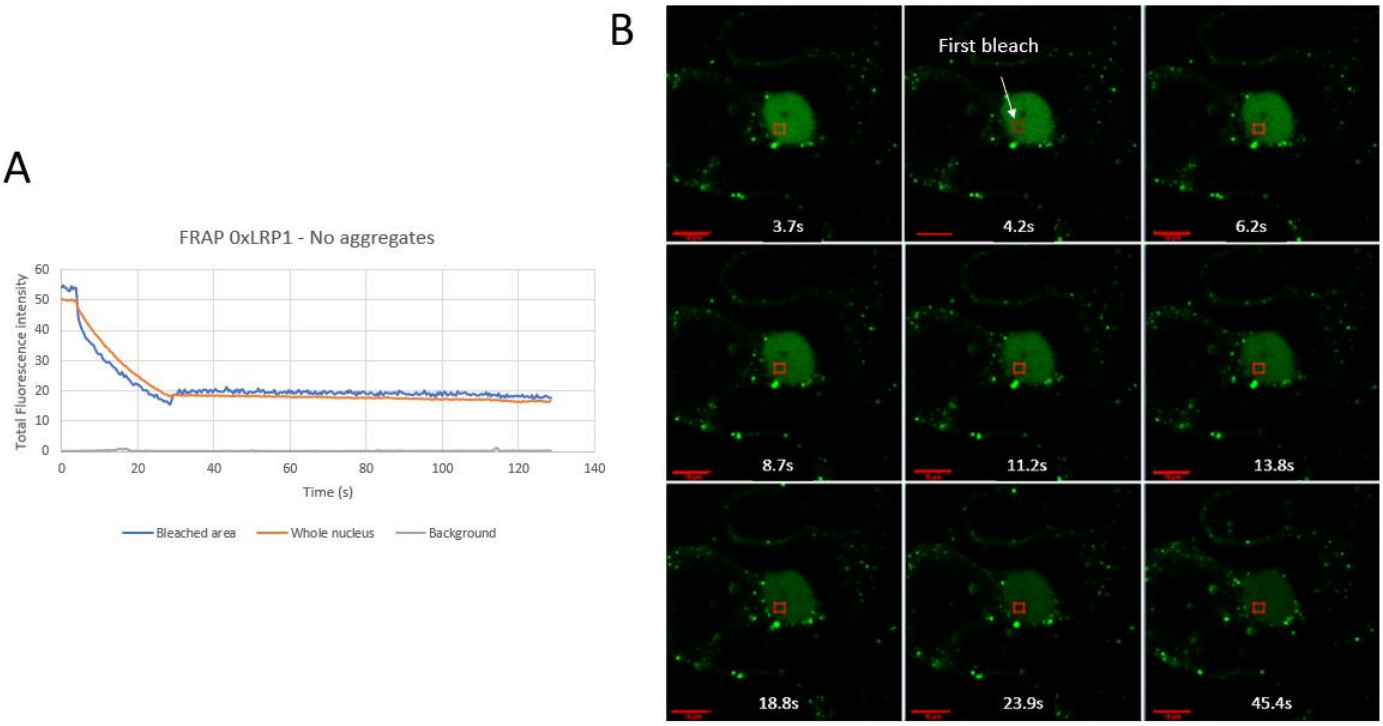

Supplementary figure 4 Fluorescence recovery after photobleaching of nucleus with no aggregates. A) Example of a FRAP curve from attempted FRAP experiment on nucleus without aggregates. The highest point is pre-bleach, the decrease in fluorescence intensity is almost identical for the bleached area and the whole nucleus meaning the unbleached proteins move into the bleach area very quickly, and the bleach was only able to reach 30 % when sufficient amount of protein had been bleached in the entire nucleus B) example pictures from the bleached nucleus without aggregates showing how the entire nucleus becomes bleached. The red square shows the bleach area.

S. Fig. 5

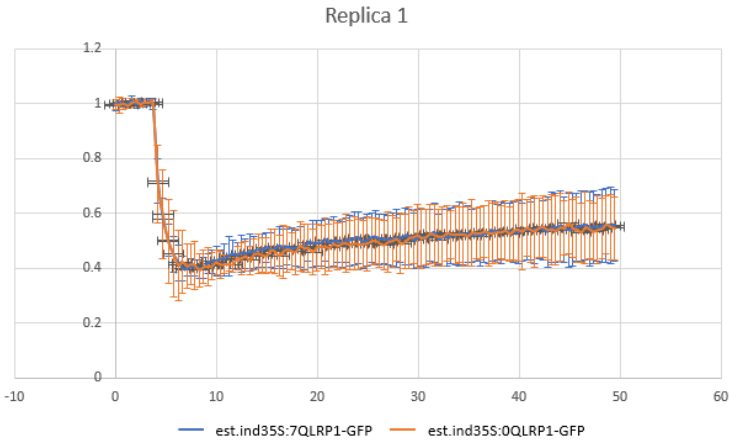

	est.ind35S::7QLRP1-GFP	est.ind35S:0QLRP1-GFP
Mf (%)	23.61	25.14

Supplementary figure 5 Fluorescence recovery after photobleaching of replica 1. The fluorescence recovery is essentially identical for *est.ind35S:7QLRP1:GFP* and *est.ind35S:0QLRP1:GFP*. The mobile fraction is also fairly identical.

S. Fig. 6

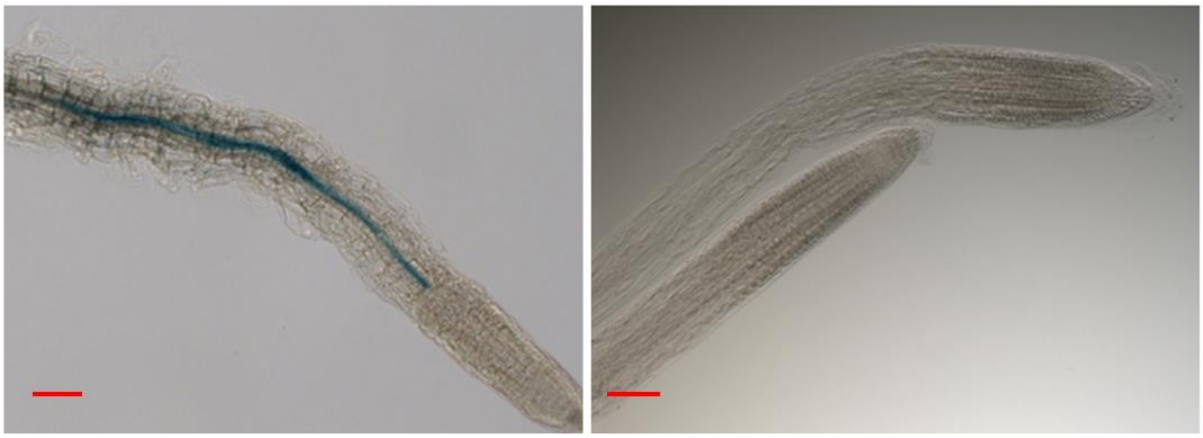

Supplementary figure 6 GUS staining of root that had grown into agar plate (left) and root that grew vertically on plate (right). Scale bar = 100 µm

S. Fig. 7

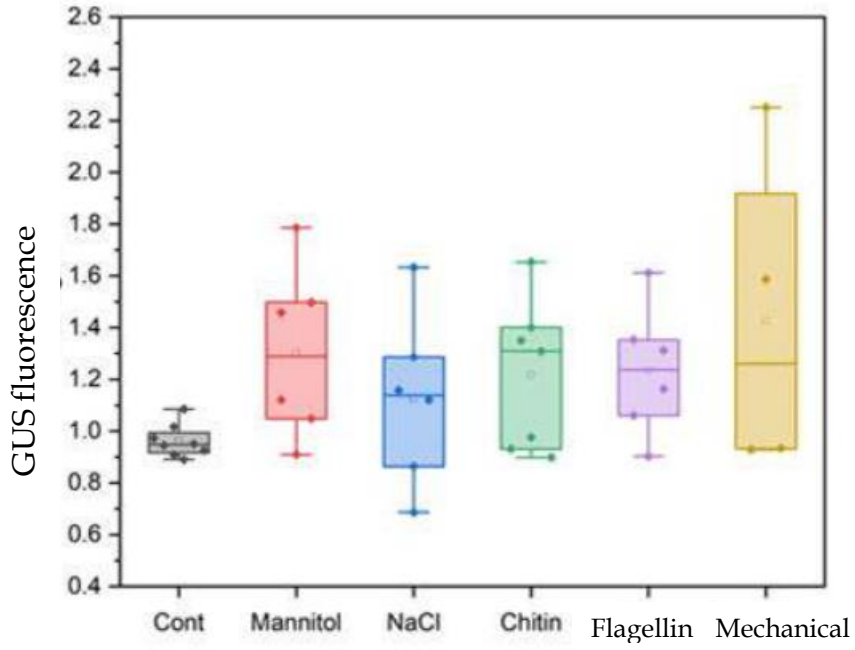

Supplementary figure 7 GUS fluorimetric assay replica 1. A slight upregulation in pLRP1 activity is seen for all treatments.

S. Fig. 8

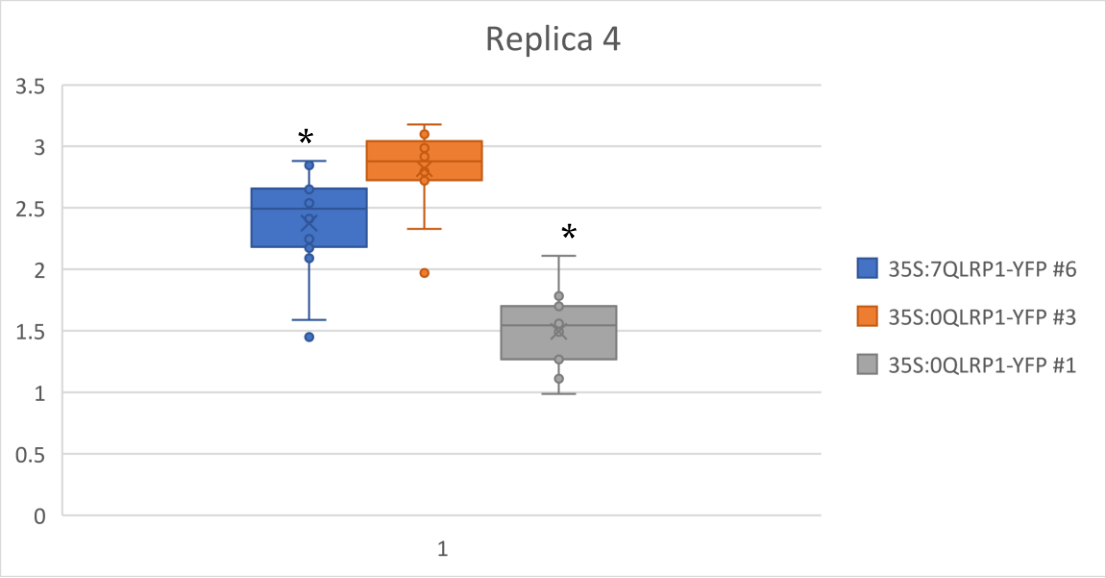

Supplementary figure 8 root length of overexpression lines after 8 days. Asterix (*) indicates statistical significance. One-way ANOVA was used for statistics. n = 18, 14, 11

S. Fig. 9

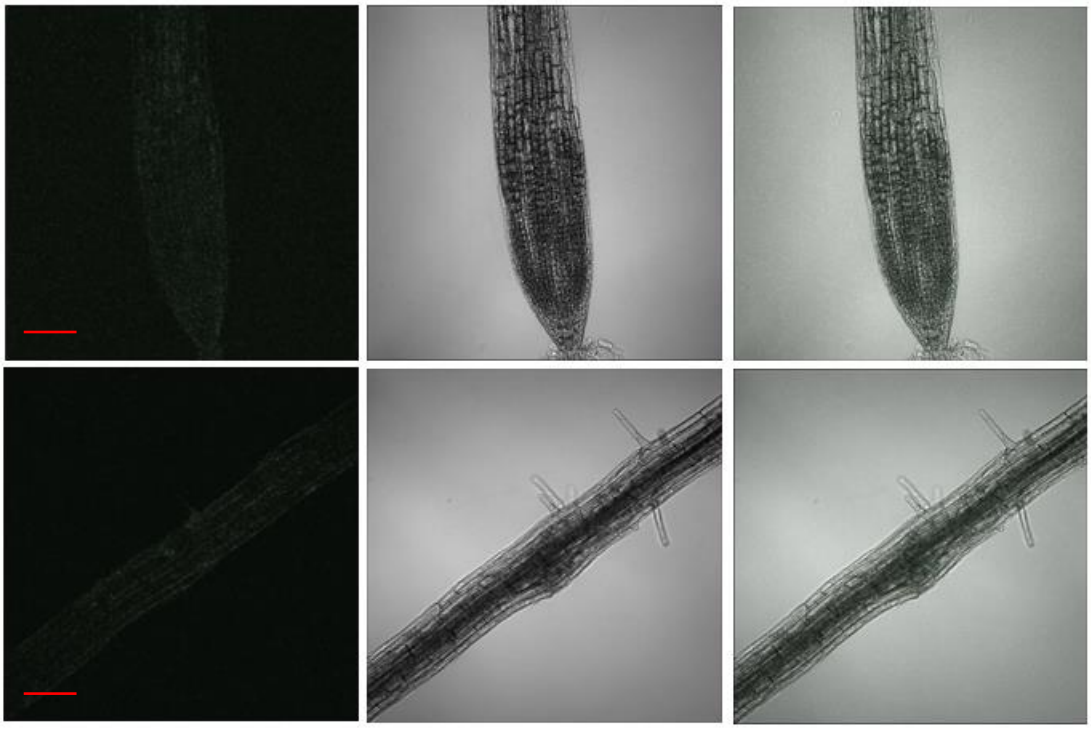

Supplementary Figure 9 Col-0 autofluorescence in root tip and along root. Scalebar = 100 µm. Picture taken with Olympus FV1000, 20 x objective.

Appendix 2 Supplementary movies

Movie 1	Nucleus containing no aggregates of 7QLRP1-GFP co-expressed with H2B-Tomat
Movie 2	Nucleus where aggregates of 7QLRP1-GFP co-expressed with H2B-Tomat appear to be inside the nucleus when seen in 2D, but aggregates are actually on the outside of the nucleus.
Movie 3	Nucleus with aggregates of 7QLRP1-GFP co-expressed with H2B-Tomat

Appendix 3 Abbreviations

4-MUG 4-Methylumbelliferyl beta-D-glucuronide

A Alanine

A. thaliana *Arabidopsis thaliana*

A. tumefaciens *Agrobacterium tumefaciens*

Accession Ecotype

ATN1 Atrophin-1

Col-0 Columbia-0

CRISPR Clustered Regularly Interspaced Palindromic Repeats

DBD DNA binding domain

ddH_2O double distilled H_2O

DSB Double stranded break

DZ Differentiation zone

ELF EARLY FLOWERING

est.ind Estradiol inducible

EtOH Ethanol

EZ Elongation zone

FRAP Fluorescence recovery after photobleaching

GA Gibberellic acid

GFP Green fluorescent protein

GUS β-glucuronidase

h Hour(s)

KO Knock-out

LB Left border

LDL1 (SWP1) LYSINE-SPECIFIC HISTONE DEMETHYLASE 1

LEP LEAFY PETIOLE

LR Lateral root

LRC Lateral root cap

LRP Lateral root primordia

LRP1 LATERAL ROOT PRIMORDIUM 1

Mf Mobile fraction

min Minute(s)

MS Murashige Skoog

MZ Meristematic zone

N Asparagine

N. benthamiana *Nicotiana benthamiana*

NASC Nottingham Arabidopsis Stock Centre

OD Optical density

OE Overexpression

pLRP1 LRP1 promoter

PR Primary root

PtAN1 Populus thrichocarpa ANGUSTIFOLIA

pYUC4 YUC4 promoter

PZ Peripheral zone

Q Glutamine

RAM Root apical meristem

RB right border

RFP Red fluorescent protein

ROI Region of interest

rpm Rotations per minute

RT Room temperature

s second(s)

SAM Shoot apical meristem

SCN Stem cell niche

sgRNA single guide RNA

SHI/STY SHORT INTERNODES/STYLISH

SNP Single nucleotide polymorphism

SRS SHI-RELATED SEQUENCE

STR Short tandem repeat

TF Transcription factor

TSS Transcription start site

TZ Transition zone

XPP Xylem pole pericycle

YEB Yeast extract beef

YFP Yellow fluorescent protein

YUC YUCCA